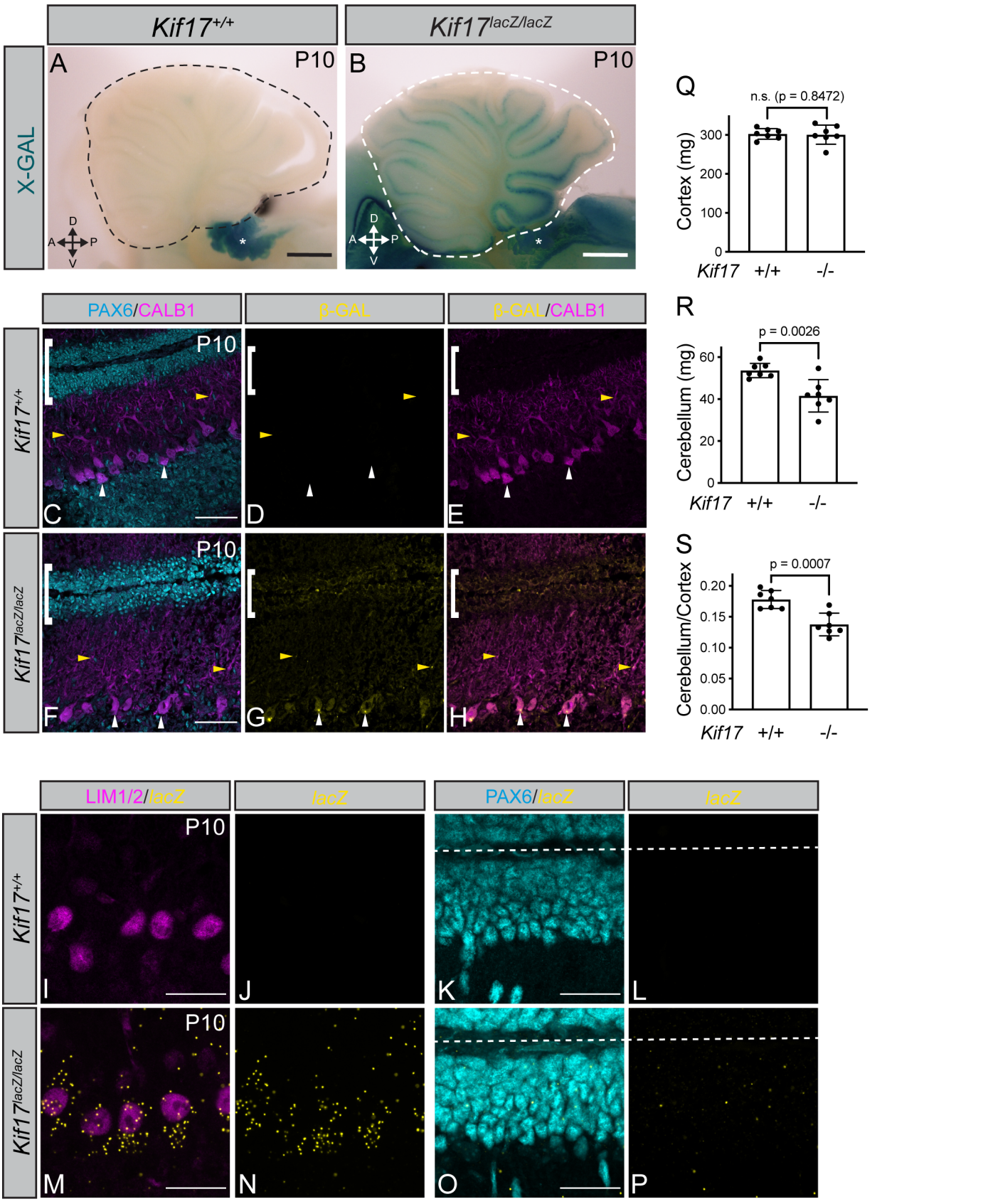
Kif17+/+
Kif17lacZ/lacZ
X-GAL
A
P10
B
P10
D
A
P
V
*
PAX6/CALB1
β-GAL
β-GAL/CALB1
Kif17+/+
Kif17lacZ/lacZ
C
D
E
F
G
H
P10
Q
n.s. (p = 0.8472)
Cortex (mg)
300
200
100
0
Kif17 +/+ -/-
R
p = 0.0026
Cerebellum (mg)
60
40
20
0
S
p = 0.0007
Cerebellum/Cortex
0.20
0.15
0.10
0.05
0.00
LIM1/2/lacZ
lacZ
PAX6/lacZ
I
J
K
L
M
N
O
P

Figure 2.2 *Kif17* is expressed within Purkinje cells and cerebellar granule neural progenitors and is required for normal cerebellar development.

Whole-mount X-gal staining of *Kif17*$^{+/+}$ (A) and *Kif17*$^{lacZ/lacZ}$ (B) cerebella at postnatal day 10 (P10). Scale bar, 500 μm. Asterisks denote endogenous Beta galactosidase (β-GAL) activity in the choroid plexus (Trifonov *et al.*, 2016). Immunofluorescent antibody detection of β-GAL (yellow) in *Kif17*$^{+/+}$ (C-E) and *Kif17*$^{lacZ/lacZ}$ (F-H) P10 posterior cerebellar lobes. Antibody detection of PAX6 (cyan) and Calbindin (CALB1, magenta) mark granule neuron nuclei and Purkinje cells, respectively. White brackets denote the external granule layers (EGL); white arrowheads indicate Purkinje cell bodies and yellow arrowheads indicate Purkinje cell dendrites. Scale bars (C, F), 50 μm. Fluorescent *in situ* detection of *lacZ* mRNA (yellow; I-P) in *Kif17*$^{+/+}$ (I-L) and *Kif17*$^{lacZ/lacZ}$ (M-P) P10 cerebella. Antibody detection of LIM1/2 (magenta; I, M) and PAX6 (cyan; K, O) identify Purkinje cell and cerebellar granule neural progenitor nuclei, respectively. Dashed lines separate individual external granule layers. Scale bars (I, K, M, O), 25 μm. Quantitation of cortex weight (Q), cerebellar weight (R), and cerebellar weight normalized to cortex weight (S) in P10 *Kif17*$^{+/+}$ and *Kif17*$^{-/-}$ mice. Data are mean ± s.d. Each dot represents an individual animal. *P*-values were determined by a two-tailed Student's *t*-test.

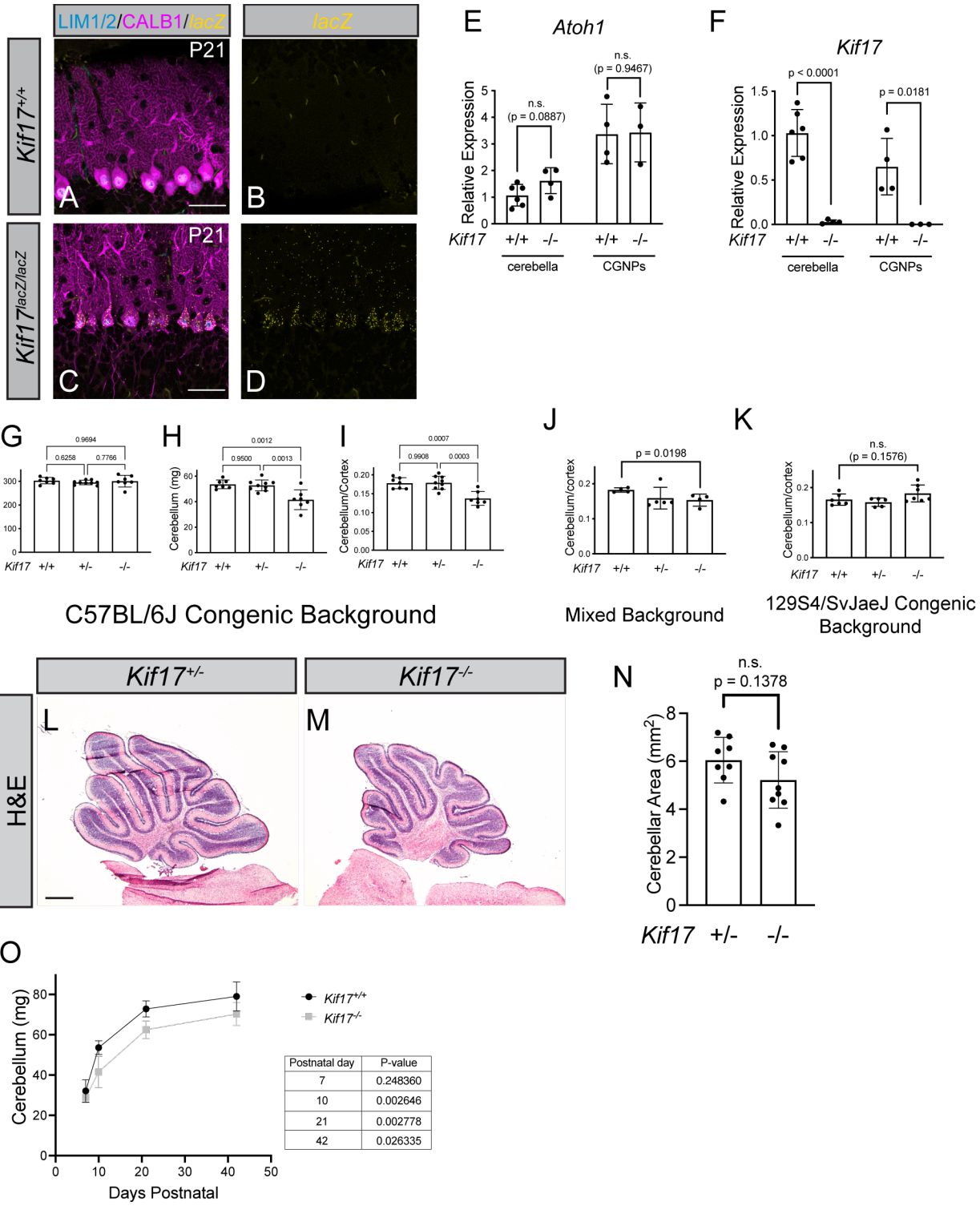

Postnatal day	P-value
7	0.248360
10	0.002646
21	0.002778
42	0.026335

Figure 2.3 Assessment of cerebellar defects on different genetic backgrounds and through postnatal cerebellar development.
Fluorescent *in situ* hybridization detection of *lacZ* (yellow, A-D) in posterior cerebellar lobes of P21 *Kif17*$^{+/+}$ (A-B) and *Kif17*$^{-/-}$ (C-D) mice. Immunofluorescent detection of LIM1/2 (cyan) and Calbindin (CALB1, magenta) were used to visualize Purkinje cells (A, C). Scale bar (A, C), 50 μm. Relative expression of *Atoh1* (E) and *Kif17* (F) measured by RT-qPCR in P8 and P10 whole cerebella and purified cerebellar granule neural progenitor cells (CGNPs). Weight of cortices (G), cerebella (H) and cerebellar weight normalized to cortical weight (I) in *Kif17*$^{+/+}$, *Kif17*$^{+/-}$ and *Kif17*$^{-/-}$ P10 littermates on a C57BL/6J genetic background. Cerebellar weight normalized to cortical weight for *Kif17*$^{+/+}$, *Kif17*$^{+/-}$ and *Kif17*$^{-/-}$ P10 littermates on a mixed genetic background (C57BL/6J and 129S4/SvJaeJ backgrounds, J) or a congenic 129S4/SvJaeJ genetic background (K). Representative hematoxylin and eosin-stained midsagittal sections (L, M) of P10 *Kif17*$^{+/+}$ (N) and *Kif17*$^{-/-}$ cerebella (N). Quantitation of cerebellar area (O) of *Kif17*$^{+/+}$ and *Kif17*$^{-/-}$ animals at P10. Cerebellar weights (O) of *Kif17*$^{+/+}$ and *Kif17*$^{-/-}$ mice through postnatal day 7 to 42. Data are means ± s.d. Each dot represents an individual animal or CGNP isolation, except in L, where it represents the average at each timepoint. P-values were determined by a two-tailed Student's t-test (E, F, J, K, N, O) or one way ANOVA (G, H, I).

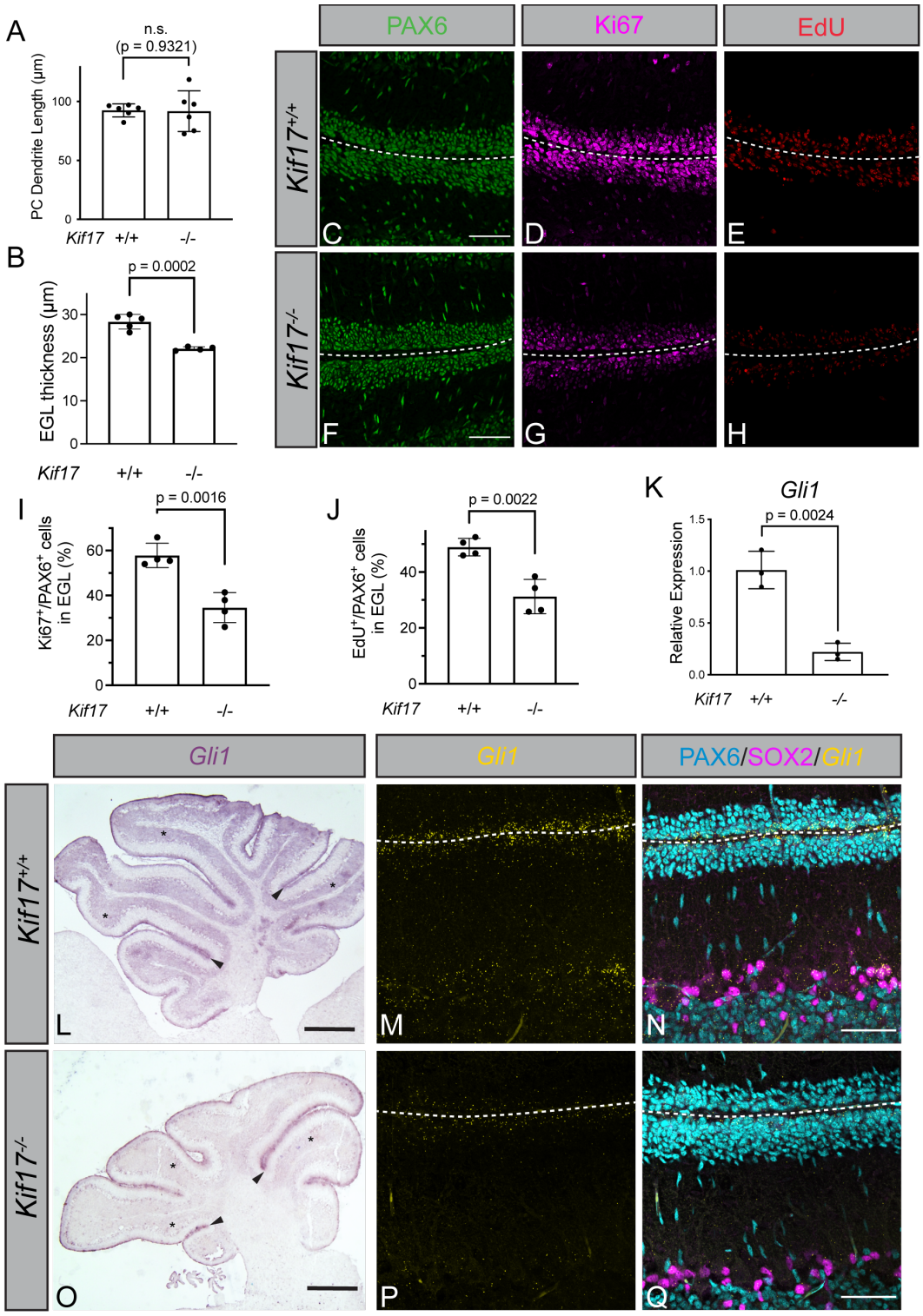

Figure 2.4 *Kif17* germline deletion results in reduced CGNP proliferation and decreased *Gli1* expression within all HH-responsive cells.

Quantitation of PC dendrite length (A) and external granule layer (EGL, B) thickness in posterior lobes of P10 *Kif17*$^{+/+}$ and *Kif17*$^{-/-}$ cerebella. Immunofluorescent analysis of CGNP proliferation

in the posterior lobes of P10 *Kif17*$^{+/+}$ (C-E) and *Kif17*$^{-/-}$ (F-H) cerebella. Antibody detection of PAX6 (green; C, F) and Ki67 (magenta; D, G). Fluorescent azide detection of EdU (red; E, H). Scale bars (C, F), 50μm. Dashed line separates individual external granule layers. Percentage of Ki67^{+} (I) and EdU^{+} (J) cells out of the PAX6^{+} EGL within the posterior lobes of P10 *Kif17*$^{+/+}$ and *Kif17*$^{-/-}$ cerebella. RT-qPCR detection of *Gli1* expression (K) in P10 *Kif17*$^{+/+}$ and *Kif17*$^{-/-}$ cerebella. Data are mean ± s.d. Each dot represents the average of 3-5 images per individual animal (A-B, I-J) or an individual animal (K). *P*-values were determined by a two-tailed Student's *t*-test. (L, O) *In situ* hybridization detection of *Gli1* in *Kif17*$^{+/+}$ (L) and *Kif17*$^{-/-}$ (O) P10 cerebella. Arrowheads point to EGL (CGNPs), while asterisk denotes inner granule layer (CGNs). Scale bars (L, O), 500 μm. Fluorescent *in situ* detection of *Gli1* (yellow; M-N, P-Q) and antibody detection (N, Q) of PAX6 (cyan) and SOX2 (magenta) to label granule neurons and Bergmann glia, respectively. Scale bars (N, Q), 50 μm. Dashed lines separate external granule layers.

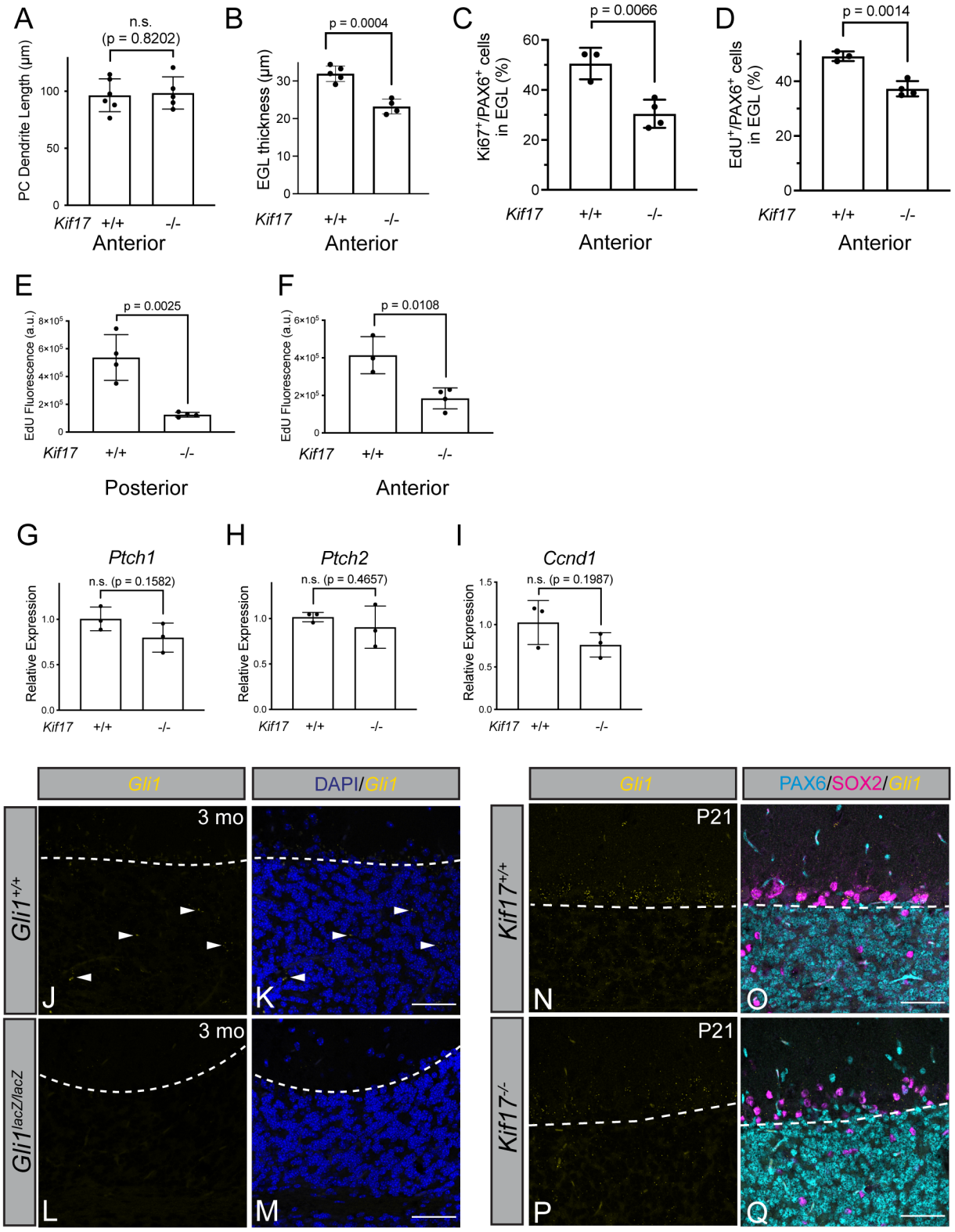
A
n.s.
(p = 0.8202)
PC Dendrite Length (μm)
Kif17 +/+ -/-
Anterior
B
p = 0.0004
EGL thickness (μm)
Kif17 +/+ -/-
Anterior
C
p = 0.0066
Ki67+/PAX6+ cells in EGL (%)
Kif17 +/+ -/-
Anterior
D
p = 0.0014
EdU+/PAX6+ cells in EGL (%)
Kif17 +/+ -/-
Anterior
E
p = 0.0025
EdU Fluorescence (a.u.)
Kif17 +/+ -/-
Posterior
F
p = 0.0108
EdU Fluorescence (a.u.)
Kif17 +/+ -/-
Anterior
G
Ptch1
n.s. (p = 0.1582)
Relative Expression
Kif17 +/+ -/-
H
Ptch2
n.s. (p = 0.4657)
Relative Expression
Kif17 +/+ -/-
I
Ccnd1
n.s. (p = 0.1987)
Relative Expression
Kif17 +/+ -/-
Gli1
DAPI/Gli1
Gli1+/+
3 mo
J
K
Gli1lacZ/lacZ
3 mo
L
M
Gli1
PAX6/SOX2/Gli1
Kif17+/+
P21
N
O
Kif17-/-
P21
P
Q

Figure 2.5 Quantitation of cerebellar phenotypes in anterior lobes of P10 *Kif17*$^{-/-}$ mice, including reduced HH target gene expression and demonstration of reduced *Gli1* expression in P21 *Kif17*$^{-/-}$ cerebella.

Measurements of the PC dendrite length (A) and EGL thickness (B) within anterior cerebellar lobes from P10 *Kif17*$^{+/+}$ and *Kif17*$^{-/-}$ mice. Percentage of Ki67^{+} (C) and EdU^{+} (D) cells out of the PAX6^{+} cells within the EGL of *Kif17*$^{+/+}$ and *Kif17*$^{-/-}$ anterior lobes in P10 cerebella. Quantitation of EdU fluorescence intensity (integrated density), within the posterior (E) and anterior (F) lobes in *Kif17*$^{+/+}$ and *Kif17*$^{-/-}$ P10 cerebella. Relative expression of *Ptch1* (G), *Ptch2* (H), *Ccnd1* (I) by RT-qPCR in P10 cerebella of *Kif17*$^{+/+}$ and *Kif17*$^{-/-}$ mice. Data are means ± s.d. Each dot represents the average of 3-5 images per animal (A-F) or an individual animal (G-I). *P*-values were determined by a two-tailed Student's *t*-test. Validation of *Gli1* fluorescent *in situ* probe (yellow, J-M) in *Gil1*$^{+/+}$ (J, K) and *Gli1*$^{lacZ/lacZ}$ (L, M) adult cerebella (3 months of age) counterstained with DAPI (blue, K, M). Dashed line separates Bergmann glia and mature CGNs, while arrowheads denote *Gli1*-expressing CGNs. Fluorescent *in situ* hybridization detection of *Gli1* (yellow; N-Q) with immunofluorescent antibody detection of PAX6 and SOX2 (magenta and cyan; O, Q) to identify CGNs and Bergmann glia, respectively, in P21 *Kif17*$^{+/+}$ (N-O) and *Kif17*$^{-/-}$ (P-Q) posterior cerebellar lobes. Dashed line separates Bergmann glia and CGNs. Scale bars (K, M, O, Q), 50 μm.

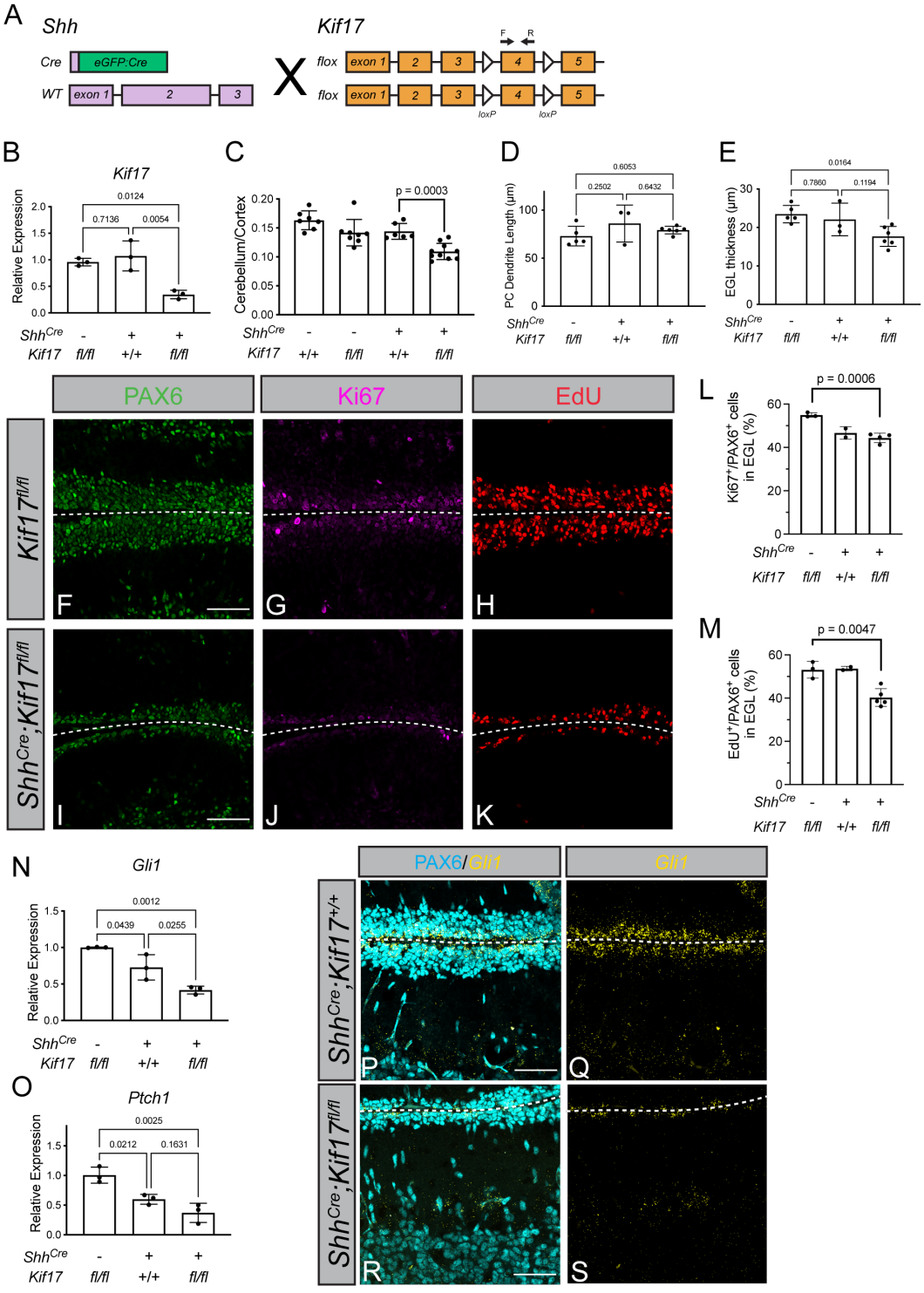
A
Shh
Cre
eGFP:Cre
WT
exon 1
2
3
X
Kif17
flox
F
R
4
5
loxP
B
Kif17
Relative Expression
0.0124
0.7136
0.0054
C
Cerebellum/Cortex
p = 0.0003
D
PC Dendrite Length (μm)
0.6053
0.2502
0.6432
E
EGL thickness (μm)
0.0164
0.7860
0.1194
Shh^Cre
Kif17
fl/fl
+/+
PAX6
Ki67
EdU
Kif17^fl/fl
Shh^Cre;Kif17^fl/fl
F
G
H
I
J
K
L
Ki67+/PAX6+ cells in EGL (%)
p = 0.0006
M
EdU+/PAX6+ cells in EGL (%)
p = 0.0047
N
Gli1
0.0012
0.0439
0.0255
O
Ptch1
0.0025
0.0212
0.1631
PAX6/Gli1
Gli1
Shh^Cre;Kif17^+/+
P
Q
R
S

Figure 2.6 Purkinje cell-specific *Kif17* deletion results in a non-cell autonomous HH loss-of-function phenotype.

(A) Schematic representing conditional Kif17 deletion within Purkinje cells using Shh^{Cre}. Arrows above exon 4 denote qPCR primers. Relative Kif17 expression (B) by RT-qPCR in $Kif17^{fl/fl}$, Shh^{Cre};$Kif17^{+/+}$ and Shh^{Cre};$Kif17^{fl/fl}$ P10 whole cerebella. Cerebellum weight normalized to cortex weight (C) P10 in P10 control and Purkinje cell-specific Kif17 deletion mice. Quantitation of PC dendrite length (D) and EGL (E) thickness within posterior lobes of P10 cerebella in $Kif17^{fl/fl}$, Shh^{Cre};$Kif17^{+/+}$ and Shh^{Cre};$Kif17^{fl/fl}$ mice. Immunofluorescent analysis of cerebellar granule neural progenitor proliferation in $Kif17^{fl/fl}$ (F-H) and Shh^{Cre};$Kif17^{fl/fl}$ (I-K) P10 cerebella. Antibody detection of PAX6 (green; F, I) and Ki67 (magenta; G, J). Fluorescent azide detection of EdU (red; H, K). Scale bars (F, I), 50 μm. Percentage of $Ki67^{+}$ (L) and EdU^{+} (M) cells out of the $PAX6^{+}$ EGL within the posterior lobes in P10 control and conditional Kif17 deletion cerebella. Relative expression of Gli1 (N) and Ptch1 (O) measured by RT-qPCR in P10 whole cerebella in $Kif17^{fl/fl}$, Shh^{Cre};$Kif17^{+/+}$ and Shh^{Cre};$Kif17^{fl/fl}$ mice. Data are mean ± s.d. Each dot represents an individual animal (B-C, N-O) or an average of 5 images per animal (D-E, L-M). P-values were determined by one way ANOVA (B, D, E, Nm O) or a two-tailed Student's t-test (C, L, M). Fluorescent in situ detection of Gli1 (yellow; P-S) and antibody detection of PAX6 (cyan; P, R) within posterior cerebellar lobes of P10 Shh^{Cre};$Kif17^{+/+}$ (P, Q) and Shh^{Cre};$Kif17^{fl/fl}$ (R, S) mice. Scale bars (P, R), 50 μm. Dashed lines separate external granule layers.

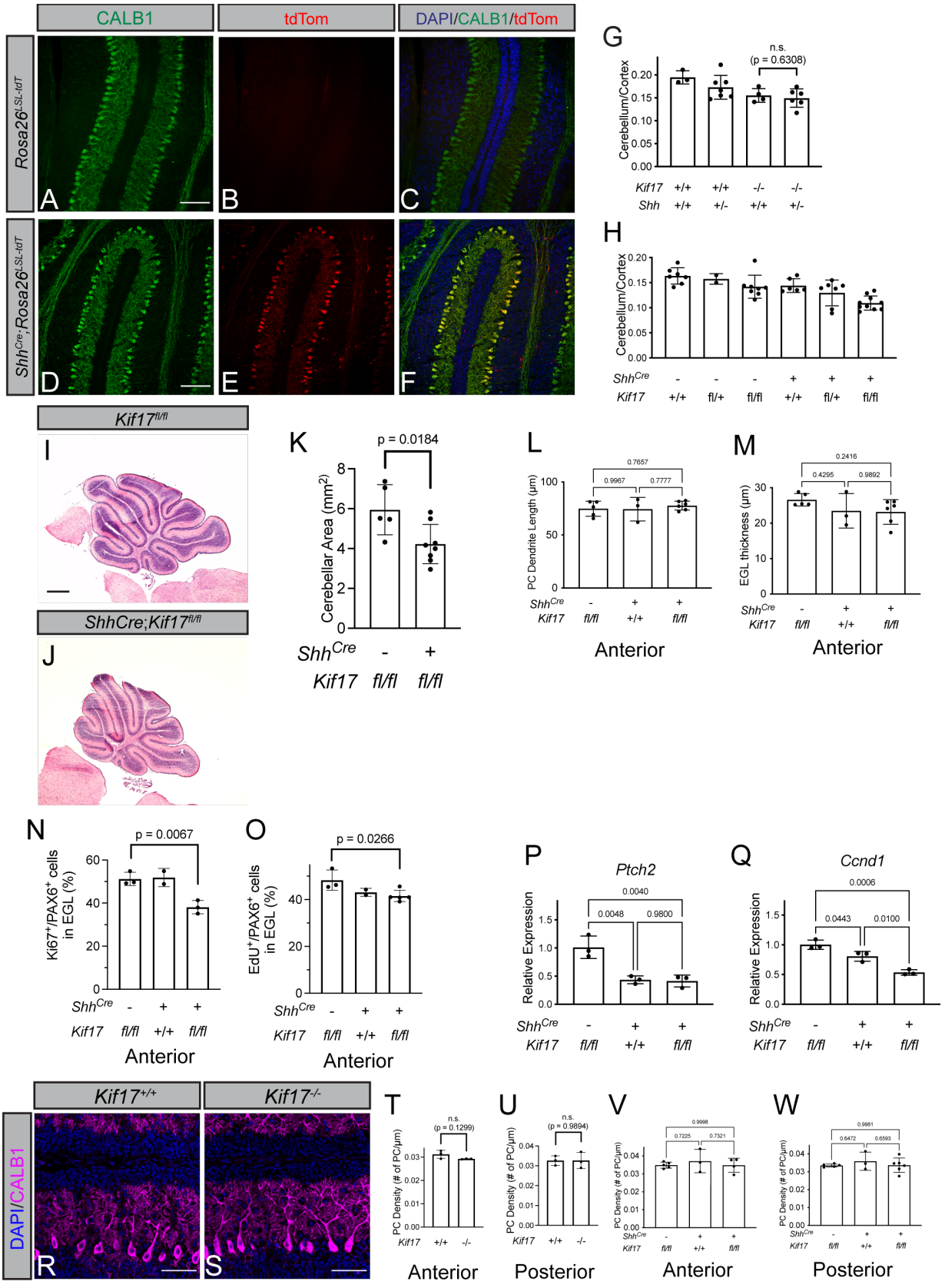
CALB1
tdTom
DAPI/CALB1/tdTom
Rosa26^L-SL-tdT
Shh^Cre;Rosa26^L-SL-tdT
A
B
C
D
E
F
G
n.s.
(p = 0.6308)
Cerebellum/Cortex
Kif17 +/+ +/+ -/- -/-
Shh +/+ +/- +/+ +/-
H
Cerebellum/Cortex
Shh^Cre - - - + + +
Kif17 +/+ fl/+ fl/fl +/+ fl/+ fl/fl
Kif17^fl/fl
I
ShhCre;Kif17^fl/fl
J
K
p = 0.0184
Cerebellar Area (mm^2)
Shh^Cre - +
Kif17 fl/fl fl/fl
L
0.7657
0.9967
0.7777
PC Dendrite Length (μm)
Shh^Cre - + +
Kif17 fl/fl +/+ fl/fl
Anterior
M
0.2416
0.4295
0.9892
EGL thickness (μm)
Shh^Cre - + +
Kif17 fl/fl +/+ fl/fl
Anterior
N
p = 0.0067
Ki67+/PAX6+ cells in EGL (%)
Shh^Cre - + +
Kif17 fl/fl +/+ fl/fl
Anterior
O
p = 0.0266
EdU+/PAX6+ cells in EGL (%)
Shh^Cre - + +
Kif17 fl/fl +/+ fl/fl
Anterior
P
Ptch2
0.0040
0.0048
0.9800
Relative Expression
Shh^Cre - + +
Kif17 fl/fl +/+ fl/fl
Q
Ccnd1
0.0006
0.0443
0.0100
Relative Expression
Shh^Cre - + +
Kif17 fl/fl +/+ fl/fl
Kif17^+/+
Kif17^-/-
DAPI/CALB1
R
S
T
n.s.
(p = 0.1299)
PC Density (# of PC/μm)
Kif17 +/+ -/-
Anterior
U
n.s.
(p = 0.9894)
PC Density (# of PC/μm)
Kif17 +/+ -/-
Posterior
V
0.9998
0.7225
0.7321
PC Density (# of PC/μm)
Shh^Cre - + +
Kif17 fl/fl +/+ fl/fl
Anterior
W
0.9981
0.6472
0.6593
PC Density (# of PC/μm)
Shh^Cre - + +
Kif17 fl/fl +/+ fl/fl
Posterior

Figure 2.7 Validation of selective *Shh^{Cre}* recombination in PCs and quantitation of cerebellar phenotypes following PC-specific *Kif17* deletion.

Immunofluorescent analysis of *Shh^{Cre}*-mediated recombination utilizing the *Rosa26$^{LSL\text{-}tdTomato}$* allele (A-F) in P10 *Rosa26$^{LSL\text{-}tdTomato}$* (A-C) and *Shh^{Cre};Rosa26$^{LSL\text{-}tdTomato}$* (D-F) cerebella. Direct fluorescence detection of tdTomato (TdTom, red; B, C, E, F) and antibody detection of Calbindin (CALB1, green; A, C, D, F) to visualize PCs. Nuclei were counterstained with DAPI (blue, C, F). Scale bars (A, D), 100 μm. Quantitation of cerebellar to cortical weights of compound *Shh/Kif17* germline mutants (G) and control and Purkinje cell-specific *Kif17* deletion (H) in P10 mice. Representative hematoxylin and eosin-stained midsagittal sections (I-J) of P10 *Kif17$^{fl/fl}$* (I) and *Shh^{Cre};Kif17$^{fl/fl}$* littermates (J). Quantitation of cerebellar area (K) of *Kif17$^{fl/fl}$* and *Shh^{Cre};Kif17$^{fl/fl}$* animals at P10. Measurements of PC dendrite length (L) and EGL (M) thickness in anterior lobes of *Kif17$^{fl/fl}$*, *Shh^{Cre};Kif17$^{+/+}$* and *Shh^{Cre};Kif17$^{fl/fl}$* P10 cerebella. Percentage of Ki67^{+} (N) and EdU^{+} (O) cells out of PAX6^{+} cells in EGL within the anterior lobes of P10 control and PC-specific *Kif17* deletion animals. Relative expression of *Ptch2* (P) and *Ccnd1* (Q) by RT-qPCR in P10 whole cerebella from *Kif17$^{fl/fl}$*, *Shh^{Cre};Kif17$^{+/+}$* and *Shh^{Cre};Kif17$^{fl/fl}$* mice. Immunofluorescent analysis of PC morphology (R, S) using detection of Calbindin (CALB1, magenta) counterstained with DAPI (blue) in *Kif17$^{+/+}$* (R) and *Kif17$^{-/-}$* (S) P10 posterior cerebellar lobes. Quantitation of PC density (number of PCs divided by the length in microns) in anterior (T) and posterior (U) in *Kif17$^{+/+}$* and *Kif17$^{-/-}$* P10 cerebella. Quantitation of PC density in anterior (V) and posterior (W) *Kif17$^{fl/fl}$*, *Shh^{Cre};Kif17$^{+/+}$* and *Shh^{Cre};Kif17$^{fl/fl}$* in P10 cerebella. Data are means ± s.d. Each dot represents an individual animal (G, H, K, P, Q) or average of 3-5 images per animal (L-O, T-W). *P*-values were determined by a two-tailed Student's *t*-test (G, K N, O, T, U) or one way ANOVA (L, M, P, Q, V, W).

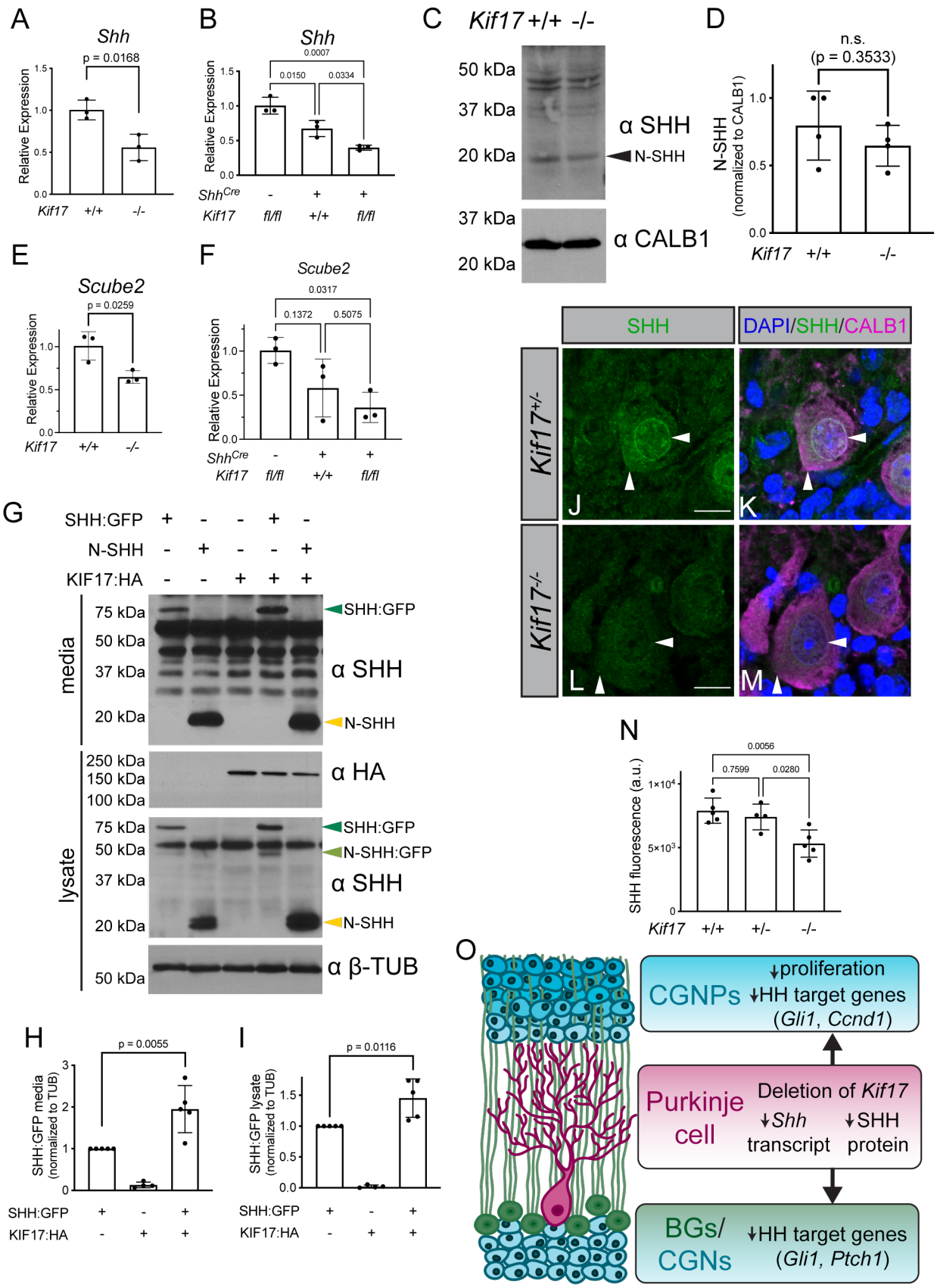
A
Shh
p = 0.0168
Relative Expression
Kif17 +/+ -/-
B
Shh
0.0007
0.0150
0.0334
Relative Expression
ShhCre - + +
Kif17 fl/fl +/+ fl/fl
C
Kif17 +/+ -/-
50 kDa
37 kDa
20 kDa
α SHH
N-SHH
37 kDa
20 kDa
α CALB1
D
n.s.
(p = 0.3533)
N-SHH (normalized to CALB1)
Kif17 +/+ -/-
E
Scube2
p = 0.0259
Relative Expression
Kif17 +/+ -/-
F
Scube2
0.0317
0.1372
0.5075
Relative Expression
ShhCre - + +
Kif17 fl/fl +/+ fl/fl
SHH
DAPI/SHH/CALB1
Kif17+/-
Kif17-/-
J
K
L
M
G
SHH:GFP + - - + -
N-SHH - + - - +
KIF17:HA - - + + +
media
75 kDa
50 kDa
37 kDa
20 kDa
SHH:GFP
α SHH
N-SHH
250 kDa
150 kDa
100 kDa
α HA
lysate
75 kDa
50 kDa
37 kDa
20 kDa
SHH:GFP
N-SHH:GFP
α SHH
N-SHH
50 kDa
α β-TUB
N
0.0056
0.7599
0.0280
SHH fluorescence (a.u.)
Kif17 +/+ +/- -/-
H
p = 0.0055
SHH:GFP media (normalized to TUB)
SHH:GFP + - +
KIF17:HA - + +
I
p = 0.0116
SHH:GFP lysate (normalized to TUB)
SHH:GFP + - +
KIF17:HA - + +
O
CGNPs
↓proliferation
↓HH target genes
(Gli1, Ccnd1)
Purkinje cell
Deletion of Kif17
↓Shh transcript
↓SHH protein
BGs/ CGNs
↓HH target genes
(Gli1, Ptch1)

Figure 2.8 KIF17 regulates SHH protein in the developing cerebellum.

Relative expression of *Shh* (A, B) by RT-qPCR in P10 whole cerebella of (A) $Kif17^{+/+}$ and $Kif17^{-/-}$ mice and (B) $Kif17^{fl/fl}$, $Shh^{Cre};Kif17^{+/+}$ and $Shh^{Cre};Kif17^{fl/fl}$ mice. Western blot analysis examining levels of SHH, using an antibody targeted to the N-terminus of SHH (C) in $Kif17^{+/+}$ and $Kif17^{-/-}$ P10 cerebella. Antibody detection of Calbindin (α-CALB1) was used to confirm equal loading across lanes. Arrowhead denotes secreted N-SHH (19kDa). The molecular masses (in kDa) of protein standards are indicated at the left of each blot. Quantitation of the levels of N-SHH (D) normalized to Calbindin in $Kif17^{+/+}$ and $Kif17^{-/-}$ in P10 cerebella. RT-qPCR analysis of *Scube2* expression (E, F) in P10 whole cerebella of (E) $Kif17^{+/+}$ and $Kif17^{-/-}$ mice and (F) $Kif17^{fl/fl}$, $Shh^{Cre};Kif17^{+/+}$ and $Shh^{Cre};Kif17^{fl/fl}$ P10 whole cerebella. Western blot analysis (G) of media and cell lysates collected from COS-7 cells expressing HA-tagged KIF17 (KIF17:HA), full length SHH fused to GFP (SHH:GFP) or N-SHH. Blots were incubated with antibodies directed against SHH (α-SHH) and HA (α-HA). Antibody detection of β-tubulin (α β-TUB) was used to confirm equal loading across lanes. Arrowheads denote full length SHH:GFP (68 kDa), N-SHH:GFP (42 kDa) or N-SHH (19 kDa). The molecular masses (in kDa) of protein standards are indicated at the left of each blot. Quantitation of full length SHH:GFP in the media (H) and in the cell lysates (I) normalized to β-tubulin within COS-7 cells. Immunofluorescent detection of SHH using an antibody targeted to the C-terminus of SHH (green; J-M). DAPI denotes nuclei (blue, K, M). Antibody detection of Calbindin, (CALB1, magenta; K, M) in P10 posterior cerebellar sections from $Kif17^{+/-}$ (J, K) and $Kif17^{-/-}$ (L, M) mice. Horizontal arrowheads indicate SHH localization to Golgi/ER, while vertical arrowheads denote cytoplasmic localization. Scale bars (J, L), 10 μm. Quantitation of SHH fluorescence (N) in posterior cerebellar lobes of P10 $Kif17^{+/+}$, $Kif17^{+/-}$ and $Kif17^{-/-}$ mice. Data are mean ± s.d. Each dot represents an individual animal (A-B, D-F), independent experiment (H-I) or the average of 5 images per animal (N). *P*-values were determined by a two-tailed Student's *t*-test (A, D, E, H, I) or one way ANOVA (B, F, N). (O) Summary of Purkinje cell-specific *Kif17* deletion on HH ligand production and HH response in the developing cerebellum.

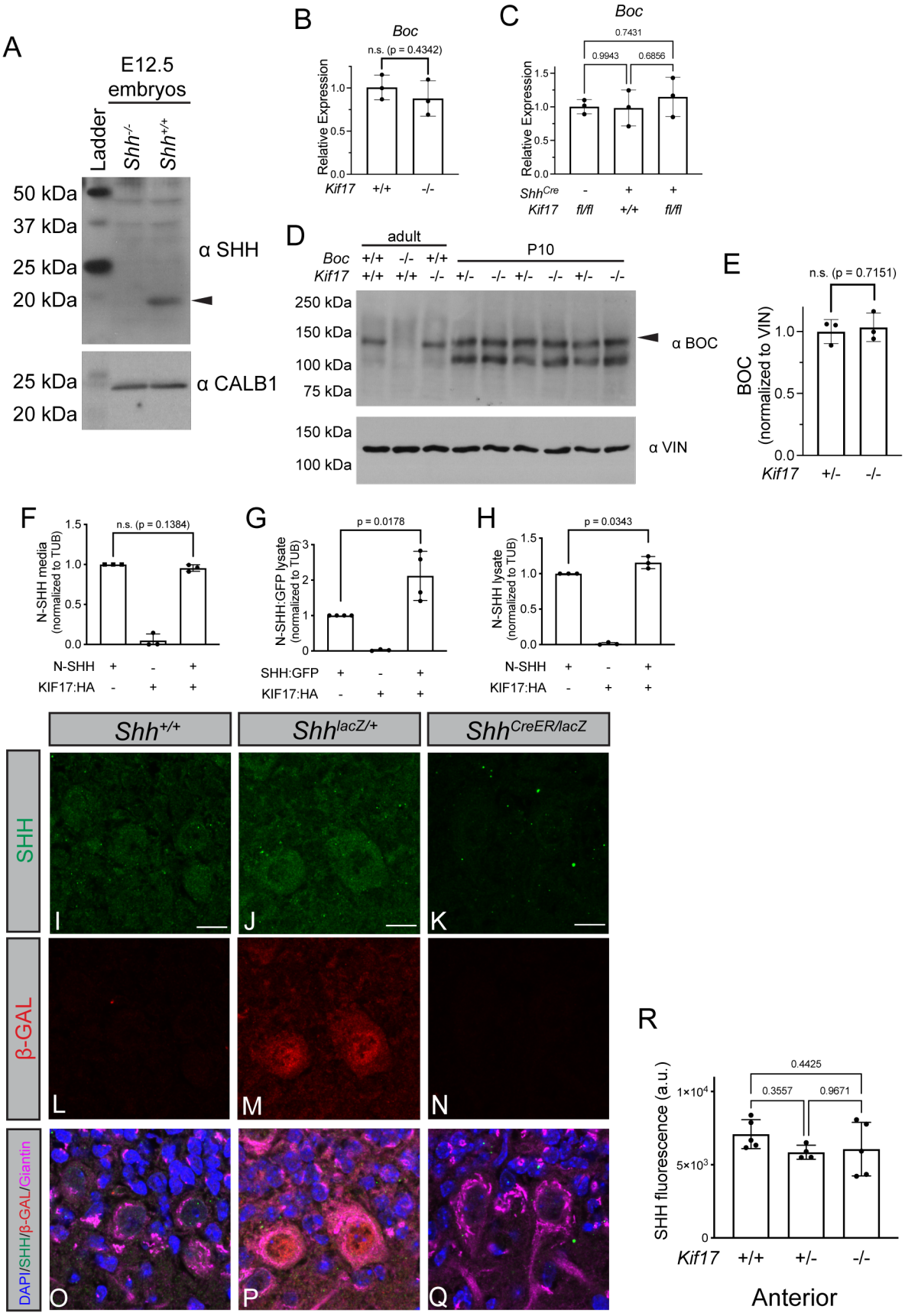
A
E12.5 embryos
Ladder
Shh-/-
Shh+/+
50 kDa
37 kDa
25 kDa
20 kDa
α SHH
25 kDa
20 kDa
α CALB1
B
Boc
n.s. (p = 0.4342)
Relative Expression
Kif17 +/+ -/-
C
Boc
0.7431
0.9943
0.6856
Relative Expression
ShhCre - + +
Kif17 fl/fl +/+ fl/fl
D
adult
P10
Boc +/+ -/- +/+
Kif17 +/+ +/+ -/- +/- -/- +/- -/- +/- -/-
250 kDa
150 kDa
100 kDa
75 kDa
α BOC
150 kDa
100 kDa
α VIN
E
n.s. (p = 0.7151)
BOC (normalized to VIN)
Kif17 +/- -/-
F
n.s. (p = 0.1384)
N-SHH media (normalized to TUB)
N-SHH + - +
KIF17:HA - + +
G
p = 0.0178
N-SHH:GFP lysate (normalized to TUB)
SHH:GFP + - +
KIF17:HA - + +
H
p = 0.0343
N-SHH lysate (normalized to TUB)
N-SHH + - +
KIF17:HA - + +
Shh+/+
ShhlacZ/+
ShhCreER/lacZ
SHH
β-GAL
DAPI/SHH/β-GAL/Giantin
I
J
K
L
M
N
O
P
Q
R
0.4425
0.3557
0.9671
SHH fluorescence (a.u.)
1×10^4
5×10^3
0
Kif17 +/+ +/- -/-
Anterior

Figure 2.9 Validation of SHH antibodies, quantitation of *Boc* transcript/BOC protein in *Kif17* mutant animals, and quantitation of SHH levels following *Kif17* expression in cells.

Western blot (A) validation of the N-terminal SHH antibody using lysates collected from E12.5 wildtype and *Shh* mutant mouse embryos. Arrowhead indicates secreted SHH (19 kDa). Antibody detection of Calbindin (α CALB1) was used to confirm equal loading across lanes. RT-qPCR analysis of *Boc* expression in $Kif17^{+/+}$ and $Kif17^{-/-}$ (B) and $Kif17^{fl/fl}$, $Shh^{Cre};Kif17^{+/+}$ and $Shh^{Cre};Kif17^{fl/fl}$ (C) P10 cerebella. Western blot (D) analysis of BOC (α BOC) in cerebella from adult *wildtype*, $Boc^{-/-}$ and $Kif17^{-/-}$ mice and P10 $Kif17^{+/-}$ and $Kif17^{-/-}$ littermates. Antibody detection of Vinculin (α VIN) was used to confirm equal loading across lanes. Quantitation of the levels of BOC (E) normalized to Vinculin in $Kif17^{+/-}$ and $Kif17^{-/-}$ P10 cerebella. Quantitation of the levels of N-SHH in media (F) normalized to β-tubulin in COS-7 cells. Quantitation of the levels of N-SHH:GFP (G) and N-SHH (H) within COS-7 cell lysates normalized to β-tubulin. Immunofluorescence validation of C-terminal SHH antibody (green; I-K, O-Q) in P10 cerebella from control and *Shh* conditional *Shh* deletion animals. Antibody detection of β-galactosidase (β-GAL; red, L-Q) and Giantin to visualize Golgi (magenta; O-Q) in $Shh^{+/+}$ (L, O), $Shh^{lacZ/+}$ (M, P) and $Shh^{CreER/lacZ}$ (O, Q) P10 posterior cerebellar lobes. Scale bar (I-K), 10 μm. Quantitation of SHH fluorescence (R) in anterior cerebellar lobes from P10 $Kif17^{+/+}$, $Kif17^{+/-}$ and $Kif17^{-/-}$ mice. Data represent the mean±s.d. Individual dots represent individual mice (B, C, E), independent samples from a single experiment (F-H) or the average of 5 images per animal (S). *P*-values were determined by a two-tailed Student's *t*-test (B, E, F, G, H) or one way ANOVA (C, R).

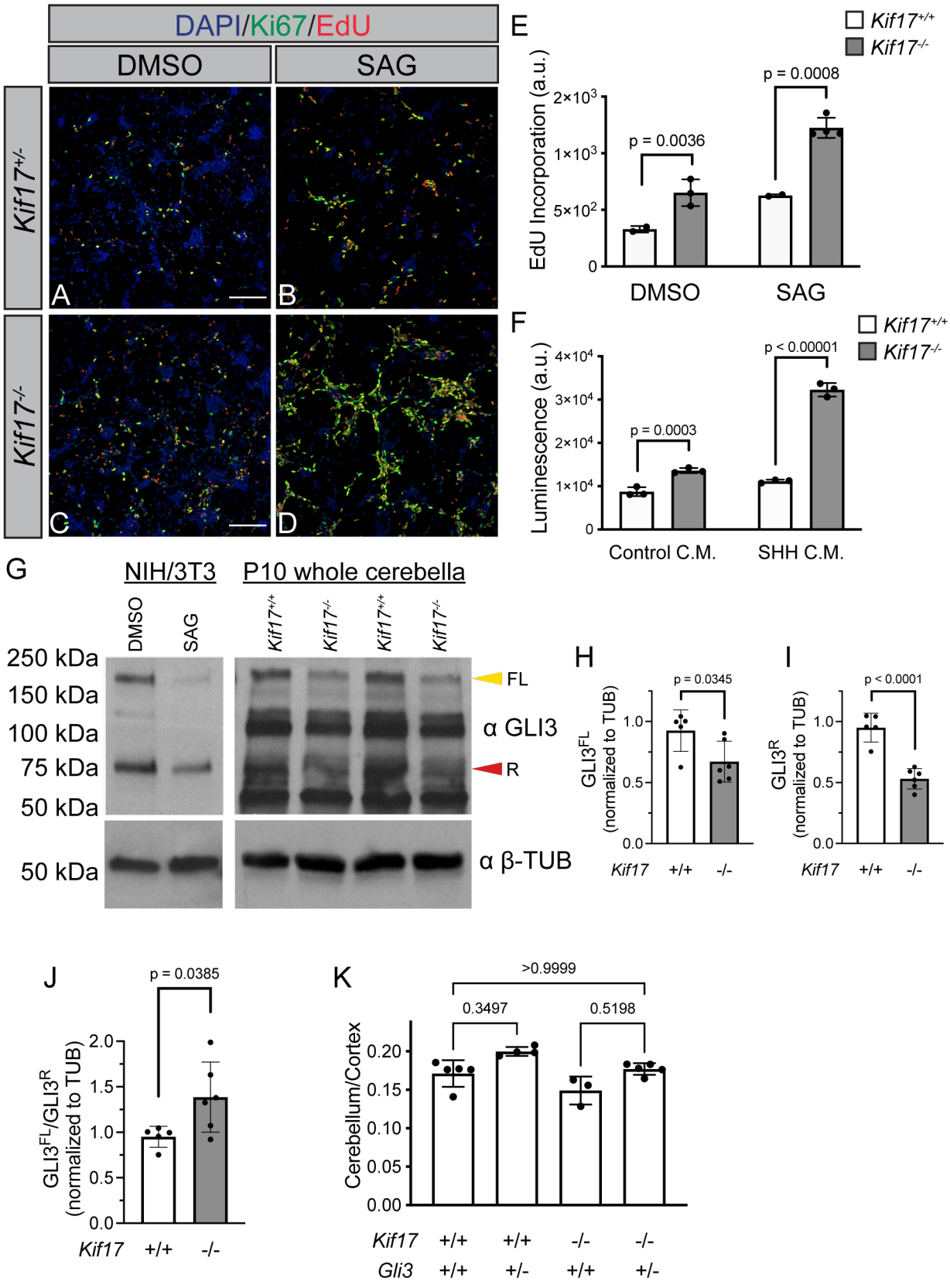
DAPI/Ki67/EdU
DMSO
SAG
Kif17+/-
Kif17-/-
A
B
C
D
E
Kif17+/+
Kif17-/-
EdU Incorporation (a.u.)
2×10³
1×10³
5×10²
0
p = 0.0036
p = 0.0008
DMSO
SAG
F
Kif17+/+
Kif17-/-
Luminescence (a.u.)
4×10⁴
3×10⁴
2×10⁴
1×10⁴
0
p = 0.0003
p < 0.00001
Control C.M.
SHH C.M.
G
NIH/3T3
P10 whole cerebella
DMSO
SAG
Kif17+/+
Kif17-/-
Kif17+/+
Kif17-/-
250 kDa
150 kDa
100 kDa
75 kDa
50 kDa
50 kDa
FL
α GLI3
R
α β-TUB
H
p = 0.0345
GLI3FL (normalized to TUB)
1.0
0.5
0.0
Kif17 +/+ -/-
I
p < 0.0001
GLI3R (normalized to TUB)
1.0
0.5
0.0
Kif17 +/+ -/-
J
p = 0.0385
GLI3FL/GLI3R (normalized to TUB)
2.0
1.5
1.0
0.5
0.0
Kif17 +/+ -/-
K
>0.9999
0.3497
0.5198
Cerebellum/Cortex
0.20
0.15
0.10
0.05
0.00
Kif17 +/+ +/+ -/- -/-
Gli3 +/+ +/- +/+ +/-

Figure 2.10 *Kif17* deletion promotes CGNP proliferation *in vitro*.

Immunofluorescent analysis of proliferation in P8 CGNP cultures from *Kif17*$^{+/-}$ (A-B) and *Kif17*$^{-/-}$ (C-D) littermates. Antibody detection of Ki67 (green), fluorescent azide detection of EdU (red), and DAPI staining of nuclei (blue). Cultures were treated with DMSO as a vehicle control (A, C) or Smoothened agonist (SAG, B, D). Scale bars (A, C), 100 μm. Quantitation of EdU incorporation (E) in *Kif17*$^{+/+}$ and *Kif17*$^{-/-}$ CGNP cultures. Quantitation of ATP levels by luminescence values (F) in *Kif17*$^{+/+}$ and *Kif17*$^{-/-}$ CGNP cultures treated with control conditioned media (C.M.) or SHH conditioned media (SHH C.M.). Western blot analysis of GLI3 (G) in NIH/3T3 fibroblasts and P10 cerebella from *Kif17*$^{+/+}$ and *Kif17*$^{-/-}$ mice. The molecular masses (in kDa) of protein standards are indicated at the left of each blot. Yellow arrowhead denotes full length GLI3 (FL, 190 kDa); red arrowhead denotes GLI3 repressor (R, 83 kDa). Antibody detection of β-tubulin (α β-TUB) was used to confirm equal loading across lanes. Quantitation of GLI3 full length (GLI3^{FL}, H) and GLI3 repressor (GLI3^{R}, I) normalized to β-tubulin. Ratio of GLI3^{FL} to GLI3^{R} (J) normalized to β-tubulin in *Kif17*$^{+/+}$ and *Kif17*$^{-/-}$ cerebella. Quantitation of cerebellar weight normalized to cortical weight in *Gli3;Kif17* compound mutants (K) at postnatal day 10. Data are mean ± s.d. Each dot represents an independent CGNP culture (E-F) or individual mouse (H-K). *P*-values were determined by a two-tailed Student's *t*-test (E, F, H, I, J) or one way ANOVA (K).

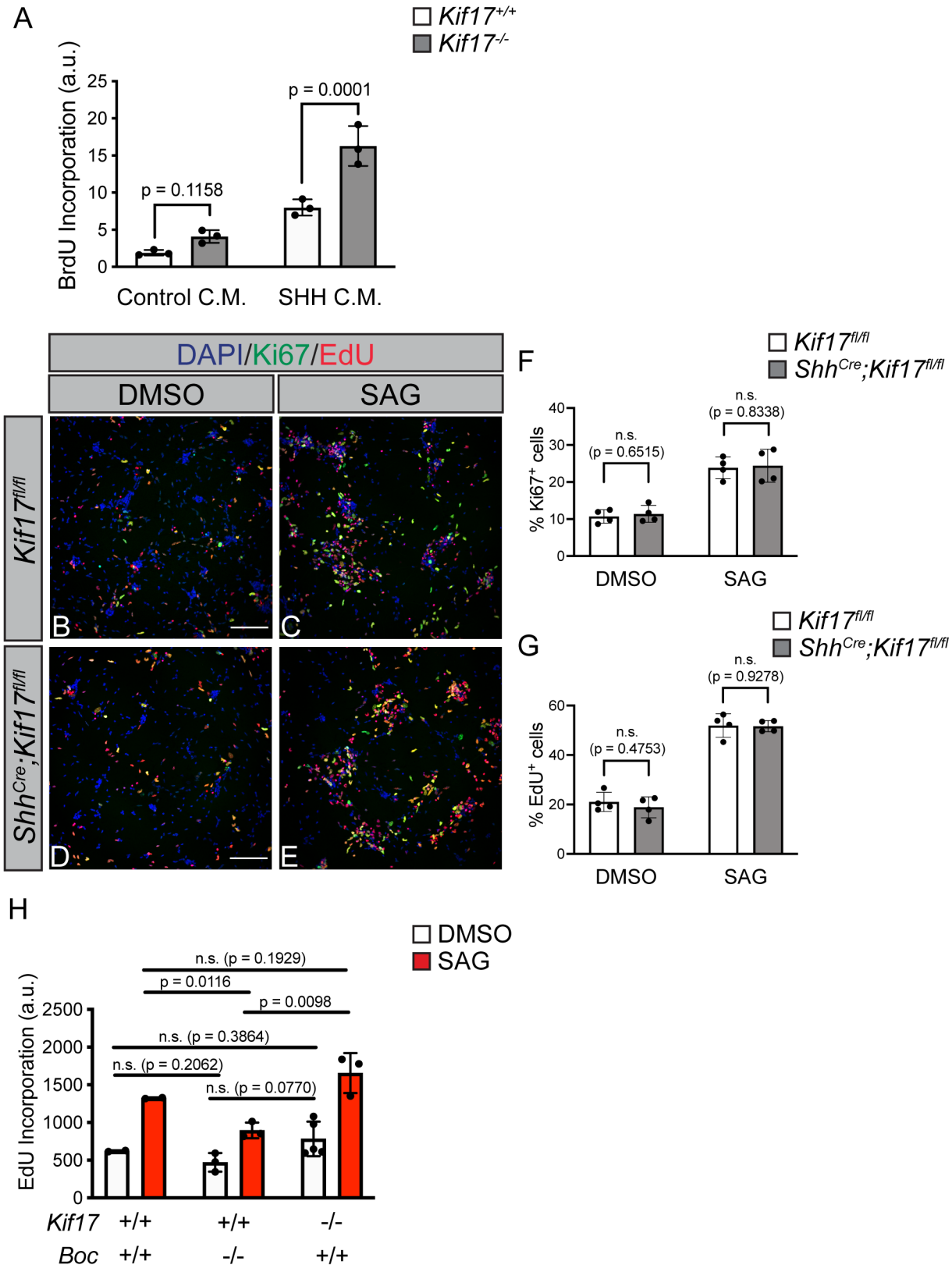
A
Kif17+/+
Kif17-/-
BrdU Incorporation (a.u.)
25
20
15
10
5
0
p = 0.0001
p = 0.1158
Control C.M.
SHH C.M.
DAPI/Ki67/EdU
DMSO
SAG
Kif17fl/fl
Shh Cre;Kif17fl/fl
B
C
D
E
F
Kif17fl/fl
Shh Cre;Kif17fl/fl
% Ki67+ cells
40
30
20
10
0
n.s.
(p = 0.6515)
n.s.
(p = 0.8338)
DMSO
SAG
G
Kif17fl/fl
Shh Cre;Kif17fl/fl
% EdU+ cells
60
40
20
0
n.s.
(p = 0.4753)
n.s.
(p = 0.9278)
DMSO
SAG
H
DMSO
SAG
EdU Incorporation (a.u.)
2500
2000
1500
1000
500
0
n.s. (p = 0.1929)
p = 0.0116
p = 0.0098
n.s. (p = 0.3864)
n.s. (p = 0.2062)
n.s. (p = 0.0770)
Kif17 +/+ +/+ -/-
Boc +/+ -/- +/+

Figure 2.11 *Kif17*$^{-/-}$ CGNPs but not CGNPs from PC-specific *Kif17* deletion display increased proliferation.

Quantitation of BrdU incorporation (A) in *Kif17*$^{+/+}$ and *Kif17*$^{-/-}$ CGNP cultures treated with either control conditioned media (control C.M.) or SHH conditioned media (SHH C.M.). Immunofluorescent analysis of *in vitro* CGNP proliferation in cultures from P8 *Kif17*$^{fl/fl}$ (B-C) and *Shh*^{Cre}*;Kif17*$^{fl/fl}$ (D-E) littermates. Nuclei were counterstained with DAPI (blue); Ki67 immunofluorescence (green) and EdU incorporation (red) were visualized in response to DMSO (B, D) and SAG treatment (C, E). Scale bars (B, D), 100 μm. Percentage of Ki67^{+} (F) and EdU^{+} (G) cells in CGNP cultures from P8 *Kif17*$^{fl/fl}$ and *Shh*^{Cre}*;Kif17*$^{fl/fl}$ littermates. Quantitation of EdU incorporation (H) in *wildtype*, *Kif17*$^{-/-}$, *Boc*$^{-/-}$ CGNPs grown in 10% calf serum in response to either DMSO or Smoothened Agonist (SAG, 500 nM) treatment. Each dot represents an individual well (A, H) or the average of 5 images per culture (F, G). *P*-values were determined by a two-tailed Student's *t*-test.

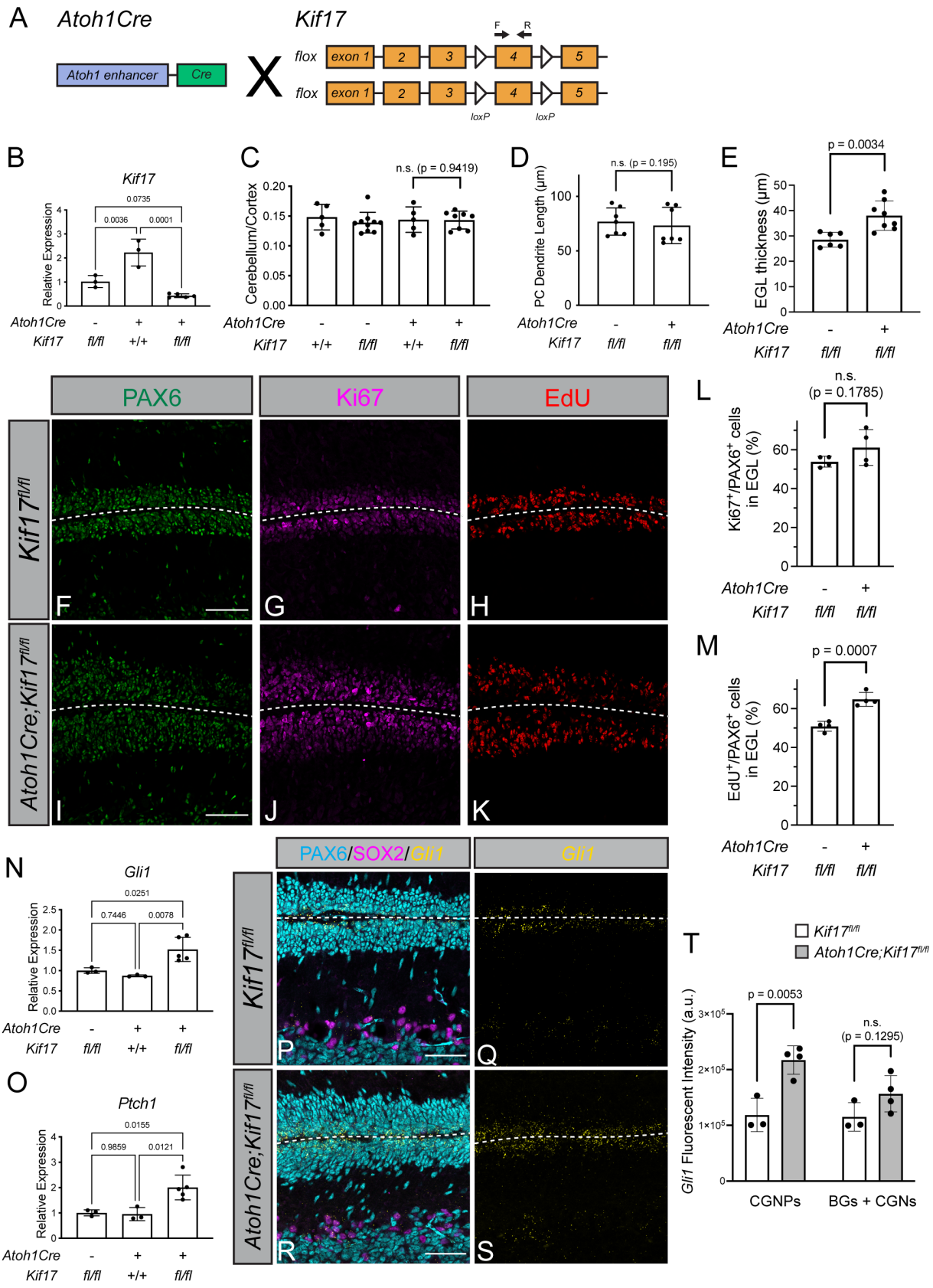
A
Atoh1Cre
Atoh1 enhancer
Cre
X
Kif17
flox
exon 1
2
3
4
5
F
R
loxP
B
Kif17
Relative Expression
0.0735
0.0036
0.0001
Atoh1Cre
Kif17
fl/fl
+/+
C
Cerebellum/Cortex
n.s. (p = 0.9419)
D
PC Dendrite Length (μm)
n.s. (p = 0.195)
E
EGL thickness (μm)
p = 0.0034
PAX6
Ki67
EdU
Kif17fl/fl
Atoh1Cre;Kif17fl/fl
F
G
H
I
J
K
L
Ki67+/PAX6+ cells in EGL (%)
n.s.
(p = 0.1785)
M
EdU+/PAX6+ cells in EGL (%)
p = 0.0007
N
Gli1
0.0251
0.7446
0.0078
O
Ptch1
0.0155
0.9859
0.0121
PAX6/SOX2/Gli1
Gli1
P
Q
R
S
T
Kif17fl/fl
Atoh1Cre;Kif17fl/fl
Gli1 Fluorescent Intensity (a.u.)
p = 0.0053
n.s.
(p = 0.1295)
CGNPs
BGs + CGNs

Figure 2.12 CGNP-specific *Kif17* deletion results in a cell-autonomous HH gain-of-function phenotype.

(A) Schematic representing conditional *Kif17* deletion within CGNPs using *Atoh11Cre*. Arrows above exon 4 denote qPCR primers. Relative *Kif17* expression (B) measured by RT-qPCR in P10 cerebella from *Kif17*$^{fl/fl}$, *Atoh1Cre;Kif17*$^{+/+}$ and *Atoh1Cre;Kif17*$^{fl/fl}$ mice. Cerebellar weights normalized to cortical weights (C) in P10 control and CGNP-specific *Kif17* deletion mice. Quantitation of PC dendrite length (D) and EGL (E) thickness in posterior lobes of *Kif17*$^{fl/fl}$ and *Atoh1Cre;Kif17*$^{fl/fl}$ P10 cerebella. Analysis of *in vivo* CGNP proliferation by immunofluorescence in *Kif17*$^{fl/fl}$ (F-H) and *Atoh1Cre;Kif17*$^{fl/fl}$ (I-K) P10 cerebella. Antibody detection of PAX6 (green; F, I) and Ki67 (magenta; G, J). Fluorescent azide detection of EdU (red; H, K). Scale bars (F, I), 50 μm. Percentage of Ki67^{+} (L) and EdU^{+} (M) cells out of the PAX6^{+} EGL within the posterior cerebellar lobes of *Kif17*$^{fl/fl}$ and *Atoh1Cre;Kif17*$^{fl/fl}$ P10 mice. Relative *Gli1* (N) and *Ptch1* (O) expression measured by RT-qPCR in *Kif17*$^{fl/fl}$, *Atoh1Cre;Kif17*$^{+/+}$ and *Atoh1Cre;Kif17*$^{fl/fl}$ P10 whole cerebella. Fluorescent *in situ Gli1* detection (yellow, P-S) with immunofluorescent detection of PAX6 to mark CGNPs and CGNs (cyan; P, R) and SOX2 to identify Bergmann glia (magenta; P, R) within posterior cerebellar lobes of P10 *Kif17*$^{fl/fl}$ and *Atoh1Cre;Kif17*$^{fl/fl}$ littermates. Scale bar (P, R), 50 μm. Quantitation of fluorescent intensity (integrated density) of *Gli1* puncta (T) within either CGNPs or Bergmann glia and cerebellar granule neurons (BGs + CGNs) in posterior cerebellar lobes of P10 *Kif17*$^{fl/fl}$ and *Atoh1Cre;Kif17*$^{fl/fl}$ mice. Data are mean ± s.d. Each dot represents an individual animal (B-E, N-O) or the average of 5 images per animal (L-M, T). *P*-values were determined by a one way ANOVA (B, N, O) or a two-tailed Student's *t*-test (C, D, E, L, M, T). Dashed lines separate external granule layers.

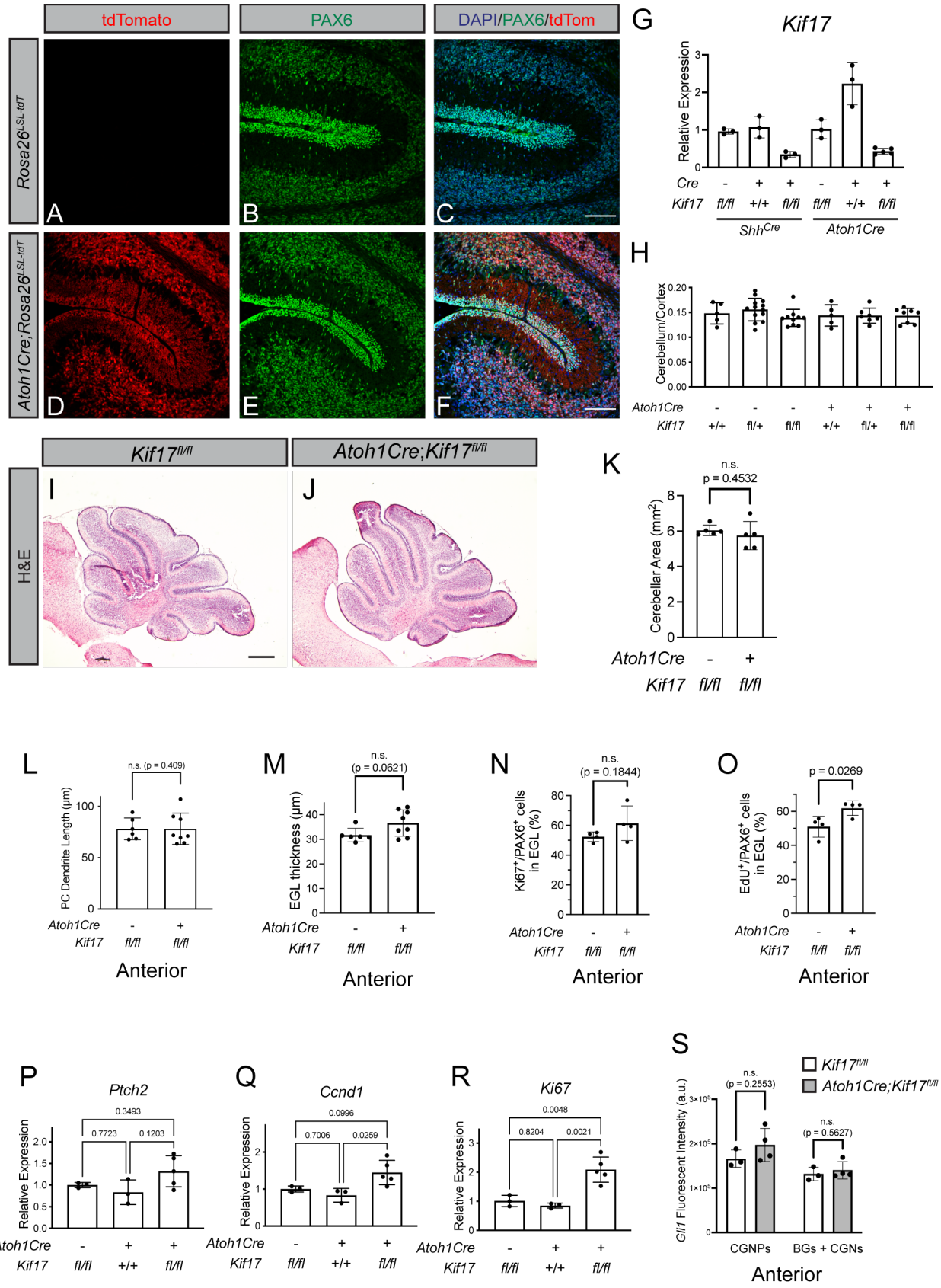
tdTomato
PAX6
DAPI/PAX6/tdTom
Rosa26LSL-tdT
Atoh1Cre;Rosa26LSL-tdT
A
B
C
D
E
F
G
Kif17
Relative Expression
Cre
Kif17
ShhCre
Atoh1Cre
H
Cerebellum/Cortex
Atoh1Cre
Kif17
Kif17fl/fl
Atoh1Cre;Kif17fl/fl
H&E
I
J
K
n.s.
p = 0.4532
Cerebellar Area (mm2)
L
n.s. (p = 0.409)
PC Dendrite Length (μm)
Anterior
M
n.s.
(p = 0.0621)
EGL thickness (μm)
N
n.s.
(p = 0.1844)
Ki67+/PAX6+ cells in EGL (%)
O
p = 0.0269
EdU+/PAX6+ cells in EGL (%)
P
Ptch2
0.3493
0.7723
0.1203
Q
Ccnd1
0.0996
0.7006
0.0259
R
Ki67
0.0048
0.8204
0.0021
S
Kif17fl/fl
Atoh1Cre;Kif17fl/fl
n.s.
(p = 0.2553)
n.s.
(p = 0.5627)
Gli1 Fluorescent Intensity (a.u.)
CGNPs
BGs + CGNs

Figure 2.13 Validation of selective *Atoh1*^{Cre} recombination in CGNPs and quantitation of cerebellar phenotypes following CGNP-specific *Kif17* deletion.

Validation of *Atoh1Cre* specificity (A-F) using immunofluorescence on sections from *Rosa26*$^{LSL\text{-}tdTomato}$ and *Atoh1Cre;Rosa26*$^{LSL\text{-}tdTomato}$ P10 posterior cerebellar lobes. Nuclei were stained with DAPI (blue; C, F), and antibody detection of PAX6 (green; B-C, E-F) to label CGNPs and CGNs. Scale bars (C, F), 100 μm. Relative *Kif17* expression (G) measured by RT-qPCR in P10 cerebella from PC conditional deletion littermates and CGNP conditional deletion littermates at P10. P10 Cerebellar weights normalized to cortical weights (H) in control and CGNP-specific *Kif17* deletion animals. Representative hematoxylin and eosin-stained midsagittal sections (I-J) of P10 *Kif17*$^{fl/fl}$ (I) and *Atoh1Cre;Kif17*$^{fl/fl}$ littermates (J). Quantitation of cerebellar area (K) of *Kif17*$^{fl/fl}$ and *Atoh1Cre;Kif17*$^{fl/fl}$ animals at P10. Measurements of PC dendrite length (L) and EGL thickness (M) in anterior lobes of *Kif17*$^{fl/fl}$ and *Atoh1Cre;Kif17*$^{fl/fl}$ P10 cerebella. Quantitation of the percentage of Ki67^{+} cells (N) and EdU^{+} cells (O) out of PAX6^{+} EGL in the anterior lobes of P10 cerebella from *Kif17*$^{fl/fl}$, and *Atoh1Cre;Kif17*$^{fl/fl}$ littermates. Expression of *Ptch2* (P), *Ccnd1* (Q), and *Ki67* (R), measured through RT-qPCR on P10 cerebella from *Kif17*$^{fl/fl}$ and *Atoh1Cre;Kif17*$^{fl/fl}$ littermates. Quantitation of fluorescent intensity (integrated density) of *Gli1* puncta (S) within CGNPs or Bergmann glia and cerebellar granule neurons (BGs + CGNs) in the anterior lobes of P10 *Kif17*$^{fl/fl}$ and *Atoh1Cre;Kif17*$^{fl/fl}$ mice. Each dot represents an individual animal (G, H, K, P-R) or the average of 5 images per animal (L-O, S). Data are means ± s.d. *P*-values were determined by a two-tailed Student's *t*-test (K, L, M, N, O, S) or one way ANOVA (P, Q, R).

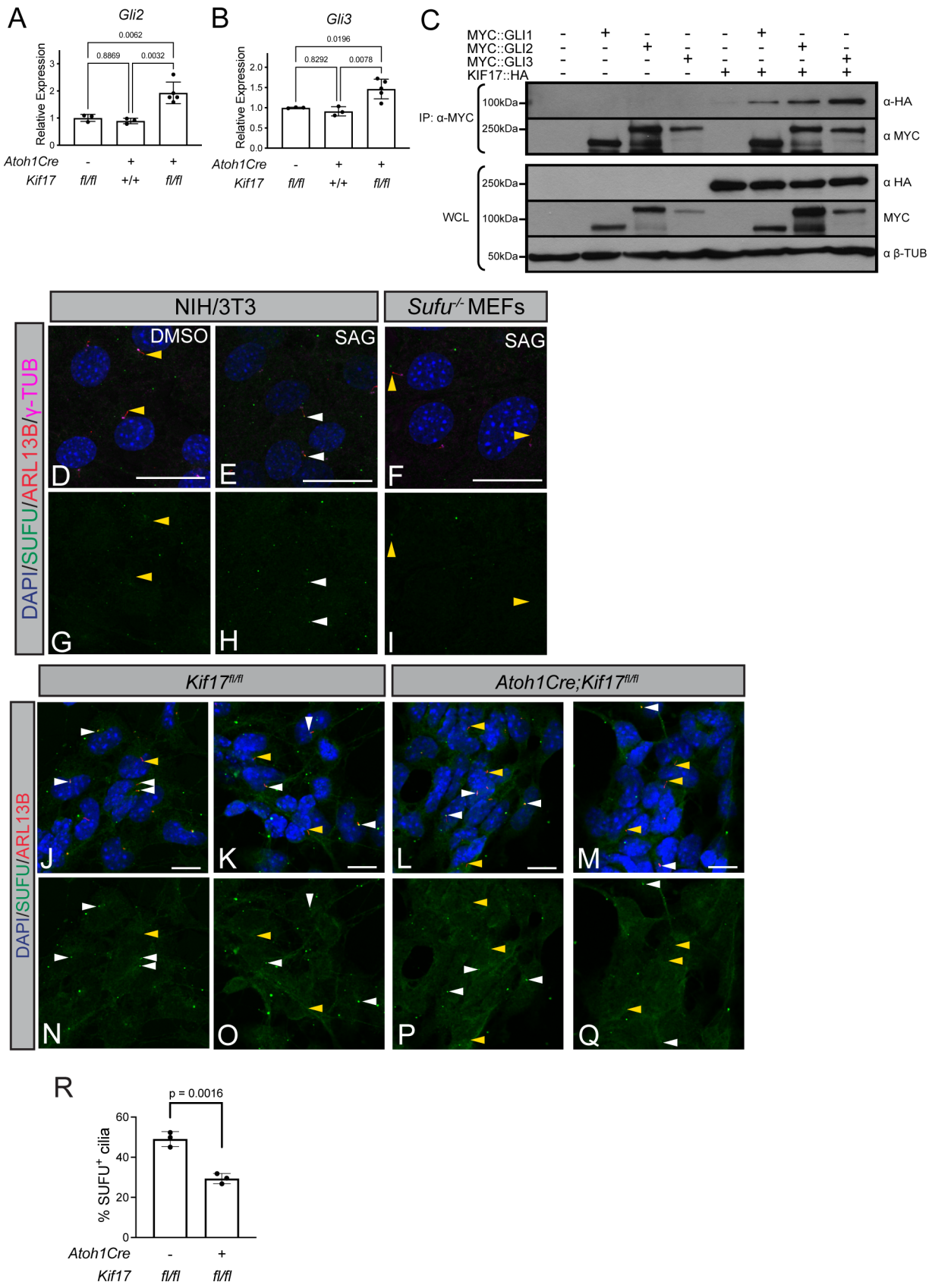
A
Gli2
0.0062
0.8869
0.0032
Relative Expression
Atoh1Cre - + +
Kif17 fl/fl +/+ fl/fl
B
Gli3
0.0196
0.8292
0.0078
Relative Expression
Atoh1Cre - + +
Kif17 fl/fl +/+ fl/fl
C
MYC::GLI1
MYC::GLI2
MYC::GLI3
KIF17::HA
IP: α-MYC
100kDa
250kDa
α-HA
α MYC
WCL
250kDa
100kDa
50kDa
α HA
MYC
α β-TUB
NIH/3T3
Sufu-/- MEFs
DMSO
SAG
SAG
DAPI/SUFU/ARL13B/γ-TUB
D
E
F
G
H
I
Kif17fl/fl
Atoh1Cre;Kif17fl/fl
DAPI/SUFU/ARL13B
J
K
L
M
N
O
P
Q
R
p = 0.0016
% SUFU+ cilia
Atoh1Cre - +
Kif17 fl/fl fl/fl

Figure 2.14 KIF17 can physically interact with GLI transcription factors, and reduction of SUFU^{+} cilia with *Kif17* deletion.

Relative expression of *Gli2* (A) and *Gli3* (B) measured by RT-qPCR in *Kif17$^{fl/fl}$*, *Atoh1Cre;Kif17$^{+/+}$* and *Atoh1Cre;Kif17$^{fl/fl}$* in P10 whole cerebella. (C) Immunoprecipitation of MYC:GLI1-3 from COS-7 cells co-expressing KIF17:HA. Immunoprecipitants (IP) and whole cell lysates (WCL) were subjected to SDS-PAGE and western blot analysis (IB) using antibodies directed against MYC (α-MYC) and HA (α-HA). Antibody detection of β-tubulin (α β-TUB) was used to confirm equal loading across lanes. The molecular weights (in kDa) of protein standards are indicated at the left of each blot. Antibody validation of SUFU antibody (green, D-I) in NIH/3T3 fibroblasts (D-E, G-H) and *Sufu$^{-/-}$* mouse embryonic fibroblasts (MEFs, F, I) treated with DMSO (vehicle) or Smo Agonist (SAG). Antibody detection of ARL13B (red) and γ-tubulin (γ-TUB, magenta) denote the axonemes and basal bodies of primary cilia, respectively; nuclei are identified with DAPI (blue). Scale bars (D-F), 25 μm. Yellow arrowheads denote cilia lacking SUFU, while white arrowheads signify SUFU^{+} cilia. Immunofluorescent analysis of SUFU localization (green, J-Q) in *Kif17$^{fl/fl}$* (J, K, N, O) and *Atoh1Cre;Kif17$^{fl/fl}$* (L, M, P, Q) CGNPs grown *in vitro* in the presence of SAG. Antibody detection of ARL13B (red) to visualize the axonemes of primary cilia; nuclei are identified with DAPI (blue). Scale bars (J-M), 10 μm. Yellow arrowheads denote cilia lacking SUFU, while white arrowheads signify SUFU^{+} cilia. Quantitation of the percentage of SUFU^{+} cilia (R) in *Kif17$^{fl/fl}$* and *Atoh1Cre;Kif17$^{fl/fl}$* CGNP cultures. Each dot represents an individual animal (A, B) or the average of 5 images in an independent CGNP culture (R). Data are means ± s.d. *P*-values were determined by a one way ANOVA (A, B) a two-tailed Student's *t*-test (R).

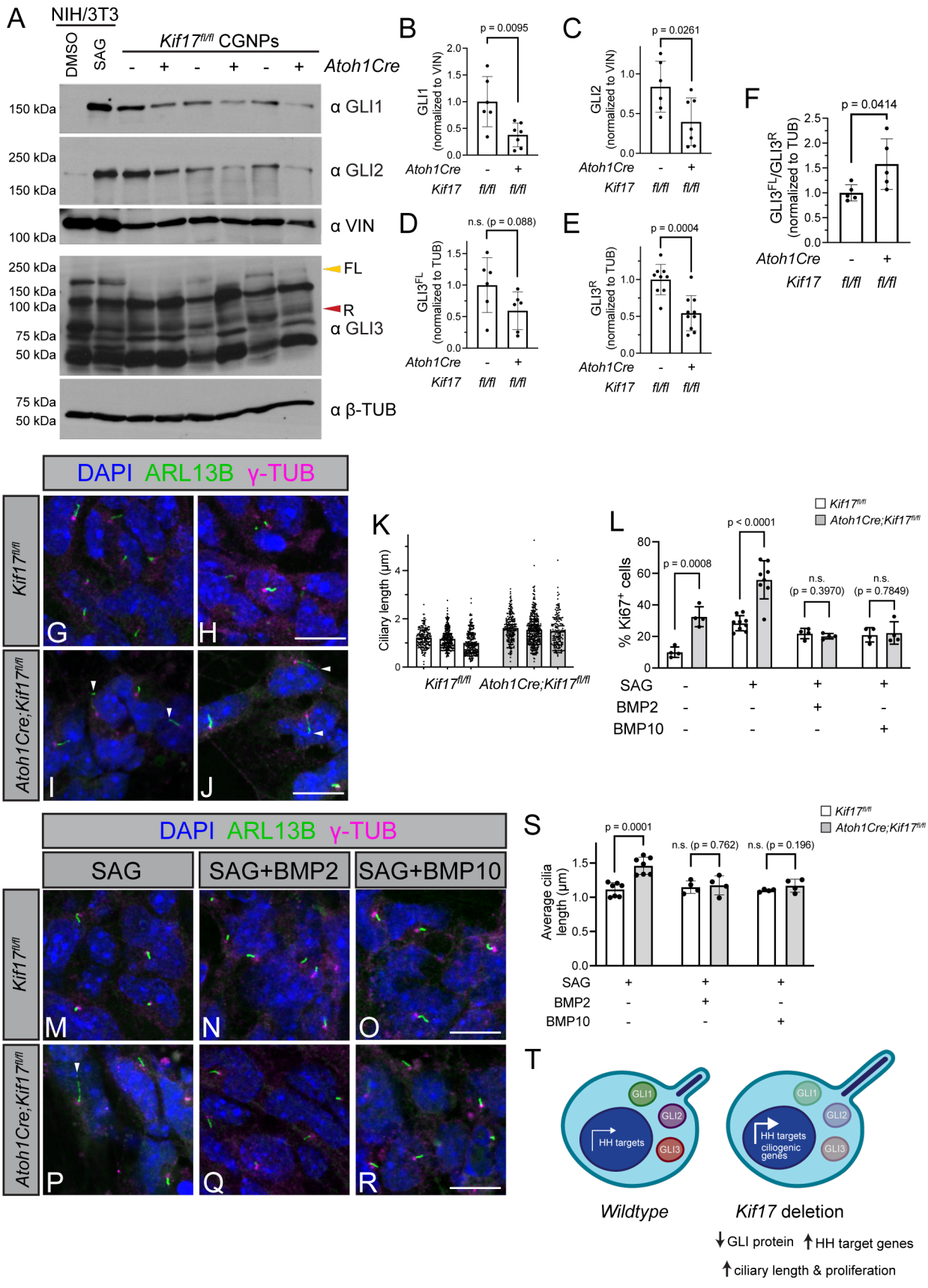
A
NIH/3T3
DMSO
SAG
Kif17fl/fl CGNPs
Atoh1Cre
150 kDa
α GLI1
250 kDa
150 kDa
α GLI2
100 kDa
α VIN
250 kDa
150 kDa
100 kDa
75 kDa
50 kDa
FL
R
α GLI3
75 kDa
50 kDa
α β-TUB
B
p = 0.0095
GLI1 (normalized to VIN)
C
p = 0.0261
GLI2 (normalized to VIN)
D
n.s. (p = 0.088)
GLI3FL (normalized to TUB)
E
p = 0.0004
GLI3R (normalized to TUB)
F
p = 0.0414
GLI3FL/GLI3R (normalized to TUB)
Kif17 fl/fl fl/fl
DAPI ARL13B γ-TUB
Kif17fl/fl
Atoh1Cre;Kif17fl/fl
G
H
I
J
K
Ciliary length (μm)
Kif17fl/fl
Atoh1Cre;Kif17fl/fl
L
Kif17fl/fl
Atoh1Cre;Kif17fl/fl
p = 0.0008
p < 0.0001
n.s. (p = 0.3970)
n.s. (p = 0.7849)
% Ki67+ cells
SAG
BMP2
BMP10
DAPI ARL13B γ-TUB
SAG
SAG+BMP2
SAG+BMP10
M
N
O
P
Q
R
S
p = 0.0001
n.s. (p = 0.762)
n.s. (p = 0.196)
Average cilia length (μm)
T
GLI1
GLI2
GLI3
HH targets
HH targets ciliogenic genes
Wildtype
Kif17 deletion
GLI protein
HH target genes
ciliary length & proliferation

Figure 2.15 CGNP-specific *Kif17* deletion results in reduced GLI protein, increased CGNP proliferation, and elongated primary cilia *in vitro.*

Western blot analysis (A) of GLI transcription factors (α GLI1, α GLI2, α GLI3) in NIH/3T3 cells and purified CGNPs isolated from *Kif17*$^{fl/fl}$ and *Atoh1Cre;Kif17*$^{fl/fl}$ littermates. Antibody detection of Vinculin (α VIN) confirmed equal loading across lanes for GLI1 and GLI2. Antibody detection of β-tubulin (α β-TUB) confirmed equal loading across lanes for GLI3. Yellow arrowhead denote full length GLI3 (FL, 180 kDa) red arrowhead indicate GLI3 repressor (R, 83 kDa). The molecular masses (in kDa) of protein standards are indicated at the left of each blot. Quantitation of GLI1 (B) and GLI2 (C) normalized to Vinculin. Levels of GLI3^{FL} (D) and GLI3^{R} (E) normalized to β-Tubulin. Ratio of GLI3^{FL} to GLI3^{R} (F) in *Kif17*$^{fl/fl}$ and *Atoh1Cre;Kif17*$^{fl/fl}$ CGNPs, normalized to β-tubulin. Visualization of primary cilia (G-J) *in vitro* from *Kif17*$^{fl/fl}$ (G-H) and *Atoh1Cre;Kif17*$^{fl/fl}$ (I-J) CGNP cultures treated with SAG. Antibody detection of ARL13B (green) and γ-tubulin (γ-TUB, magenta) denote the axonemes and basal bodies of primary cilia, respectively; nuclei are identified with DAPI (blue). Scale bars (H, J), 10 μm. Ciliary length (K) quantitation of CGNPs from three representative cultures of *Kif17*$^{fl/fl}$ and *Atoh1Cre;Kif17*$^{fl/fl}$ littermates. Each dot represents an individual cilium. Percentages of Ki67^{+} (L) cells in CGNP cultures from P8 *Kif17*$^{fl/fl}$ and *Atoh1Cre;Kif17*$^{fl/fl}$ littermates. Cells were treated with vehicle (DMSO) or SMO Agonist (SAG), with or without BMP2 or BMP10. Immunofluorescent detection of primary cilia *in vitro* from *Kif17*$^{fl/fl}$ (M-O) and *Atoh1Cre;Kif17*$^{fl/fl}$ (P-R) CGNP cultures treated with SAG and BMP ligands. Antibody detection of ARL13B (green) and γ-Tubulin (γ-TUB, magenta) label the axonemes and basal bodies of primary cilia; nuclei are identified with DAPI (blue). Scale bar (O, R), 10 μm. Average CGNP ciliary length (S) from *Kif17*$^{fl/fl}$ and *Atoh1Cre;Kif17*$^{fl/fl}$ littermates, where each dot represents the average length of an individual culture. Data are mean ± s.d. *P*-values were determined by a two-tailed Student's *t*-test. (T) Summary of CGNP-specific *Kif17* deletion on GLI proteins, CGNP proliferation and primary cilia length.

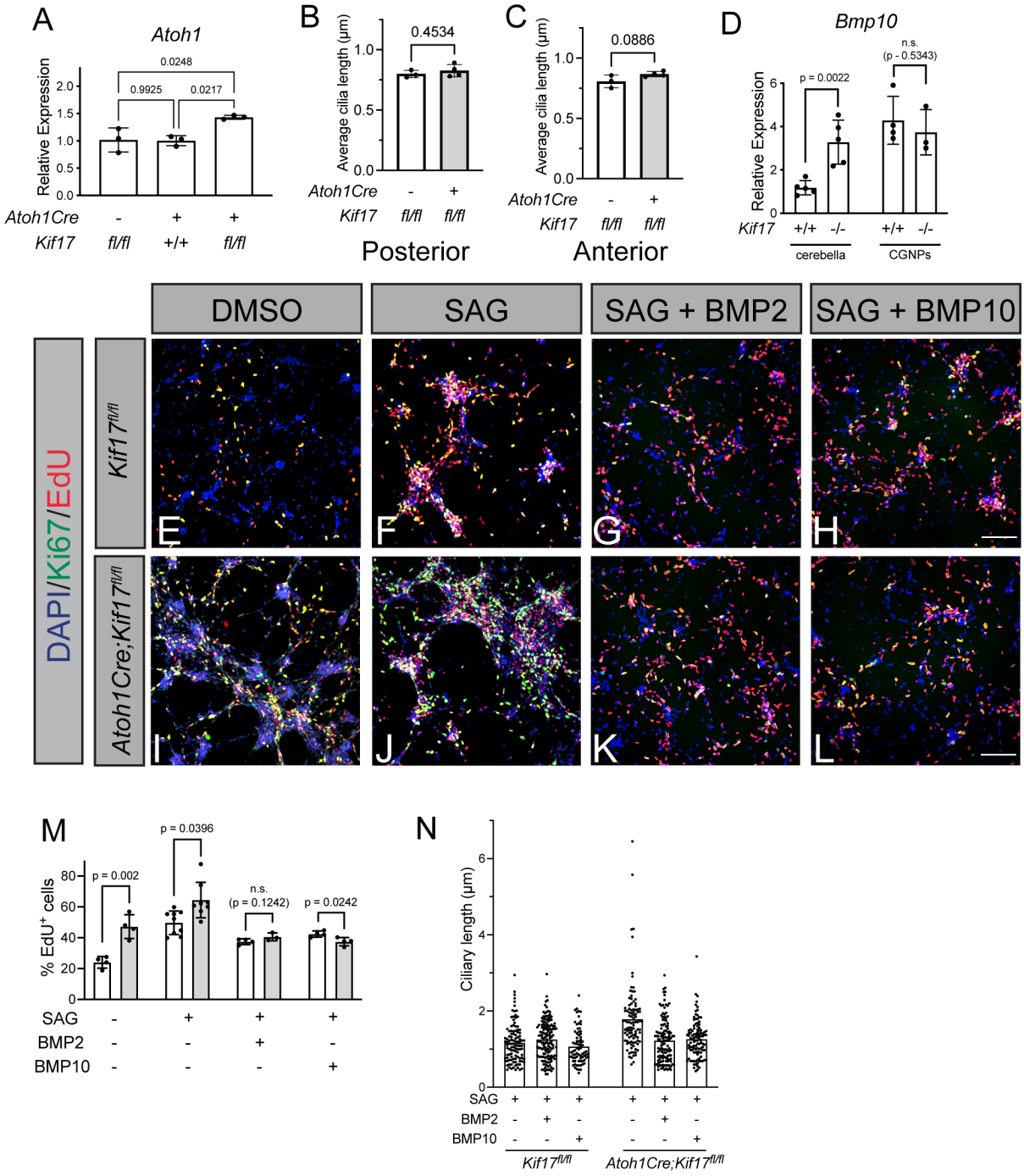

Figure 2.16 Figure S9: Deletion of *Kif17* results in increased CGNP proliferation *in vitro*, which can be attenuated with addition of BMP ligands.

Relative expression of *Atoh1* (A) measured by RT-qPCR in *Kif17*$^{fl/fl}$, *Atoh1Cre;Kif17*$^{+/+}$ and *Atoh1Cre;Kif17*$^{fl/fl}$ in P10 whole cerebella. Average ciliary length of CGNPs within the posterior (B) and anterior (C) lobes of *Kif17*$^{fl/fl}$ and *Atoh1Cre;Kif17*$^{fl/fl}$ at P10. Relative expression of

Bmp10 (D) by RT-qPCR in *Kif17*$^{+/+}$ and *Kif17*$^{-/-}$ P8-P10 whole cerebella and purified CGNPs. Immunofluorescent analysis of *in vitro* proliferation in CGNP cultures from P8 *Kif17*$^{fl/fl}$ (E-H) and *Atoh1Cre;Kif17*$^{fl/fl}$ (I-L) littermates. Nuclei were counterstained with DAPI (blue); Ki67 immunofluorescence (green) and EdU incorporation (red) were visualized in response to DMSO (E, I), SAG (F, J), SAG + BMP2 (G, K), or SAG + BMP10 (H, L) treatment. Scale bars (H, L), 100 μm. Percentage of EdU^{+} (M) cells in CGNP cultures from P8 *Kif17*$^{fl/fl}$ and *Atoh1Cre;Kif17*$^{fl/fl}$ littermates. Ciliary lengths (N) measured *in vitro* from CGNP cultures from *Kif17*$^{fl/fl}$ and *Atoh1Cre;Kif17*$^{fl/fl}$ littermates. Each dot represents an individual animal (A, B, D), the average of 5 images per animal (B, C), the average of 5 images per independent CGNP culture (M) or measurement of an individual cilium (N). Data are means ± s.d. *P*-values were determined by a one way ANOVA (A) or a two-tailed Student's *t*-test (B, C, D, M).

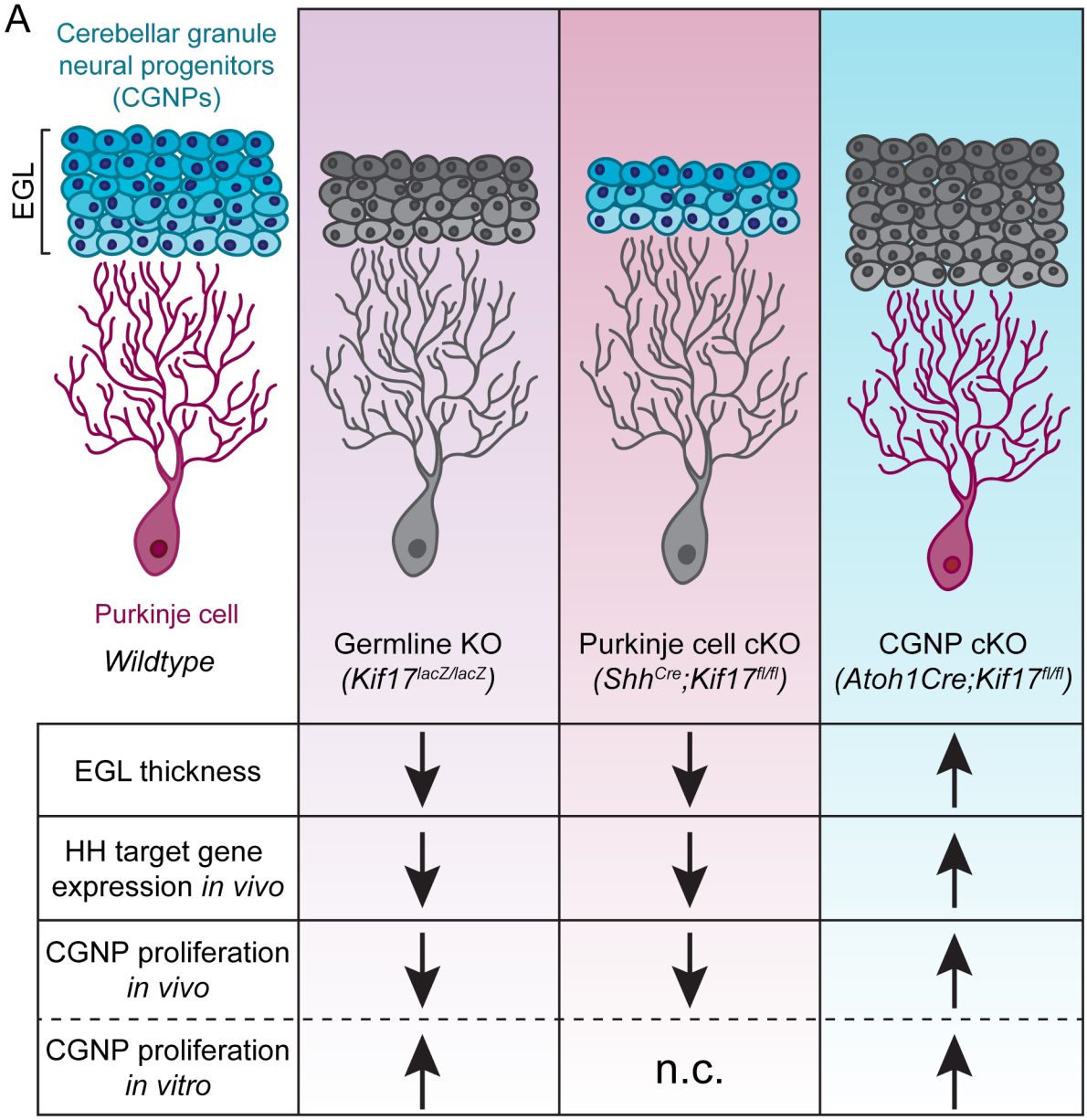

Figure 2.17 KIF17 has dual and opposing roles in HH signaling in the developing cerebella.

(A) Schematic demonstrating the consequences of KIF17 deletion on cerebellar development. Germline or Purkinje cell-specific *Kif17* deletion (magenta) results in a HH loss-of-function phenotype *in vivo*, while CGNP-specific *Kif17* deletion yields a HH gain-of-function phenotype (cyan). Notably, germline *Kif17* deletion results in increased CGNP proliferation *in vitro*, similar to CGNP-specific *Kif17* deletion both *in vivo* and *in vitro*.

2.10 References

Allen, B.L., Song, J.Y., Izzi, L., Althaus, I.W., Kang, J.S., Charron, F., Krauss, R.S., and McMahon, A.P. (2011). Overlapping roles and collective requirement for the coreceptors GAS1, CDO, and BOC in SHH pathway function. Dev Cell *20*, 775-787. 10.1016/j.devcel.2011.04.018.

Bangs, F., and Anderson, K.V. (2017). Primary Cilia and Mammalian Hedgehog Signaling. Cold Spring Harb Perspect Biol *9*. 10.1101/cshperspect.a028175.

Blaess, S., Stephen, D., and Joyner, A.L. (2008). Gli3 coordinates three-dimensional patterning and growth of the tectum and cerebellum by integrating Shh and Fgf8 signaling. Development *135*, 2093-2103. 10.1242/dev.015990.

Breunig, J.J., Sarkisian, M.R., Arellano, J.I., Morozov, Y.M., Ayoub, A.E., Sojitra, S., Wang, B., Flavell, R.A., Rakic, P., and Town, T. (2008). Primary cilia regulate hippocampal neurogenesis by mediating sonic hedgehog signaling. Proc Natl Acad Sci U S A *105*, 13127-13132. 10.1073/pnas.0804558105.

Bumcrot, D.A., Takada, R., and McMahon, A.P. (1995). Proteolytic processing yields two secreted forms of sonic hedgehog. Mol Cell Biol *15*, 2294-2303. 10.1128/MCB.15.4.2294.

Carpenter, B.S., Barry, R.L., Verhey, K.J., and Allen, B.L. (2015). The heterotrimeric kinesin-2 complex interacts with and regulates GLI protein function. J Cell Sci *128*, 1034-1050. 10.1242/jcs.162552.

Chang, C.H., Zanini, M., Shirvani, H., Cheng, J.S., Yu, H., Feng, C.H., Mercier, A.L., Hung, S.Y., Forget, A., Wang, C.H., et al. (2019). Atoh1 Controls Primary Cilia Formation to Allow for SHH-Triggered Granule Neuron Progenitor Proliferation. Dev Cell *48*, 184-199 e185. 10.1016/j.devcel.2018.12.017.

Cheng, F.Y., Fleming, J.T., and Chiang, C. (2018). Bergmann glial Sonic hedgehog signaling activity is required for proper cerebellar cortical expansion and architecture. Dev Biol *440*, 152-166. 10.1016/j.ydbio.2018.05.015.

Chennathukuzhi, V., Morales, C.R., El-Alfy, M., and Hecht, N.B. (2003). The kinesin KIF17b and RNA-binding protein TB-RBP transport specific cAMP-responsive element modulator-regulated mRNAs in male germ cells. Proc Natl Acad Sci U S A *100*, 15566-15571. 10.1073/pnas.2536695100.

Chu, T., Chiu, M., Zhang, E., and Kunes, S. (2006). A C-terminal motif targets Hedgehog to axons, coordinating assembly of the Drosophila eye and brain. Dev Cell *10*, 635-646. 10.1016/j.devcel.2006.03.003.

Clark, A.M., Garland, K.K., and Russell, L.D. (2000). Desert hedgehog (Dhh) gene is required in the mouse testis for formation of adult-type Leydig cells and normal development of peritubular cells and seminiferous tubules. Biol Reprod *63*, 1825-1838. 10.1095/biolreprod63.6.1825.

Corrales, J.D., Blaess, S., Mahoney, E.M., and Joyner, A.L. (2006). The level of sonic hedgehog signaling regulates the complexity of cerebellar foliation. Development *133*, 1811-1821. 10.1242/dev.02351.

Corrales, J.D., Rocco, G.L., Blaess, S., Guo, Q., and Joyner, A.L. (2004). Spatial pattern of sonic hedgehog signaling through Gli genes during cerebellum development. Development *131*, 5581-5590. 10.1242/dev.01438.

Cruz, C., Ribes, V., Kutejova, E., Cayuso, J., Lawson, V., Norris, D., Stevens, J., Davey, M., Blight, K., Bangs, F., et al. (2010). Foxj1 regulates floor plate cilia architecture and modifies the response of cells to sonic hedgehog signalling. Development *137*, 4271-4282. 10.1242/dev.051714.

Dahmane, N., and Ruiz i Altaba, A. (1999). Sonic hedgehog regulates the growth and patterning of the cerebellum. Development *126*, 3089-3100. 10.1242/dev.126.14.3089.

Ding, Q., Fukami, S., Meng, X., Nishizaki, Y., Zhang, X., Sasaki, H., Dlugosz, A., Nakafuku, M., and Hui, C. (1999). Mouse suppressor of fused is a negative regulator of sonic hedgehog signaling and alters the subcellular distribution of Gli1. Curr Biol *9*, 1119-1122. 10.1016/s0960-9822(99)80482-5.

Dishinger, J.F., Kee, H.L., Jenkins, P.M., Fan, S., Hurd, T.W., Hammond, J.W., Truong, Y.N., Margolis, B., Martens, J.R., and Verhey, K.J. (2010). Ciliary entry of the kinesin-2 motor KIF17 is regulated by importin-beta2 and RanGTP. Nat Cell Biol *12*, 703-710. 10.1038/ncb2073.

Endoh-Yamagami, S., Evangelista, M., Wilson, D., Wen, X., Theunissen, J.W., Phamluong, K., Davis, M., Scales, S.J., Solloway, M.J., de Sauvage, F.J., and Peterson, A.S. (2009). The mammalian Cos2 homolog Kif7 plays an essential role in modulating Hh signal transduction during development. Curr Biol *19*, 1320-1326. 10.1016/j.cub.2009.06.046.

Engelke, M.F., Waas, B., Kearns, S.E., Suber, A., Boss, A., Allen, B.L., and Verhey, K.J. (2019). Acute Inhibition of Heterotrimeric Kinesin-2 Function Reveals Mechanisms of Intraflagellar Transport in Mammalian Cilia. Curr Biol *29*, 1137-1148 e1134. 10.1016/j.cub.2019.02.043.

Hall, E.T., Dillard, M.E., Stewart, D.P., Zhang, Y., Wagner, B., Levine, R.M., Pruett-Miller, S.M., Sykes, A., Temirov, J., Cheney, R.E., et al. (2021). Cytoneme delivery of Sonic Hedgehog from ligand-producing cells requires Myosin 10 and a Dispatched-BOC/CDON co-receptor complex. Elife *10*. 10.7554/eLife.61432.

Han, Y.G., Spassky, N., Romaguera-Ros, M., Garcia-Verdugo, J.M., Aguilar, A., Schneider-Maunoury, S., and Alvarez-Buylla, A. (2008). Hedgehog signaling and primary cilia are required for the formation of adult neural stem cells. Nat Neurosci *11*, 277-284. 10.1038/nn2059.

Haque, F., Freniere, C., Ye, Q., Mani, N., Wilson-Kubalek, E.M., Ku, P.I., Milligan, R.A., and Subramanian, R. (2022). Cytoskeletal regulation of a transcription factor by DNA mimicry via coiled-coil interactions. Nat Cell Biol *24*, 1088-1098. 10.1038/s41556-022-00935-7.

Harfe, B.D., Scherz, P.J., Nissim, S., Tian, H., McMahon, A.P., and Tabin, C.J. (2004). Evidence for an expansion-based temporal Shh gradient in specifying vertebrate digit identities. Cell *118*, 517-528. 10.1016/j.cell.2004.07.024.

He, M., Agbu, S., and Anderson, K.V. (2017). Microtubule Motors Drive Hedgehog Signaling in Primary Cilia. Trends Cell Biol *27*, 110-125. 10.1016/j.tcb.2016.09.010.

He, M., Subramanian, R., Bangs, F., Omelchenko, T., Liem, K.F., Jr., Kapoor, T.M., and Anderson, K.V. (2014). The kinesin-4 protein Kif7 regulates mammalian Hedgehog signalling by organizing the cilium tip compartment. Nat Cell Biol *16*, 663-672. 10.1038/ncb2988.

Han, Y., Xiong, Y., Shi, X., Wu, J., Zhao, Y., and Jiang, J. (2017). Regulation of Gli ciliary localization and Hedgehog signaling by the PY-NLS/karyopherin-beta2 nuclear import system. PLoS Biol *15*, e2002063. 10.1371/journal.pbio.2002063.

Hor, C.H.H., Lo, J.C.W., Cham, A.L.S., Leong, W.Y., and Goh, E.L.K. (2021). Multifaceted Functions of Rab23 on Primary Cilium-Mediated and Hedgehog Signaling-Mediated Cerebellar Granule Cell Proliferation. J Neurosci *41*, 6850-6863. 10.1523/JNEUROSCI.3005-20.2021.

Hirokawa, N., Noda, Y., Tanaka, Y., and Niwa, S. (2009). Kinesin superfamily motor proteins and intracellular transport. Nat Rev Mol Cell Biol *10*, 682-696. 10.1038/nrm2774.

Hollway, G.E., Maule, J., Gautier, P., Evans, T.M., Keenan, D.G., Lohs, C., Fischer, D., Wicking, C., and Currie, P.D. (2006). Scube2 mediates Hedgehog signalling in the zebrafish embryo. Dev Biol *294*, 104-118. 10.1016/j.ydbio.2006.02.032.

Huangfu, D., and Anderson, K.V. (2005). Cilia and Hedgehog responsiveness in the mouse. Proc Natl Acad Sci U S A *102*, 11325-11330. 10.1073/pnas.0505328102.

Huangfu, D., Liu, A., Rakeman, A.S., Murcia, N.S., Niswander, L., and Anderson, K.V. (2003). Hedgehog signalling in the mouse requires intraflagellar transport proteins. Nature *426*, 83-87. 10.1038/nature02061.

Insinna, C., Pathak, N., Perkins, B., Drummond, I., and Besharse, J.C. (2008). The homodimeric kinesin, Kif17, is essential for vertebrate photoreceptor sensory outer segment development. Dev Biol *316*, 160-170. 10.1016/j.ydbio.2008.01.025.

Izzi, L., Levesque, M., Morin, S., Laniel, D., Wilkes, B.C., Mille, F., Krauss, R.S., McMahon, A.P., Allen, B.L., and Charron, F. (2011). Boc and Gas1 each form distinct Shh receptor complexes with Ptch1 and are required for Shh-mediated cell proliferation. Dev Cell *20*, 788-801. 10.1016/j.devcel.2011.04.017.

Jiwani, T., Kim, J.J., and Rosenblum, N.D. (2020). Suppressor of fused controls cerebellum granule cell proliferation by suppressing Fgf8 and spatially regulating Gli proteins. Development *147*. 10.1242/dev.170274.

Kawakami, A., Nojima, Y., Toyoda, A., Takahoko, M., Satoh, M., Tanaka, H., Wada, H., Masai, I., Terasaki, H., Sakaki, Y., et al. (2005). The zebrafish-secreted matrix protein you/scube2 is implicated in long-range regulation of hedgehog signaling. Curr Biol *15*, 480-488. 10.1016/j.cub.2005.02.018.

Kimmins, S., Kotaja, N., Fienga, G., Kolthur, U.S., Brancorsini, S., Hogeveen, K., Monaco, L., and Sassone-Corsi, P. (2004). A specific programme of gene transcription in male germ cells. Reprod Biomed Online *8*, 496-500. 10.1016/s1472-6483(10)61094-2.

Kotaja, N., Lin, H., Parvinen, M., and Sassone-Corsi, P. (2006). Interplay of PIWI/Argonaute protein MIWI and kinesin KIF17b in chromatoid bodies of male germ cells. J Cell Sci *119*, 2819-2825. 10.1242/jcs.03022.

Lee, H.Y., Greene, L.A., Mason, C.A., and Manzini, M.C. (2009). Isolation and culture of post-natal mouse cerebellar granule neuron progenitor cells and neurons. J Vis Exp. 10.3791/990.

Lee, J.J., Ekker, S.C., von Kessler, D.P., Porter, J.A., Sun, B.I., and Beachy, P.A. (1994). Autoproteolysis in hedgehog protein biogenesis. Science *266*, 1528-1537. 10.1126/science.7985023.

Lewis, P.M., Gritli-Linde, A., Smeyne, R., Kottmann, A., and McMahon, A.P. (2004). Sonic hedgehog signaling is required for expansion of granule neuron precursors and patterning of the mouse cerebellum. Dev Biol *270*, 393-410. 10.1016/j.ydbio.2004.03.007.

Lewis, T.R., Kundinger, S.R., Link, B.A., Insinna, C., and Besharse, J.C. (2018). Kif17 phosphorylation regulates photoreceptor outer segment turnover. BMC Cell Biol *19*, 25. 10.1186/s12860-018-0177-9.

Lewis, T.R., Kundinger, S.R., Pavlovich, A.L., Bostrom, J.R., Link, B.A., and Besharse, J.C. (2017). Cos2/Kif7 and Osm-3/Kif17 regulate onset of outer segment development in zebrafish photoreceptors through distinct mechanisms. Dev Biol *425*, 176-190. 10.1016/j.ydbio.2017.03.019.

Lin, Y.C., Roffler, S.R., Yan, Y.T., and Yang, R.B. (2015). Disruption of Scube2 Impairs Endochondral Bone Formation. J Bone Miner Res *30*, 1255-1267. 10.1002/jbmr.2451.

Liu, Y., Du, S.Y., Ding, M., Dou, X., Zhang, F.F., Wu, Z.Y., Qian, S.W., Zhang, W., Tang, Q.Q., and Xu, C.J. (2017). The BMP4-Smad signaling pathway regulates hyperandrogenism development in a female mouse model. J Biol Chem *292*, 11740-11750. 10.1074/jbc.M117.781369.

Macho, B., Brancorsini, S., Fimia, G.M., Setou, M., Hirokawa, N., and Sassone-Corsi, P. (2002). CREM-dependent transcription in male germ cells controlled by a kinesin. Science *298*, 2388-2390. 10.1126/science.1077265.

Machold, R., Hayashi, S., Rutlin, M., Muzumdar, M.D., Nery, S., Corbin, J.G., Gritli-Linde, A., Dellovade, T., Porter, J.A., Rubin, L.L., et al. (2003). Sonic hedgehog is required for progenitor cell maintenance in telencephalic stem cell niches. Neuron *39*, 937-950. 10.1016/s0896-6273(03)00561-0.

Madison, B.B., Braunstein, K., Kuizon, E., Portman, K., Qiao, X.T., and Gumucio, D.L. (2005). Epithelial hedgehog signals pattern the intestinal crypt-villus axis. Development *132*, 279-289. 10.1242/dev.01576.

Matei, V., Pauley, S., Kaing, S., Rowitch, D., Beisel, K.W., Morris, K., Feng, F., Jones, K., Lee, J., and Fritzsch, B. (2005). Smaller inner ear sensory epithelia in Neurog 1 null mice are related to earlier hair cell cycle exit. Dev Dyn *234*, 633-650. 10.1002/dvdy.20551.

Mille, F., Tamayo-Orrego, L., Levesque, M., Remke, M., Korshunov, A., Cardin, J., Bouchard, N., Izzi, L., Kool, M., Northcott, P.A., et al. (2014). The Shh receptor Boc promotes progression of early medulloblastoma to advanced tumors. Dev Cell *31*, 34-47. 10.1016/j.devcel.2014.08.010.

Nonaka, S., Tanaka, Y., Okada, Y., Takeda, S., Harada, A., Kanai, Y., Kido, M., and Hirokawa, N. (1998). Randomization of left-right asymmetry due to loss of nodal cilia generating leftward flow of extraembryonic fluid in mice lacking KIF3B motor protein. Cell *95*, 829-837. 10.1016/s0092-8674(00)81705-5.

Peterson, K.A., Nishi, Y., Ma, W., Vedenko, A., Shokri, L., Zhang, X., McFarlane, M., Baizabal, J.M., Junker, J.P., van Oudenaarden, A., et al. (2012). Neural-specific Sox2 input and differential Gli-binding affinity provide context and positional information in Shh-directed neural patterning. Genes Dev *26*, 2802-2816. 10.1101/gad.207142.112.

Petrov, K., Wierbowski, B.M., and Salic, A. (2017). Sending and Receiving Hedgehog Signals. Annu Rev Cell Dev Biol *33*, 145-168. 10.1146/annurev-cellbio-100616-060847.

Porter, J.A., von Kessler, D.P., Ekker, S.C., Young, K.E., Lee, J.J., Moses, K., and Beachy, P.A. (1995). The product of hedgehog autoproteolytic cleavage active in local and long-range signalling. Nature *374*, 363-366. 10.1038/374363a0.

Rios, I., Alvarez-Rodriguez, R., Marti, E., and Pons, S. (2004). Bmp2 antagonizes sonic hedgehog-mediated proliferation of cerebellar granule neurones through Smad5 signalling. Development *131*, 3159-3168. 10.1242/dev.01188.

Saade, M., Irla, M., Govin, J., Victorero, G., Samson, M., and Nguyen, C. (2007). Dynamic distribution of Spatial during mouse spermatogenesis and its interaction with the kinesin KIF17b. Exp Cell Res *313*, 614-626. 10.1016/j.yexcr.2006.11.011.

Santos, N., and Reiter, J.F. (2014). A central region of Gli2 regulates its localization to the primary cilium and transcriptional activity. J Cell Sci *127*, 1500-1510. 10.1242/jcs.139253.

Scales, M.K., Velez-Delgado, A., Steele, N.G., Schrader, H.E., Stabnick, A.M., Yan, W., Mercado Soto, N.M., Nwosu, Z.C., Johnson, C., Zhang, Y., et al. (2022). Combinatorial Gli activity directs immune infiltration and tumor growth in pancreatic cancer. PLoS Genet *18*, e1010315. 10.1371/journal.pgen.1010315.

Shimokawa, T., Tostar, U., Lauth, M., Palaniswamy, R., Kasper, M., Toftgard, R., and Zaphiropoulos, P.G. (2008). Novel human glioma-associated oncogene 1 (GLI1) splice variants reveal distinct mechanisms in the terminal transduction of the hedgehog signal. J Biol Chem *283*, 14345-14354. 10.1074/jbc.M800299200.

Signor, D., Wedaman, K.P., Rose, L.S., and Scholey, J.M. (1999). Two heteromeric kinesin complexes in chemosensory neurons and sensory cilia of Caenorhabditis elegans. Mol Biol Cell *10*, 345-360. 10.1091/mbc.10.2.345.

Snow, J.J., Ou, G., Gunnarson, A.L., Walker, M.R., Zhou, H.M., Brust-Mascher, I., and Scholey, J.M. (2004). Two anterograde intraflagellar transport motors cooperate to build sensory cilia on C. elegans neurons. Nat Cell Biol *6*, 1109-1113. 10.1038/ncb1186.

Spassky, N., Han, Y.G., Aguilar, A., Strehl, L., Besse, L., Laclef, C., Ros, M.R., Garcia-Verdugo, J.M., and Alvarez-Buylla, A. (2008). Primary cilia are required for cerebellar development and Shh-dependent expansion of progenitor pool. Dev Biol *317*, 246-259. 10.1016/j.ydbio.2008.02.026.

Takeda, S., Yonekawa, Y., Tanaka, Y., Okada, Y., Nonaka, S., and Hirokawa, N. (1999). Left-right asymmetry and kinesin superfamily protein KIF3A: new insights in determination of laterality and mesoderm induction by kif3A-/- mice analysis. J Cell Biol *145*, 825-836. 10.1083/jcb.145.4.825.

Trifonov, S., Yamashita, Y., Kase, M., Maruyama, M., and Sugimoto, T. (2016). Overview and assessment of the histochemical methods and reagents for the detection of beta-galactosidase activity in transgenic animals. Anat Sci Int *91*, 56-67. 10.1007/s12565-015-0300-3.

Tukachinsky, H., Lopez, L.V., and Salic, A. (2010). A mechanism for vertebrate Hedgehog signaling: recruitment to cilia and dissociation of SuFu-Gli protein complexes. J Cell Biol *191*, 415-428. 10.1083/jcb.201004108.

Tuson, M., He, M., and Anderson, K.V. (2011). Protein kinase A acts at the basal body of the primary cilium to prevent Gli2 activation and ventralization of the mouse neural tube. Development *138*, 4921-4930. 10.1242/dev.070805.

Wang, S., Tanaka, Y., Xu, Y., Takeda, S., and Hirokawa, N. (2022). KIF3B promotes a PI3K signaling gradient causing changes in a Shh protein gradient and suppressing polydactyly in mice. Dev Cell *57*, 2273-2289 e2211. 10.1016/j.devcel.2022.09.007.

Wechsler-Reya, R.J., and Scott, M.P. (1999). Control of neuronal precursor proliferation in the cerebellum by Sonic Hedgehog. Neuron *22*, 103-114. 10.1016/s0896-6273(00)80682-0.

Wen, X., Lai, C.K., Evangelista, M., Hongo, J.A., de Sauvage, F.J., and Scales, S.J. (2010). Kinetics of hedgehog-dependent full-length Gli3 accumulation in primary cilia and subsequent degradation. Mol Cell Biol *30*, 1910-1922. 10.1128/MCB.01089-09.

Wu, Y., Wang, C., Sun, H., LeRoith, D., and Yakar, S. (2009). High-efficient FLPo deleter mice in C57BL/6J background. PLoS One *4*, e8054. 10.1371/journal.pone.0008054.

Yang, Z., Roberts, E.A., and Goldstein, L.S. (2001). Functional analysis of mouse kinesin motor Kif3C. Mol Cell Biol *21*, 5306-5311. 10.1128/MCB.21.16.5306-5311.2001.

Yin, X., Feng, X., Takei, Y., and Hirokawa, N. (2012). Regulation of NMDA receptor transport: a KIF17-cargo binding/releasing underlies synaptic plasticity and memory in vivo. J Neurosci *32*, 5486-5499. 10.1523/JNEUROSCI.0718-12.2012.

Yin, X., Takei, Y., Kido, M.A., and Hirokawa, N. (2011). Molecular motor KIF17 is fundamental for memory and learning via differential support of synaptic NR2A/2B levels. Neuron *70*, 310-325. 10.1016/j.neuron.2011.02.049.

Zhao, C., Omori, Y., Brodowska, K., Kovach, P., and Malicki, J. (2012). Kinesin-2 family in vertebrate ciliogenesis. Proc Natl Acad Sci U S A *109*, 2388-2393. 10.1073/pnas.1116035109.

Chapter 3 KIF3C is Required for Cerebellar Development

3.1 Abstract

The heterodimeric kinesin-2 motor complex, consisting of KIF3A and KIF3B, is required for ciliogenesis in mice– loss of this motor complex results in cerebellar hypoplasia due to reduced HH-dependent CGNP proliferation. We recently identified dual and opposing roles for the accessory kinesin-2 motor, KIF17, within SHH-producing Purkinje cells and HH-responsive CGNPs. Here, we investigated the contribution of the remaining kinesin-2 motor, KIF3C, to cerebellar development. Germline *Kif3c* deletion does not affect embryonic development or gross cerebellar morphology in adult mice (Yang *et al*., 2001). However, examination of these mice during cerebellar development reveals cerebellar hypoplasia due to reduced CGNP proliferation. While decreased CGNP proliferation is often associated with reduced Hedgehog (HH) signaling, we did not detect a change in the levels of HH signaling in *Kif3c*$^{-/-}$ cerebella. Instead, we observed altered Bergmann glia density and localization in *Kif3c* mutants, which correlates with *Hes1* downregulation and reduced Notch signaling. These data suggest that KIF3C is required for proper cerebellar development in a HH-independent manner.

3.2 Introduction

The postnatal expansion of the cerebellum is dependent on several mitogenic pathways. Sonic Hedgehog, SHH, induces proliferation of cerebellar granule neurons (CGNPs), which give

rise to cerebellar granule neurons, the most abundant type of neuron in the brain (Dahmane and Ruiz i Altaba, 1999; Wechsler-Reya and Scott, 1999). *Shh* deletion results in reduced proliferation and cerebellar hypoplasia (Lewis *et al*., 2004). Additionally, the loss of other essential HH pathway components, such as *Gli2*, *Gas1* or *Boc*, negatively impacts CGNP proliferation and cerebellar size (Corrales *et al*., 2006; Izzi *et al*., 2011). Another signaling pathway required for proper cerebellar development is Notch signaling (Adachi et al., 2021; Hiraoka et al., 2013; Komine et al., 2007; Solecki *et al*., 2001; Weller et al., 2006). Stimulation of the Notch pathway with JAG1 induces proliferation and inhibits differentiation of CGNPs (Solecki *et al*., 2001). Consistently, deletion of Notch pathway components, such as *Jag1*, *Notch1*, *Notch2* or *Dll-1*, results in CGNP migration defects and abnormal localization of Bergmann glia, which undergo apoptosis (Adachi *et al*., 2021; Hiraoka *et al*., 2013; Komine *et al*., 2007; Weller *et al*., 2006).

Intracellular transport is an important aspect of cell signaling. Receptors, transcription factors, or other essential pathway components must be trafficked to their proper localization to respond appropriately to morphogens during development. Transport of cargo along microtubules is accomplished through kinesin and dynein motors. Kinesin-2 motors regulate Hedgehog (HH) signaling [(Huangfu *et al*., 2003; Spassky *et al*., 2008), Chapter 2]. The kinesin-2 family consists of three motor complexes: heterodimeric KIF3A/KIF3B, homodimeric KIF17 and heterodimeric KIF3A/KIF3C [reviewed in (Hirokawa *et al*., 2009)]. Heterodimeric KIF3A/KIF3B is well known for its role in ciliogenesis and HH signaling during embryogenesis (Engelke *et al*., 2019; Huangfu *et al*., 2003; Nonaka *et al*., 1998; Takeda *et al*., 1999). Further, KIF3A/KIF3B physically interact with and regulate GLI proteins, transcriptional effectors of the HH pathway (Carpenter *et al*., 2015). Recently, homodimeric KIF17 has been implicated in the regulation of HH signaling both

at the level of SHH ligand production and release in HH-producing Purkinje cells and at the level of GLI processing in HH-responsive CGNPs in the developing cerebellum.

The KIF3A/KIF3C motor complex has not been investigated in the context of HH signaling or cerebellar development. Unlike other Kinesin-2 family members, KIF3C loss does not result in ciliary phenotypes, and *Kif3c* deletion is well tolerated across multiple model organisms (Jimeno *et al*., 2006; Yang *et al*., 2001; Zhao *et al*., 2012). However, *Kif3c* mutant mice display defects in neuronal regeneration (Gumy *et al*., 2013). Specifically, growth cones of *Kif3c*$^{-/-}$ neurons display stable, overgrown, and looped microtubules that impair regeneration (Gumy *et al*., 2013). Given the roles of other kinesin-2 motors in HH-dependent cerebellar development, we investigated the contribution of KIF3C in HH signaling within the developing cerebellum.

Here we find that *Kif3c* is widely expressed in the developing cerebellum, including within CGNPs, Bergmann glia, Purkinje cells and CGNs. Germline *Kif3c* deletion results in cerebellar hypoplasia and reduced body size. We observe reduced CGNP proliferation in *Kif3c*$^{-/-}$ mice, but unexpectedly, HH signaling is not affected. Instead, *Hes1* downregulation and changes to Bergmann glia density and localization in *Kif3c* mutant cerebella suggests KIF3C has a role in regulating Notch signaling in the developing cerebellum. Altogether, these data suggest a novel, HH-independent role for KIF3C in cerebellar development.

3.3 Results

3.3.1 Kif3c is ubiquitously expressed in the developing cerebella and is required for proper cerebellar development.

To investigate a potential role for *Kif3c* in cerebellar development, *Kif3c* mutant mice carrying a deletion of exon 1 were acquired and maintained on a C57BL/6J genetic background

(Figure 3.1A). Consistent with the literature and similar to *Kif17*, *Kif3c*$^{-/-}$ mice are viable and fertile (Yang *et al*., 2001). To determine if *Kif3c* is expressed in the developing cerebellum, RT-qPCR was performed on postnatal day 10 (P10) *Kif3c*$^{+/+}$ and *Kif3c*$^{-/-}$ cerebella (Figure 3.1B). Importantly, *Kif3c* transcript was detected in *Kif3c*$^{+/+}$ cerebella not in *Kif3c*$^{-/-}$ cerebella. Whole-mount *in situ* hybridization of *Kif3c* was performed on P10 *Kif3c*$^{+/+}$ and *Kif3c*$^{-/-}$ cerebella (Figure 3.1C-D). Distinct from *Kif17*, *Kif3c* appears to be uniformly expressed across the lobes of the cerebellum and within all cell layers of the cerebellum (Figure 3.1C-D). To determine which cell populations express *Kif3c*, fluorescence *in situ* hybridization was performed in anterior lobes (Figure 3.1E-P) and posterior lobes (Figure 3.2A-L) of *Kif3c*$^{+/-}$ and *Kif3c*$^{-/-}$ P10 cerebella. For analysis, we examined mid-sagittal cerebellar sections, where lobes I-III were considered anterior, while lobes VI-VIII were considered posterior (Figure 2.1H-I). In both anterior and posterior lobes, *Kif3c* puncta were observed in CGNPs (Figure 3.1E-H, Figure 3.2A-D), surrounding Purkinje cells and Bergmann glia (Figure 3.1I-L, Figure 3.2E-H) and within mature CGNs (Figure 3.1M-P, Figure 3.2I-L). These data suggest that *Kif3c* is expressed ubiquitously in the developing cerebellum.

Quantitation of cortical (Figure 3.2M) and cerebellar (Figure 3.2N) weights revealed *Kif3c*$^{-/-}$ animals display a significant reduction in cerebellar size when normalized to cortical weight (Figure 3.2O), suggesting a contribution of *Kif3c* to cerebellar development. Additionally, *Kif3c*$^{-/-}$ mice display reduced body weight compared to *Kif3c*$^{+/+}$ littermates at P10 (Figure 3.2P). Analysis of body weights from postnatal day 7 to 43 (Figure 3.2Q) revealed *Kif3c* deletion results in reduced body size during the first three weeks of life. Importantly, the difference between *Kif3c*$^{+/+}$ and *Kif3c*$^{-/-}$ body sizes is not significant by 6 weeks of age, distinct from HH loss- or gain-of-function animals, which maintain significant differences during adulthood (Goodrich *et al*., 1997; Zhang et

al., 2015). These data demonstrate that *Kif3c* is expressed ubiquitously in the developing cerebellum and that *Kif3c* deletion disrupts normal cerebellar development.

3.3.2 Kif3c deletion results in reduced CGNP proliferation but does not alter HH pathway activity.

To investigate which cell layers were affected by *Kif3c* deletion, the length of Purkinje cell (PC) dendrites and thickness of the external granule layer (EGL; where CGNPs reside) were measured at P10 in the anterior (Figure 3.3A-B) and posterior lobes (Figure 3.3C-D). No differences were noted in Purkinje cell dendrite length compared to *Kif3c*$^{+/+}$ mice in either anterior or posterior lobes (Figure 3.3A, C). However, *Kif3c*$^{-/-}$ cerebella have a significant reduction of EGL thickness in both regions (Figure 3.3B, D). In other studies, (Izzi *et al*., 2011) and the previous chapter, reduced EGL thickness was associated with decreased CGNP proliferation, which was examined in *Kif3c*$^{+/+}$ and *Kif3c*$^{-/-}$ littermates (Figure 3.3E-P). In the anterior (Figure 3.3E-J) and posterior (Figure 3.3K-P) lobes, *Kif3c*$^{-/-}$ cerebella display a decrease in proliferating CGNPs. Further, expression of the proliferative CGNP marker, *Atoh1*, measured by RT-qPCR, is significantly reduced in *Kif3c*$^{-/-}$ P10 cerebella (Figure 3.3Q). Collectively, these data suggest that the cerebellar hypoplasia observed in *Kif3c*$^{-/-}$ mice is due to reduced CGNP proliferation.

As reduced levels of HH signaling are often associated with reduced CGNP proliferation and cerebellar hypoplasia (Corrales *et al*., 2006; Izzi *et al*., 2011; Lewis *et al*., 2004; Spassky *et al*., 2008), we next assessed the levels of HH signaling through fluorescence *in situ* hybridization of *Gli1* (Figure 3.4A-J). In the anterior (Figure 3.4A-E) and posterior (Figure 3.4F-J) lobes at P10, we do not detect any significant changes in the levels of *Gli1* expression when normalized to the number of HH-responsive cells in *Kif3c*$^{-/-}$ cerebella. Analysis of other HH target genes, *Ptch1*, and

Ptch2, measured by RT-qPCR revealed no significant changes in the levels of expression (Figure 3.4K-L). Furthermore, expression of *Shh* is unchanged in *Kif3c*$^{-/-}$ cerebella (Figure 3.4M). Together, these data suggest that *Kif3c* deletion does not disrupt HH signaling.

3.3.3 Reduced Notch signaling and abnormal Bergmann glia localization in Kif3c mutant cerebella.

As HH signaling was not affected by *Kif3c* deletion, we next assessed the levels of Notch signaling components, another mitogenic pathway in the developing cerebellum (Adachi *et al*., 2021; Solecki *et al*., 2001). The Notch target gene, *Hes1*, and Notch ligand, *Jag1*, were measured by RT-qPCR (Figure 3.5A-B). *Hes1* expression was significantly reduced, while *Jag1* levels were not significantly changed in *Kif3c* mutants. In addition to decreased CGNP proliferation, reduced levels of Notch signaling can result in a change Bergmann glia density and localization (Komine *et al*., 2007). We assessed the density of Bergmann glia and Purkinje cells in the anterior (Figure 3.5C-H) and posterior lobes (Figure 3.5I-N) of *Kif3c*$^{+/+}$ and *Kif3c*$^{-/-}$ P10 cerebella. There was no change in Purkinje cell density in the anterior (Figure 3.5C, E, G) or posterior (Figure 3.5I, K, M) lobes with *Kif3c* deletion. However, we detected an increase in Bergmann glia density within the anterior (Figure 3.5D, F, H) and posterior (Figure 3.5J, L, N) lobes of *Kif3c*$^{-/-}$ cerebella. Furthermore, we observed abnormal localization of Bergmann glia in *Kif3c*$^{-/-}$ mice, more frequently in the posterior lobes (Figure 3.5L, white arrowheads). Notably, some Bergmann glia resided within the EGL. Collectively, these data suggest *Kif3c* deletion results in reduced CGNP proliferation and abnormal Bergmann glia patterning that correlates with reduced Notch signaling.

3.3.4 Kif17 is epistatic to Kif3c in the developing cerebellum.

Given that both *Kif17* and *Kif3c* contribute to cerebellar development, we investigated the consequences of deleting both accessory kinesin-2 motors through the generation of *Kif3c;Kif17* double mutant animals. *Kif17* and *Kif3c* expression were measured by RT-qPCR at P10 (Figure 3.6A-B). While we did not detect a change in expression of *Kif17* in $Kif3c^{-/-}$ cerebella (Figure 3.6A), we did observe reduced *Kif3c* expression in $Kif17^{-/-}$ cerebella (Figure 3.6B). We next evaluated whether loss of both accessory kinesin-2 motors, KIF17 and KIF3C, would result in embryonic lethality or a more severe cerebellar phenotype. Mice lacking both motors ($Kif17^{-/-};Kif3c^{-/-}$) were viable, fertile, and grossly indistinguishable from their littermates. We assessed the cerebellar size of the double mutants at P10 (Figure 3.6C). Remarkably, while the individual germline deletion of these motors results in significant reduction in cerebellar size, loss of both accessory-2 motors does not result in decreased cerebellar size.

Since CGNP-specific *Kif17* deletion results in increased EGL thickness (Chapter 2, Figure 2.12), we hypothesized that the lack of a cerebellar phenotype in $Kif17^{-/-};Kif3c^{-/-}$ mice could be due to the partial HH gain-of-function phenotype observed in *Kif17* mutants. To test this hypothesis, we evaluated cerebellar size in mice with *Kif3c* germline deletion and Purkinje cell-specific *Kif17* deletion (Figure 3.6D). Indeed, cerebellar size was reduced in $Shh^{Cre/+};Kif17^{fl/fl};Kif3c^{-/-}$ animals (Figure 3.6E). We next examined *in vivo* CGNP proliferation in the posterior lobes of these animals (Figure 3.6E-M). In the $Shh^{Cre/+};Kif17^{fl/fl};Kif3c^{-/-}$ cerebella, we observed a severe reduction in EGL thickness and number of proliferative CGNPs. These data suggest loss of *Kif17* in CGNPs can rescue cerebellar size of $Kif17^{-/-};Kif3c^{-/-}$ mutants or that *Kif17* is epistatic to *Kif3c*. Additionally, KIF17 and KIF3A/KIF3C may have partially redundant roles within Purkinje cells, as the loss of

both motors in Purkinje cells (*Shh*$^{Cre/+}$;*Kif17*$^{fl/fl}$;*Kif3c*$^{-/-}$) result in a severe reduction in EGL thickness.

3.4 Discussion

Here, we identified a novel role for KIF3C in the developing mouse cerebellum. We found that *Kif3c* deletion results in reduced cerebellar size due to decreased CGNP proliferation. Unlike *Kif17* mutants, *Kif3*c mutant cerebella do not exhibit altered HH signaling but instead display abnormal Bergmann glia density and localization, a phenotype consistent with reduced Notch signaling. Surprisingly, germline deletion of both accessory kinesin-2 motors does not result in a more severe cerebellar phenotype; instead, our data suggest that *Kif17* is epistatic to *Kif3c*. However, Purkinje cell-specific *Kif17* deletion combined with *Kif3c* germline deletion results in a severe reduction in EGL thickness.

3.4.1 KIF3C regulation of Notch signaling in the developing cerebellum.

Here we demonstrated that *Kif3c* deletion results in reduced Notch signaling in the developing cerebellum. Specifically, we detected decreased expression of the Notch target, *Hes1* and reduced CGNP proliferation. Further, *Kif3c*$^{-/-}$ cerebella display a change in the density and localization of Bergmann glia, consistent with previous Notch loss-of-function studies (Komine *et al*., 2007). In the vertebrate nervous system, Notch promotes glial differentiation and represses neural progenitor differentiation [reviewed in (Louvi and Artavanis-Tsakonas, 2006)]. Notably in the cerebellum, activating the Notch pathway with JAG1 *in vitro* inhibits differentiation of CGNPs and acts synergistically with SHH ligand to promote proliferation (Solecki *et al*., 2001). Further,

cerebellar *Jag1* deletion resulted in delayed CGNP migration, as well as abnormally localized Bergmann glia, which underwent apoptosis in the postnatal cerebellum (Weller *et al*., 2006). Conditional deletion of the Notch transcription factor, RBP-J, within Bergmann glia resulted in cerebellar hypoplasia, aberrantly localized Bergmann glia, and apoptosis of Bergmann glia and CGNPs (Komine *et al*., 2007). Conditional deletion of *Notch1*, *Notch2* and *Dll-1* specific to Bergmann glia yielded similar outcomes – abnormal radial fiber projections, disrupted monolayer alignment, and Bergmann glia apoptosis (Hiraoka *et al*., 2013; Komine *et al*., 2007). Notably, the disrupted monolayer alignment was observed only in the posterior lobes in these animals, similar to *Kif3c*$^{-/-}$ cerebella (Figure 3.5).

Considering our data in the context of previously published studies, one model that emerges for KIF3C function in the developing cerebellum is the regulation of Notch signaling levels. Since *Kif3c* is ubiquitously expressed in cerebellar cell types, we cannot distinguish which cell population(s) contribute to the phenotype observed in germline *Kif3c* mutants. However, we did observe a reduction in EGL thickness, suggesting there is not a delay in CGNP migration and that Notch signaling is intact in those cells. Additionally, we observed aberrant localization of Bergmann glia most significantly in posterior lobes of *Kif3c*$^{-/-}$ animals, phenocopying Bergmann glia-specific deletion of *Notch1*, *Notch2* and *Dll-1* (Hiraoka *et al*., 2013; Komine *et al*., 2007). It will be important to assess whether the aberrantly localized Bergmann glia observed in *Kif3c*$^{-/-}$ animals are undergoing apoptosis and whether the increase in Bergmann glia density is maintained in adult *Kif3c*$^{-/-}$ mice. *In vitro* cultures isolating Bergmann glia to evaluate their response to recombinant Notch ligands, such as JAG1 and DLL-1, will be critical to determine KIF3C contribution to Notch signaling. We also cannot rule out the possibility that KIF3C regulates Notch ligand presentation from Purkinje cells, similar to KIF17-mediated regulation of SHH in Purkinje

cells (Chapter 2). Conditional *Kif3c* deletion within Bergmann glia and Purkinje cells will be crucial to furthering our understanding of how KIF3C regulates cerebellar development.

3.4.2 KIF3C regulates microtubule stability.

Kif3c$^{-/-}$ cerebella display decreased CGNP proliferation and disrupted Bergmann glia patterning. One potential function for KIF3C in cerebellar development is the regulation of microtubule stability. Previous work found *Kif3c*$^{-/-}$ neurons displayed impaired regeneration due to stable, overgrown, and looped microtubules at the growth cones of dorsal root ganglion neurons (Gumy *et al.*, 2013). Further, KIF3C localized to the growing ends of microtubules and preferentially bound to tyrosinated (unstable) microtubules (Gumy *et al.*, 2013). Forced homodimerization of KIF3C motors, which has not been observed endogenously, was also found to increase microtubule catastrophe frequency (Guzik-Lendrum *et al.*, 2017).

Microtubules are essential in neuronal development. Cell migration, cue-dependent navigation of the growing end of axons and the arborization of dendrites all depend on microtubules [reviewed in, (Baas et al., 2016)]. Bergmann glia project foot processes that attach to the basement membrane, which are required for supporting the cerebellar cytoarchitecture, and Purkinje cell axon growth and dendrite arborization are dependent on proper microtubule growth; CGNPs undergo vast remodeling of their cytoskeleton during differentiation and migration [reviewed in (Leto *et al.*, 2016)]. It will be important to investigate KIF3C localization to the tips of the growing ends of microtubules in the developing cerebellum. Further, examining *Kif3c*$^{-/-}$ cells to determine if they display abnormal morphology or overgrown/looped microtubules will be vital to assessing the contribution of *Kif3c* to cerebellar development.

3.4.3 Redundancy and Compensation in Kinesin-2 Motors

Germline *Kif17* or *Kif3c* deletion result in cerebellar hypoplasia, yet simultaneous germline deletion of both *Kif17* and *Kif3c* does not appear to affect embryogenesis or cerebellar size. However, in mice with germline *Kif3*c deletion and Purkinje cell-specific *Kif17* deletion ($Shh^{Cre/+};Kif17^{fl/fl};Kif3c^{-/-}$), we observed cerebellar hypoplasia and reduced CGNP proliferation. Without examination of *Kif3c* germline mutants with a CGNP specific deletion of *Kif17* ($Atoh1Cre;Kif17^{fl/fl};Kif3c^{-/-}$), we cannot distinguish whether loss of *Kif17* in CGNPs can rescue cerebellar size or if *Kif17* is epistatic to *Kif3c*.

The requirement of kinesin-2 motors varies significantly across different model organisms. For example, in *C. elegans*, the KIF3A/KIF3B homologue, KLP20/KLP11, contributes to building the middle segment of amphid-channel sensory cilia, while the KIF17 homologue, OSM-3, is responsible for generating the distal segment of cilia (Evans *et al*., 2006; Snow *et al*., 2004). However, OSM-3 can compensate for the loss of KLP20/KLP11, while KLP20/KLP11 cannot compensate in OSM-3 mutants. In the developing zebrafish, loss of *Kif17* results in ciliary defects in the retina and olfactory pit (Insinna *et al*., 2008; Lewis *et al*., 2018; Lewis *et al*., 2017; Zhao *et al*., 2012), suggesting the other kinesin-2 motors cannot compensate for its loss in those tissues. Loss of *Kif3b* in zebrafish results in delayed outer segment development and shortened cilia in the retina, suggesting *Kif17* or *Kif3c* can partially compensate for *Kif3b*. Further supporting this notion, injection of either *Kif17* or *Kif3c* mRNA in *Kif3b* mutant embryos can rescue ciliogenesis in specialized cell types (Zhao *et al*., 2012). However, this redundancy appears to be abolished in mice. Loss of *Kif3a* or *Kif3b* result in defective ciliogenesis and mid-gestation lethality (Nonaka *et al*., 1998; Takeda *et al*., 1999), while loss of *Kif17* or *Kif3c* does not result in ciliary phenotypes or embryonic lethality (Yang *et al*., 2001; Yin *et al*., 2011). Due to the lack of detected *Kif3c* or

Kif17 expression during mouse embryogenesis, it is not surprising that these motors cannot compensate for KIF3A/KIF3B. However, KIF17 or KIF3C expression in *Kif3a*$^{-/-}$;*Kif3b*$^{-/-}$ NIH/3T3 cells cannot rescue ciliogenesis (Engelke *et al*., 2019), demonstrating that accessory kinesin-2 motors are not sufficient to compensate for KIF3A/KIF3B loss in mice. The cerebellum is an ideal tissue to examine the contribution of individual kinesin-2 motors because all motors are endogenously expressed during development and homeostasis.

Examination of CGNP proliferation in *Kif17*$^{-/-}$;*Kif3c*$^{-/-}$ cerebella compared to single mutants will be important to determine if the *Kif17*-mediated reduction in GLI3 (detailed in the previous chapter) is retained in *Kif17;Kif3c* double mutants. This could be addressed through investigating *Kif3c* mutants with CGNP conditional deletion of *Kif17* (*Atoh1Cre;Kif17*$^{fl/fl}$;*Kif3c*$^{-/-}$) or *Kif3c*/*Gli3* compound mutants. While *Kif17* expression was unchanged in *Kif3c* mutants, we detected a reduction in *Kif3c* expression in *Kif17*$^{-/-}$ animals (Figure 3.6A-B). It will be essential for future studies to identify which cell population(s) have reduced *Kif3c* expression. Further, examination of a true kinesin-2 null cerebellum (*En2Cre;Kif3a*$^{fl/fl}$;*Kif17*$^{-/-}$) will shed light on the requirement of the kinesin-2 family in cerebellar development (it is important to note that *Kif3a* deletion will be sufficient, as KIF3B/KIF3C has not been observed endogenously). Examination of mice with deletion of kinesin-2 motors in Purkinje cells (*Shh*$^{Cre/+}$;*Kif3a*$^{fl/fl}$;*Kif17*$^{fl/fl}$) or CGNPs (*Atoh1Cre;Kif3a*$^{fl/fl}$;*Kif17*$^{fl/fl}$) will also be crucial, considering two these cell types express all kinesin-2 motors. Kinesin-2 null Purkinje cells will be of particular importance, considering new studies demonstrating KIF3B function in SHH-producing cells in the developing limb (Wang *et al*., 2022), as well as the requirement of cilia in the survival of Purkinje cells (Bowie and Goetz, 2020).

3.5 Materials and Methods

Reagents

Primers used for RT-qPCR (Table 3.1); antibodies utilized (Table 3.2)

Animal models

Kif3c germline mutant mice have been previously described (Yang *et al*., 2001). *Kif17*^{lacZ} germline mutant mice have been previously described (22). *Kif17*^{fl} animals carrying *Kif17* conditional alleles were generated from the initial knock-in allele from EUCOMM through crossing *Kif17*^{tm1A} animals to ubiquitous Flippase mice obtained from The Jackson Laboratory [strain 011065, (64)] to generate *Kif17*^{tm1C}/*Kif17*^{flox} mice. Mice carrying the *Shh*^{Cre} allele [strain 005622] were provided by Dr. Deb Gumucio and previously described (26). All mice were maintained on a congenic C57BL/6J background. All animal procedures were reviews and approved by the Institutional Animal Care and Use Committee (IACUC) at the University of Michigan, USA. Experiments performed in this paper were completed with littermate controls.

RT-qPCR

Cerebella were dissected in 1X PBS, and RNA was isolated using a PureLink RNA Mini Kit (ThermoFisher Scientific, 12183025). Following isolation, 2μg of RNA were used to generate cDNA libraries using a High-Capacity cDNA reverse transcription kit (Applied Biosystems, 4368814). RT-qPCR was performed using PowerUP SYBR Green Master Mix (Applied Biosystems, A25742) in a QuantStudio 3 Real-Time PCR System (Applied Biosystems). Primers used in this paper can be found in Table 3.1. Gene expression was normalized to *Gapdh,* and

relative expression analyses were performed using the 2(-ddCT) method. For RT-qPCR analysis, biological replicates were analyzed in triplicate.

Wholemount digoxigenin in situ hybridization

Wholemount digoxigenin in situ hybridization was performed as previously described (Allen at al., 2011; Wilkinson, 1992). First, cerebella were dissected in 1X PBS (pH 7.4), cut in half with a razor and fixed for 24 h with 4% paraformaldehyde at 4°C on rocking platform. The *Kif3c* probe was designed to bind to the end of the mRNA transcript:

(GCTGCTCCACTGGACTGAATGGCGGAGCCTTGCGGCTGCCTGCCCTTCAAAGGGAT
CCCAGGTTTCTGTCAGAACCCTGTGATTGACACTCAGGATTCAAATCAGAGGAATGG
CTTTCTCTGGAACAGGAGCTGTGTGTAGAAATCTCCTGATGTGAACTGGGCATTGAG
GGACCTCCCCCTGAGCTCTCTGTCATTTGTAGATGAAGCTGCATGAGTCACCCCATT
CATCACTTGGACACACTGACTCCACATTGTCTGGTCCACTACCCTCACAGTCTTATA
GCACAATACACCCCACTTCAGCACCGCAGCCAAAGGCTGGGCCCAAGGTGTGGTCA
GAAGAGGTGCTCCTGCCTGTGGTATTATATGTGTGTGTTTATGTGTGTGTTTATGTTC
ACCTGTACAGGGGGCACTACACTCAATGTAAGATACCCTGGAGACAGGACTCCTGG
AGGTGGCTGGATCTCAGTCTCTGTCTCTCTCCTTTTTCTTTTACTGTATCACACATTTG
ATTGACAAAGTACGGGCCTTAATTAGGATCAAATTTCTATGTCTGTTGCTATGGCCTT
TAATTAAAGTTACACAAAGTGGCCCATTCTTGTCACTCTATACATATGGGACATATG
TATATCTAGGACATATGTAATATATAAATATATAAATATATATAAAGCATTAACCTC
TGCCCCC). Probe hybridization was performed with the *Kif3c* digoxigenin probe at a concentration of 1ng/μl overnight at 70°C. The samples were incubated in AP-conjugated anti-DIG antibody (Table 3.2). AP-anti-DIG was visualized with BM Purple (Roche, 11442074001),

and signal was developed for 4h at 37°C. After the signal was developed, development was stopped with 3 x 5min washes with 1X PBS (pH 4.5). Cerebella were post-fixed in 4% PFA + 0.2% glutaraldehyde for 30min, then washed 3 x 5min in 1X PBS (pH 7.4). Cerebella were photographed using a Nikon SMZ1500 microscope and stored in 1X PBS (pH 7.4).

Fluorescent in situ hybridization

Cerebella were dissected in 1X PBS (pH 7.4) and cut in half using a razor. Cerebella were fixed with 10% neutral buffered formalin (Fisher, 245-685) on a rocking platform at room temperature for 24h. Following fixation, cerebella were washed 3 x 5min with 1X PBST^{X} on a rocking platform and cryoprotected overnight in 1X PBS + 30% sucrose on a rocking platform. Cerebella were then washed 3 x 1h with 50% OCT compound before embedding in 100% OCT. Sections were collected on a Leica CM1950 cryostat at 12μm thickness. Slides were processed using RNAscope Multiplex Fluorescent Detection kit (ACD, 323110) using a protocol adapted from (Holloway et al., 2021). Prior to probe hybridization, samples underwent antigen retrieval for 15min and treated with Protease Plus (ACD, 322381) for 5min. Probes used in this paper were a custom probe for *Mm-Kif3c*, designed to bind to exon 1, and *Mm-Gli1* (ACD, 311001). After probe detection, slides were subsequently stained using the below-described section immunofluorescence protocol.

Section Immunofluorescence

Section immunofluorescence was performed as described in (65). Briefly, cerebella were dissected in 1X PBS (pH 7.4) and cut in half using a razor. Cerebella were fixed with 4% paraformaldehyde (Electron Microscopy Sciences) for 1h on ice. Following fixation, cerebella were washed 3 x 5min with 1X PBS (pH 7.4) on a rocking platform and cryoprotected overnight in 1X PBS + 30% sucrose

on a rocking platform. Then, cerebella were washed 3 x 1h in 50% OCT (Fisher Scientific, 23-730-571) before embedding in 100% OCT. Sections were collected on a Leica CM1950 cryostat at 12μm thickness for all experiments. Slides were then washed 3 x 5min with 1X PBS (pH 7.4). For mouse primary antibodies, citric acid antigen retrieval (10mM citric acid + 0.5% Tween-20, pH 6.0) at 92°C for 10 min was performed prior to primary antibody incubation. Primary antibodies were diluted in blocking buffer (3% bovine serum albumin, 1% heat-inactivated sheep serum, 0.1% Triton X-100) and incubated overnight at 4°C in a humidified chamber. After primary antibody incubation, slides were washed 3 x 10min with 1X PBST^X (1X PBS + 0.1% Triton X-100, pH 7.4). Secondary antibodies were diluted in blocking buffer and incubated for 1 h at room temperature, followed by 3 x 5min washes with 1X PBST^X. Nuclei were labeled using DAPI (0.5μg/mL in blocking buffer) for 10min and washed twice with 1X PBS. Coverslips were mounted using Immu-mount aqueous mounting medium (Thermo Fisher Scientific, 9990412). Images were taken on a Leica SP5X upright confocal. A list of all primary and secondary antibodies and their working concentrations is provided in Table 3.2.

Weight analyses

For weight measurements, the date litters were born were noted as postnatal day 0 and were dissected on postnatal day 10. Pups were first weighed and then placed on ice briefly before decapitation. The cortices and cerebella were dissected in 1X PBS (pH 7.4). To weigh cortices and cerebella, a specimen jar was first filled with PBS on an analytical scale. The tissue was transferred with forceps to the specimen jar, and its weight was recorded. Genotyping samples were taken after dissection, allowing the weights to be recorded without prior knowledge of the genotype.

EGL and PC Dendrite quantitation

To measure the thickness of the external granule layer (EGL) and PC dendrite length, ImageJ software was utilized. Images were first blinded before measuring. For EGL thickness, the area was divided by the length of the EGL. For PC dendrite length, measurements were taken just below the bottommost nuclei in the EGL to the center of Purkinje cell nuclei within the molecular layer. For each animal, at least three images were acquired in the posterior lobes and an additional three images in the anterior lobes.

EdU incorporation assay (in vivo)

On postnatal day 9, pups were intraperitoneally injected with 100mg/kg of EdU (Invitrogen, A10044), dissolved in 1X PBS (pH 7.4). 24h later, cerebella were dissected and processed for section immunofluorescence as described above. Prior to primary antibody incubation, EdU incorporation was visualized with an azide staining solution [100 mM Tris HCl (pH 8.3), 0.5 mM CuSO4, 50 mM ascorbic acid, 50 μM Alexa Fluor 555 Azide, Triethylammonium Salt (Thermo Fisher Scientific, A20012)] for 30min at room temperature. Sections were then washed 3 x 10min in $PBST^{X}$ followed by immunofluorescence staining as described above.

Image quantitation

To quantify *Gli1* fluorescence, ImageJ software was used to measure the integrated density fluorescent signal contained to either the external granule layer (EGL, CGNPs) or lower molecular layer and inner granule layer (IGL, Bergmann glia and CGNs). The signal was then divided by the number of HH-responsive cells in each layer (number of $PAX6^{+}$ cells in the EGL; number of

PAX6$^+$ and SOX2$^+$ cells in the molecular layer and IGL). At least three images were analyzed per region per mouse. For all image analyses, images were blinded.

Quantitation and statistical analysis

All the data are mean ± s.d. All statistical analyses were performed using GraphPad Prism (www.graphpad.com). Statistical significance was determined by using a two-tailed Student's t-test for comparison of two groups or one way ANOVA analysis for more than two groups. For all the experimental analyses, a minimum of three mice of each genotype were analyzed, each n represents a mouse. All the statistical details (statistical test used, adjusted P-value, statistical significance and exact value of each n) for each experiment are specified in the figure legends.

3.6 Acknowledgements

We thank past and present Allen lab members for their valuable feedback and suggestions. We thank members of the Department of Cell and Developmental Biology who provided access to equipment, including the laboratories of Sue O'Shea, Doug Engel, and Jason Spence. PAX6 and LIM1/2 antibodies were obtained from the Developmental Studies Hybridoma Bank, created by the Eunice Kennedy Shriver National Institute of Child Health and Human Development of the National Institutes of Health and maintained at The University of Iowa, Department of Biology, Iowa City, IA 52242, USA. Finally, we acknowledge the Biomedical Research Core Facilities Microscopy Core, which is supported by the Rogel Cancer Center, for providing access to confocal microscopy equipment.

3.7 Author Contributions

Conceptualization: B.W., B.L.A. Data Curation: B.W. Formal Analysis: B.W. Funding Acquisition: B.W., B.L.A. Investigation: B.W., B.L.A. Methodology: B.W. Project Administration: B.L.A. Supervision: B.L.A. Validation: B.W. Visualization: B.W. Writing/editing: B.W., B.L.A.

3.8 Tables

Table 3.1 Table of RT-qPCR Primers

Gene	forward primer (5-3)	reverse primer (5-3)	Reference
Gapdh	GTGGTGAAGCAGGCATCTGA	GCCATGTAGGCCATGAGGTC	[Han et al., 2017 (PLoS Biology)]
Kif3c	CAGGCCGACCTGTATGACG	GTCCCCTGCATGGTGTAGG	designed by BW
Atoh1	AGTCAATGAAGTTGTTTCCC	ACAGATACTCTTATCTGCCC	[Hor et al., 2021 (Journal of Neuroscience)]
Ptch1	GAAGCCACAGAAAACCCTGTC	GCCGCAAGCCTTCTCTAGG	[Han et al., 2017 (PLoS Biology)]
Ptch2	CCCGTGGTAATCCTCGTGGCCT CTAT	TCCATCAGTCACAGGGGCAAA GGTC	[Shimokawa et al., 2008 (JBC)]
Shh	GCTGTGGAAGCAGGTTTCG	GGAAGGTGAGGAAGTCGCTC	[Madison et al., 2005 (Development)]
Hes1	CAGCCAGTGTCAACACGACAC	TCGTT CATGCACTCGCTGAAG	[Solecki et al., 2001 (Neuron)]

Jag1	TGCTTGGTGACAGCCTTCTACT GG	CTCTGGGCACTTTCCAAGTC	[Solecki et al., 2001 (Neuron)]
Kif17	CATGCACACGGTACACAAC	GAACGGGAGGAGTCCTTATTC	designed by BW

Table 3.2 Table of Antibodies

Antibody	Source	Catalog Number	Application	Dilution
Mouse IgG1 anti-PAX6	DSHB	PAX6	IF	1:20
Mouse IgG1 anti-LIM1+2	DSHB	4F2	IF	1:20
Rabbit IgG anti-SOX2	Seven Hills Bioreagent	WRAB-1236	IF	1:2000
Rabbit IgG anti-Ki67	Abcam	ab15580	IF	1:1000
AP-conjugated anti-DIG antibody	Roche (Millipore Sigma)	11093274910	WISH	1:4000
Alexa Fluor 488 goat anti-mouse IgG1	Invitrogen	A21121	IF	1:500
Alexa Fluor 647 goat anti-mouse IgG1	Invitrogen	A21240	IF	1:500
Alexa Fluor 647 donkey anti-rabbit IgG	Invitrogen	A31573	IF	1:500

3.9 Figures

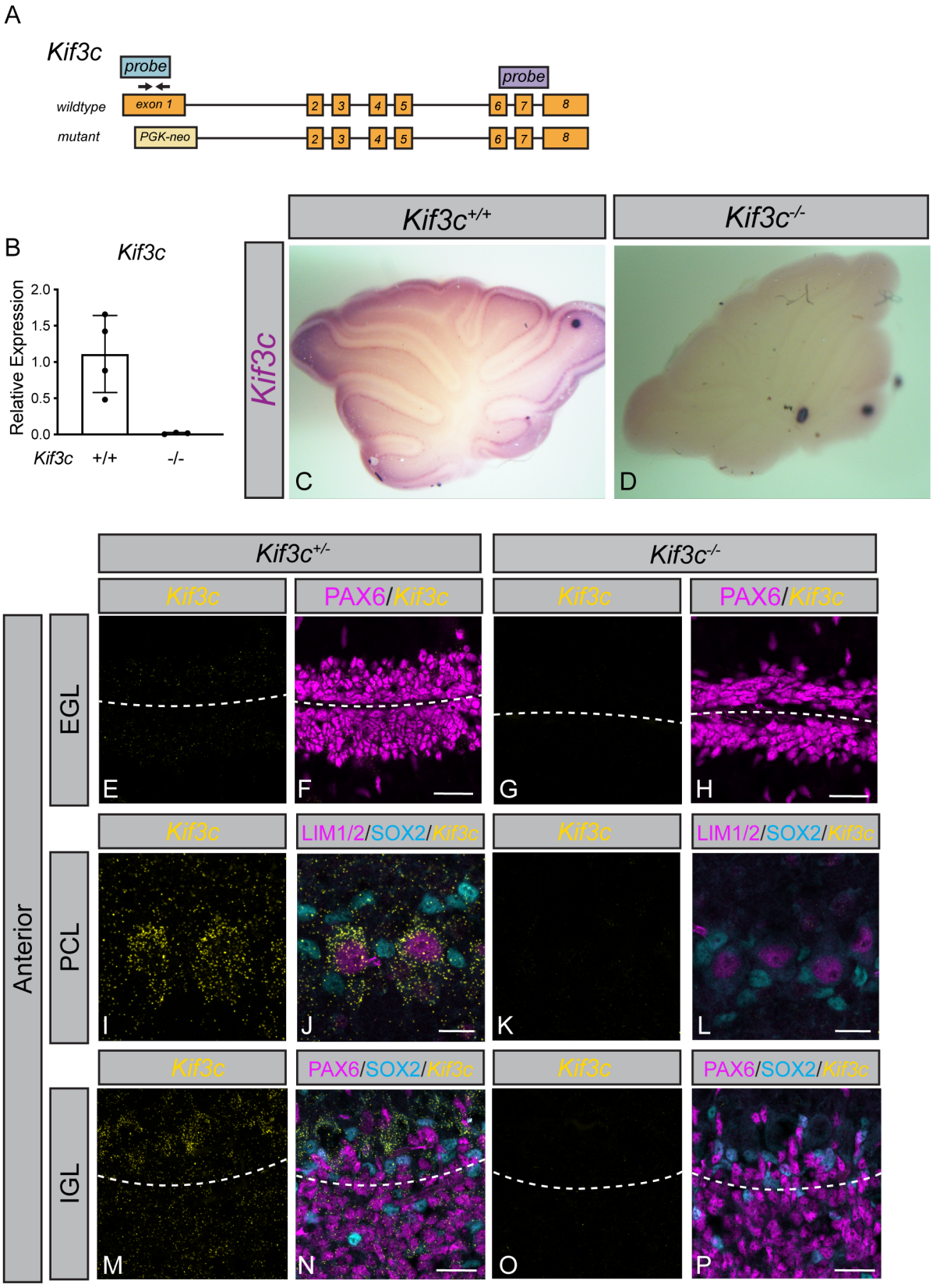
A
Kif3c
probe
probe
wildtype
exon 1
2
3
4
5
6
7
8
mutant
PGK-neo
B
Kif3c
Relative Expression
2.0
1.5
1.0
0.5
0.0
Kif3c
+/+
-/-
Kif3c+/+
Kif3c-/-
Kif3c
C
D
Kif3c+/-
Kif3c-/-
Kif3c
PAX6/Kif3c
Anterior
EGL
PCL
IGL
LIM1/2/SOX2/Kif3c
PAX6/SOX2/Kif3c
E
F
G
H
I
J
K
L
M
N
O
P

Figure 3.1 *Kif3c* is ubiquitously expressed in the developing postnatal mouse cerebellum.

Schematic of *Kif3c* wildtype and mutant alleles (A). Wildtype *Kif3c* is encoded by 8 exons, while a PGK-neo cassette replaces exon 1 and part of the first intron in the mutant allele; this results in the loss of amino acids 1-518 (out of 796 total amino acids), including the entire motor domain, yielding a null allele (CITATION). Blue probe denotes the fluorescent in situ probe binding site, while the purple probe indicates the digoxigenin probe. Arrowheads above exon 1 represent RT-qPCR primers. RT-qPCR detection of Kif3c expression (B) in P10 $Kif3c^{+/+}$ and $Kif3c^{-/-}$ cerebella. Whole-mount *in situ* hybridization of $Kif3c^{+/+}$ (C) and $Kif3c^{-/-}$ (D) cerebella at postnatal day 10 (P10). Data are mean ± s.d. Each dot represents an individual animal. P-values were determined by a two-tailed Student's t-test. Fluorescent in situ detection of *Kif3c* mRNA (yellow; E-P) in $Kif3c^{+/-}$ (E-F, I-J, M-N) and $Kif3c^{-/-}$ (G-H, K-L, O-P) within anterior lobes in P10 cerebella. Antibody detection of PAX6 (magenta; F, H) to label cerebellar granule neural progenitor nuclei. Dashed lines separate individual external granule layers. Antibody detection of LIM1/2 (magenta; J, L) and SOX2 (cyan; J, L) to label Purkinje cells and Bergmann glia, respectively. Antibody detection of PAX6 (magenta; N, P) and SOX2 (cyan; N, P) to label CGNs and Bergmann glia, respectively. Dashed lines separate molecular layer (MCL) and inner granule layer (IGL). Scale bars (F, H, N, P), 25μm. Scale bars (J, L), 15μm.

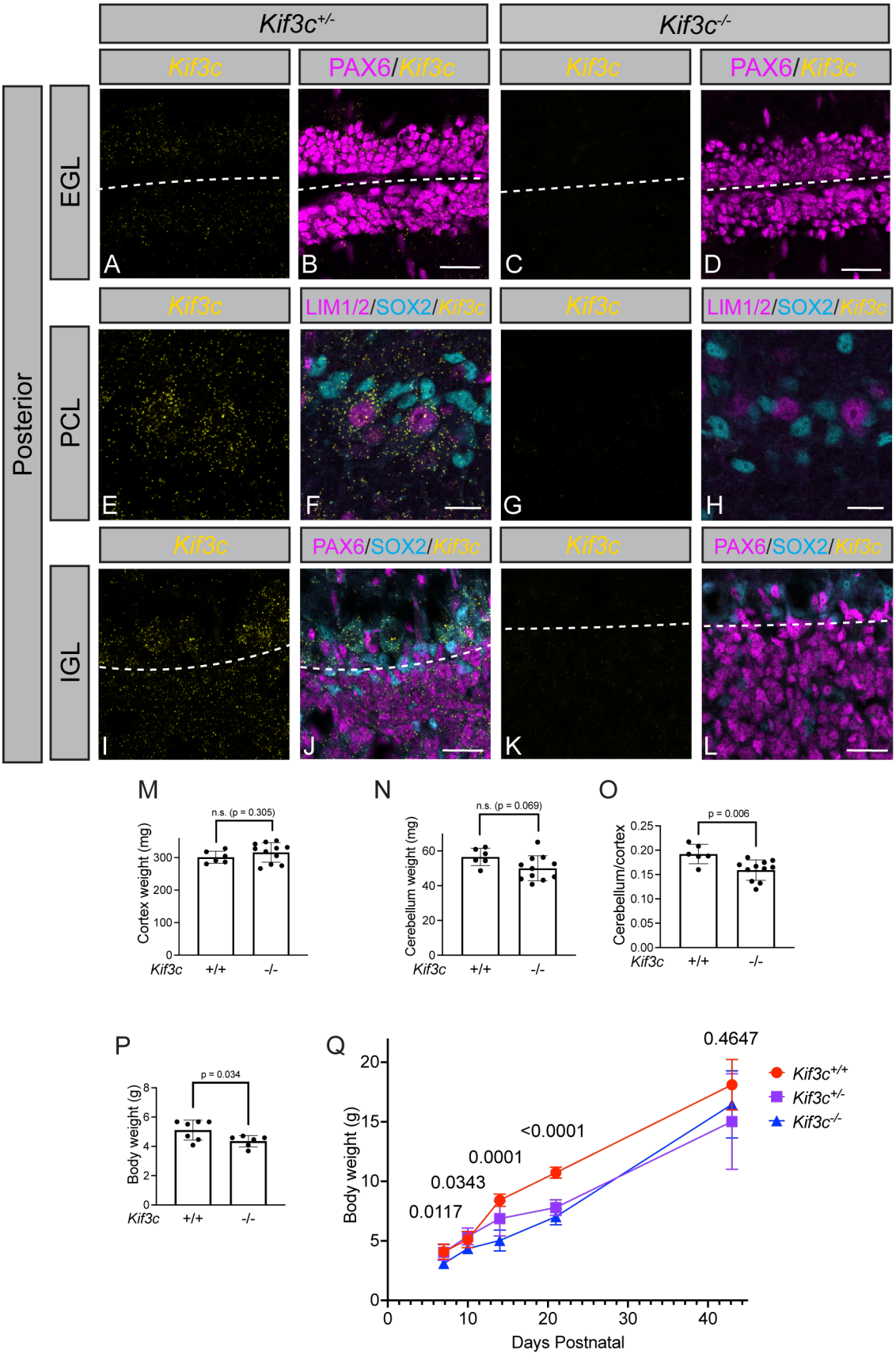
Kif3c+/-
Kif3c-/-
Kif3c
PAX6/Kif3c
LIM1/2/SOX2/Kif3c
PAX6/SOX2/Kif3c
Posterior
EGL
PCL
IGL
A
B
C
D
E
F
G
H
I
J
K
L
M
Cortex weight (mg)
n.s. (p = 0.305)
N
Cerebellum weight (mg)
n.s. (p = 0.069)
O
Cerebellum/cortex
p = 0.006
P
Body weight (g)
p = 0.034
Kif3c +/+ -/-
Q
Body weight (g)
Days Postnatal
0.4647
<0.0001
0.0001
0.0343
0.0117
Kif3c+/+
Kif3c+/-
Kif3c-/-

Figure 3.2 *Kif3c* is required for proper cerebellar size.

Fluorescent *in situ* detection of *Kif3c* mRNA (yellow; A-L) in *Kif3c*$^{+/-}$ (A-B, E-F, I-J) and *Kif3c*$^{-/-}$ (C-D, G-H, K-L) posterior lobes of P10 cerebella. Antibody detection of PAX6 (magenta; B, D) to label cerebellar granule neural progenitor nuclei. Dashed lines separate individual external granule layers. Antibody detection of LIM1/2 (magenta; F, H) and SOX2 (cyan; F, H) to label Purkinje cells and Bergmann glia, respectively. Antibody detection of PAX6 (cyan; J, L) to label CGNs and Bergmann glia, respectively. Dashed lines separate molecular layer (MCL) and inner granule layer (IGL). Scale bars (B, D, J, L), 25 μm. Scale bars (F, H), 15 μm. Quantitation of cortex weight (M), cerebellar weight (N), and cerebellar weight normalized to cortex weight (O) in P10 *Kif3c*$^{+/+}$ and *Kif3c*$^{-/-}$ mice. Quantitation of body weight (P) in P10 *Kif3c*$^{+/+}$ and *Kif3c*$^{-/-}$ mice at P10. Body weight over time (Q) of *Kif3c*$^{+/+}$, *Kif3c*$^{+/-}$ and *Kif3c*$^{-/-}$ mice beginning at P7 to P43. Data are mean ± s.d. Each dot represents an individual animal. P-values were determined by a two-tailed Student's t-test.

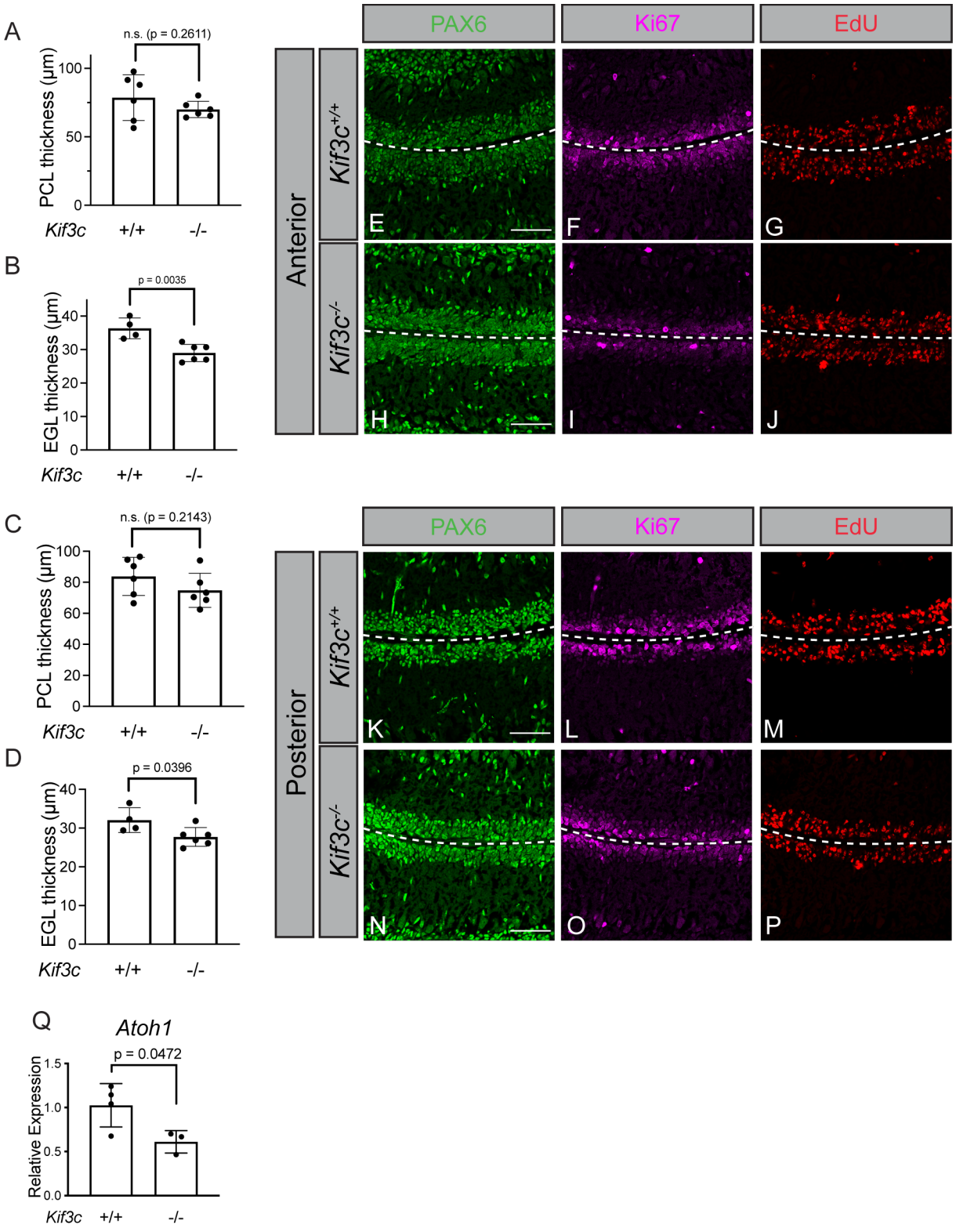
A
n.s. (p = 0.2611)
PCL thickness (μm)
100
50
0
Kif3c +/+ -/-
B
p = 0.0035
EGL thickness (μm)
40
30
20
10
0
Kif3c +/+ -/-
C
n.s. (p = 0.2143)
PCL thickness (μm)
100
80
60
40
20
0
Kif3c +/+ -/-
D
p = 0.0396
EGL thickness (μm)
40
30
20
10
0
Kif3c +/+ -/-
Q
Atoh1
p = 0.0472
Relative Expression
1.5
1.0
0.5
0.0
Kif3c +/+ -/-
PAX6
Ki67
EdU
Anterior
Kif3c+/+
Kif3c-/-
E
F
G
H
I
J
Posterior
K
L
M
N
O
P

Figure 3.3 *Kif3c* deletion results in reduced CGNP proliferation.

Quantitation of PC dendrite length (A) and external granule layer (EGL, B) thickness in the anterior lobes of P10 *Kif3c*$^{+/+}$ and *Kif3c*$^{-/-}$ cerebella. Quantitation of PC dendrite length (C) and external granule layer (EGL, D) thickness in the posterior lobes of P10 *Kif3c*$^{+/+}$ and *Kif3c*$^{-/-}$ cerebella. Each dot represents the average of three images per individual animal. Immunofluorescent analysis of CGNP proliferation of *Kif3c*$^{+/+}$ (E-G, K-M) and *Kif3c*$^{-/-}$ (H-J, N-P) anterior (E-J) and posterior (K-P) lobes in P10 cerebella. Antibody detection of PAX6 (green; E, H, K, N) and Ki67 (magenta; F, I, L, O). Fluorescent azide detection of EdU (red; G, J, M, P). Scale bars (E, H, K, N), 50μm. Dashed line separates individual external granule layers. RT-qPCR detection of Atoh1 expression (Q) in P10 *Kif3c*$^{+/+}$ and *Kif3c*$^{-/-}$ cerebella. Data are mean ± s.d. Each dot represents an individual animal. P-values were determined by a two-tailed Student's t-test.

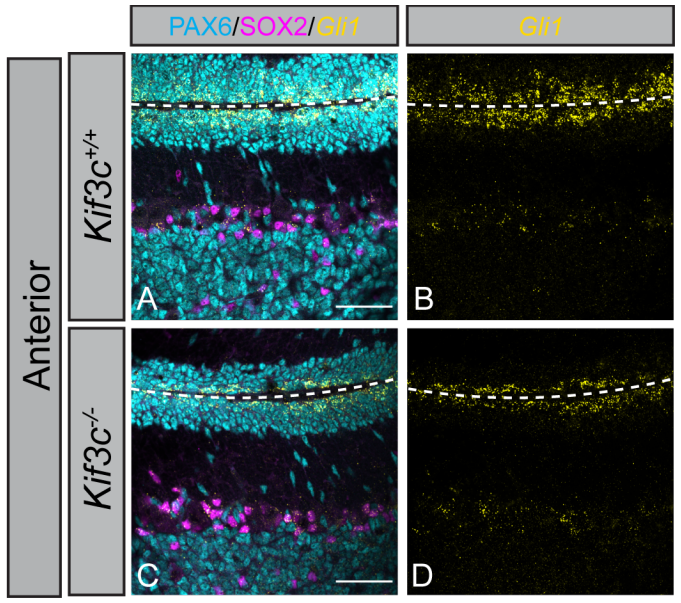
PAX6/SOX2/Gli1
Gli1
Anterior
Kif3c+/+
Kif3c-/-
A
B
C
D

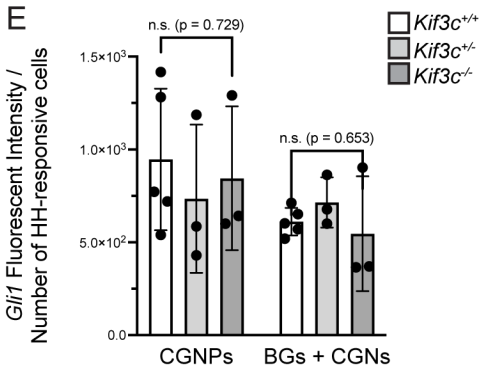
E
n.s. (p = 0.729)
n.s. (p = 0.653)
Kif3c+/+
Kif3c+/-
Kif3c-/-
Gli1 Fluorescent Intensity / Number of HH-responsive cells
1.5×10³
1.0×10³
5.0×10²
0.0
CGNPs
BGs + CGNs

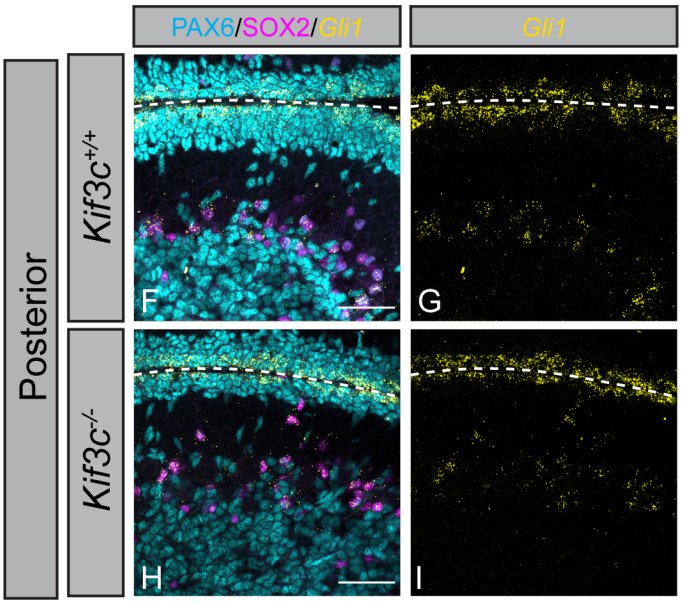
PAX6/SOX2/Gli1
Gli1
Posterior
Kif3c+/+
Kif3c-/-
F
G
H
I

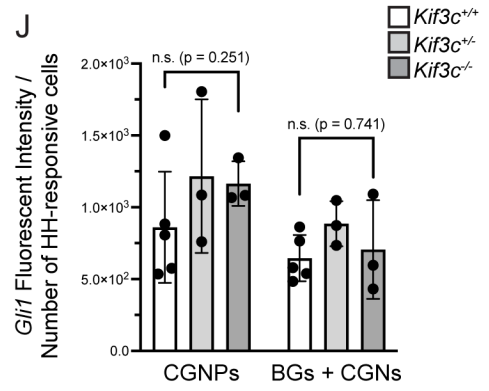
J
n.s. (p = 0.251)
n.s. (p = 0.741)
Kif3c+/+
Kif3c+/-
Kif3c-/-
Gli1 Fluorescent Intensity / Number of HH-responsive cells
2.0×10³
1.5×10³
1.0×10³
5.0×10²
0.0
CGNPs
BGs + CGNs

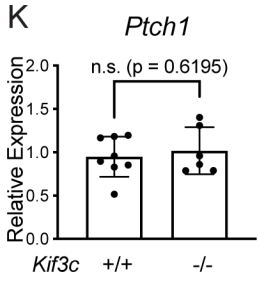
K
Ptch1
n.s. (p = 0.6195)
Relative Expression
2.0
1.5
1.0
0.5
0.0
Kif3c
+/+
-/-

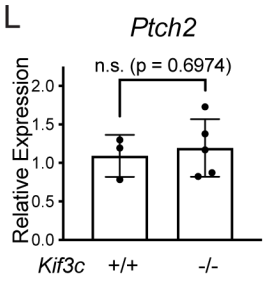
L
Ptch2
n.s. (p = 0.6974)
Relative Expression
2.0
1.5
1.0
0.5
0.0
Kif3c
+/+
-/-

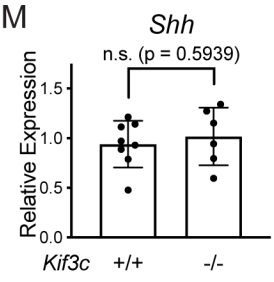
M
Shh
n.s. (p = 0.5939)
Relative Expression
1.5
1.0
0.5
0.0
Kif3c
+/+
-/-

Figure 3.4 HH signaling is intact in *Kif3c*$^{-/-}$ cerebella.

Fluorescent in situ *Gli1* detection (yellow; A-D) in P10 *Kif3c*$^{+/+}$ and *Kif3c*$^{-/-}$ anterior cerebella. Antibody detection (A, C) of PAX6 (cyan) and SOX2 (magenta) to label granule neurons and Bergmann glia, respectively. Quantitation of fluorescent intensity (integrated density) of *Gli1* puncta normalized to the number of HH-responsive cells within the EGL (CGNPs) or MCL/IGL [(Bergmann glia and cerebellar granule neurons (BGs + CGNs)] in P10 *Kif3c*$^{+/+}$ and *Kif3c*$^{-/-}$ anterior (E) lobes. Fluorescent *in situ Gli1* detection (yellow; F-I) in P10 *Kif3c*$^{+/+}$ and *Kif3c*$^{-/-}$ posterior cerebella. Antibody detection (F, H) of PAX6 (cyan) and SOX2 (magenta) to label granule neurons and Bergmann glia, respectively. Quantitation of fluorescent intensity (integrated density) of *Gli1* puncta normalized to the number of HH-responsive cells within the EGL (CGNPs) or MCL/IGL [(Bergmann glia and cerebellar granule neurons (BGs + CGNs)] in P10 *Kif3c*$^{+/+}$ and *Kif3c*$^{-/-}$ posterior (J) lobes. Scale bars (A, C, F, H), 50 μm. Dashed lines separate external granule layers. Each dot represents the average of 3 images per animal. RT-qPCR detection of *Ptch1* (K), *Ptch2* (L) and *Shh* (M) expression P10 *Kif3c*$^{+/+}$ and *Kif3c*$^{-/-}$ cerebella. Data are mean ± s.d. Each dot represents an individual animal. P-values were determined by a two-tailed Student's t-test.

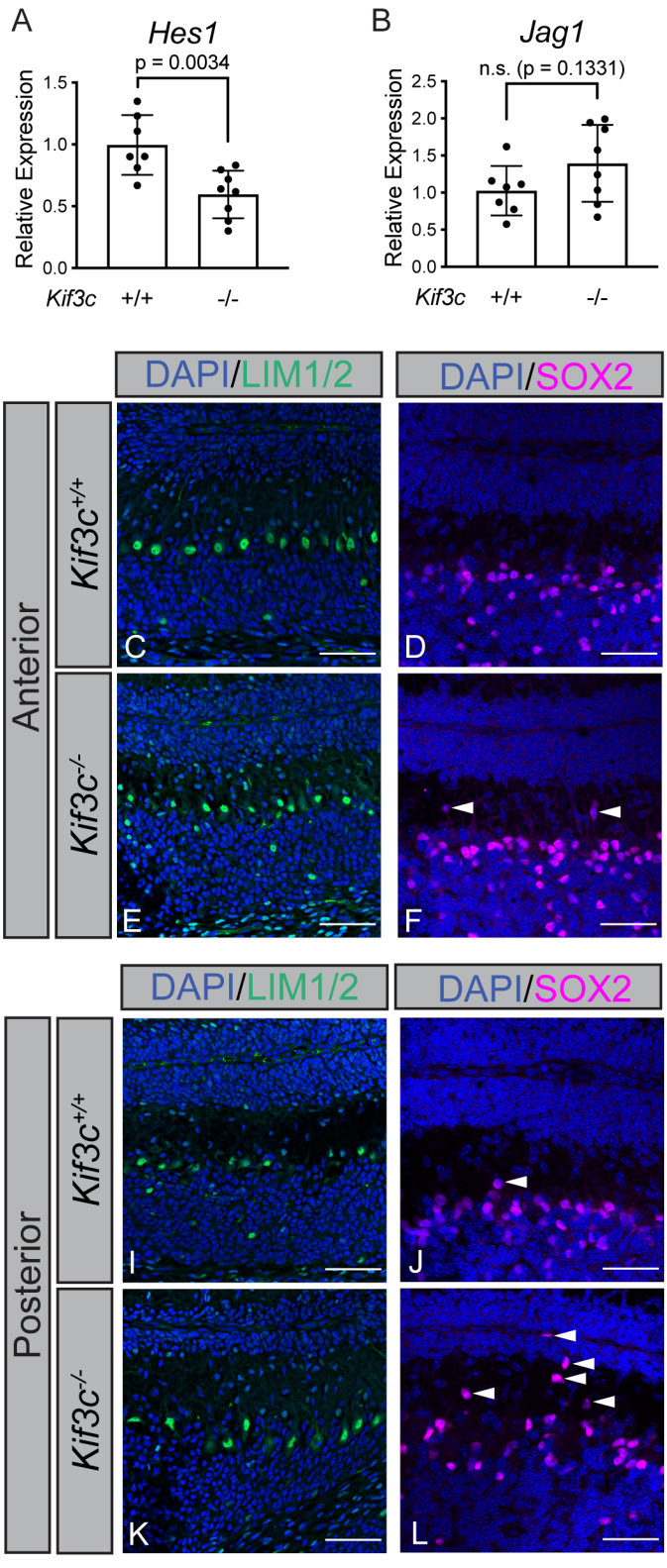
A
Hes1
p = 0.0034
Relative Expression
1.5
1.0
0.5
0.0
Kif3c +/+ -/-
B
Jag1
n.s. (p = 0.1331)
Relative Expression
2.5
2.0
1.5
1.0
0.5
0.0
Kif3c +/+ -/-
DAPI/LIM1/2
DAPI/SOX2
Anterior
Kif3c+/+
Kif3c-/-
C
D
E
F
Posterior
Kif3c+/+
Kif3c-/-
I
J
K
L

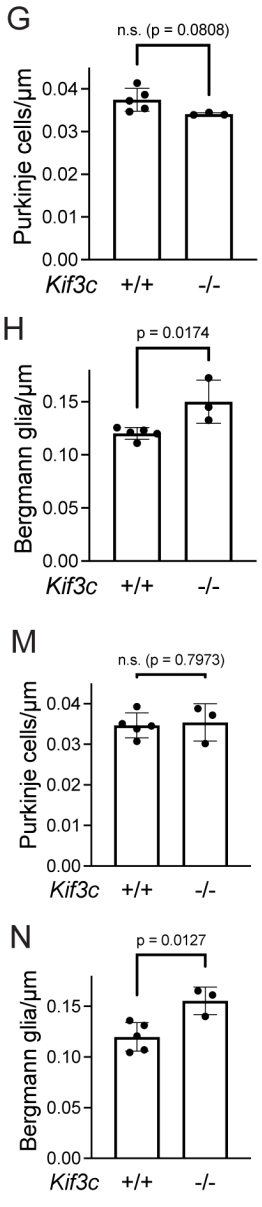
G
n.s. (p = 0.0808)
Purkinje cells/µm
0.04
0.03
0.02
0.01
0.00
Kif3c +/+ -/-
H
p = 0.0174
Bergmann glia/µm
0.15
0.10
0.05
0.00
Kif3c +/+ -/-
M
n.s. (p = 0.7973)
Purkinje cells/µm
0.04
0.03
0.02
0.01
0.00
Kif3c +/+ -/-
N
p = 0.0127
Bergmann glia/µm
0.15
0.10
0.05
0.00
Kif3c +/+ -/-

Figure 3.5 Increased density and disorganization of Bergmann glia with *Kif3c* deletion.

RT-qPCR detection of *Hes1* (A) and *Jag1* (B) expression in P10 *Kif3c*$^{+/+}$ and *Kif3c*$^{-/-}$ cerebella. Each dot represents an individual animal. Immunofluorescent analysis of Purkinje cell (PC) and Bergmann glia (BG) density in P10 anterior (C-F) and posterior (I-L) cerebella using immunofluorescent detection of LIM1/2 and SOX2 (green, magenta) to mark Purkinje cells and Bergmann glia, respectively, and counterstained with DAPI (blue) in *Kif3c*$^{+/+}$ (C-D, I-J) and *Kif3c*$^{-/-}$ (E-F, K-L) cerebellar lobes. White arrowheads denote abnormally localized Bergmann glia. Quantitation of Purkinje cell (G) and Bergmann glia density (H) in anterior lobes of *Kif3c*$^{+/+}$ and *Kif3c*$^{-/-}$ P10 cerebella. Quantitation of Purkinje cell (G) and Bergmann glia density (H) in posterior lobes of *Kif3c*$^{+/+}$ and *Kif3c*$^{-/-}$ P10 cerebella. Each dot represents the average of 3 images per animal. Data are mean ± s.d. P-values were determined by a two-tailed Student's t-test.

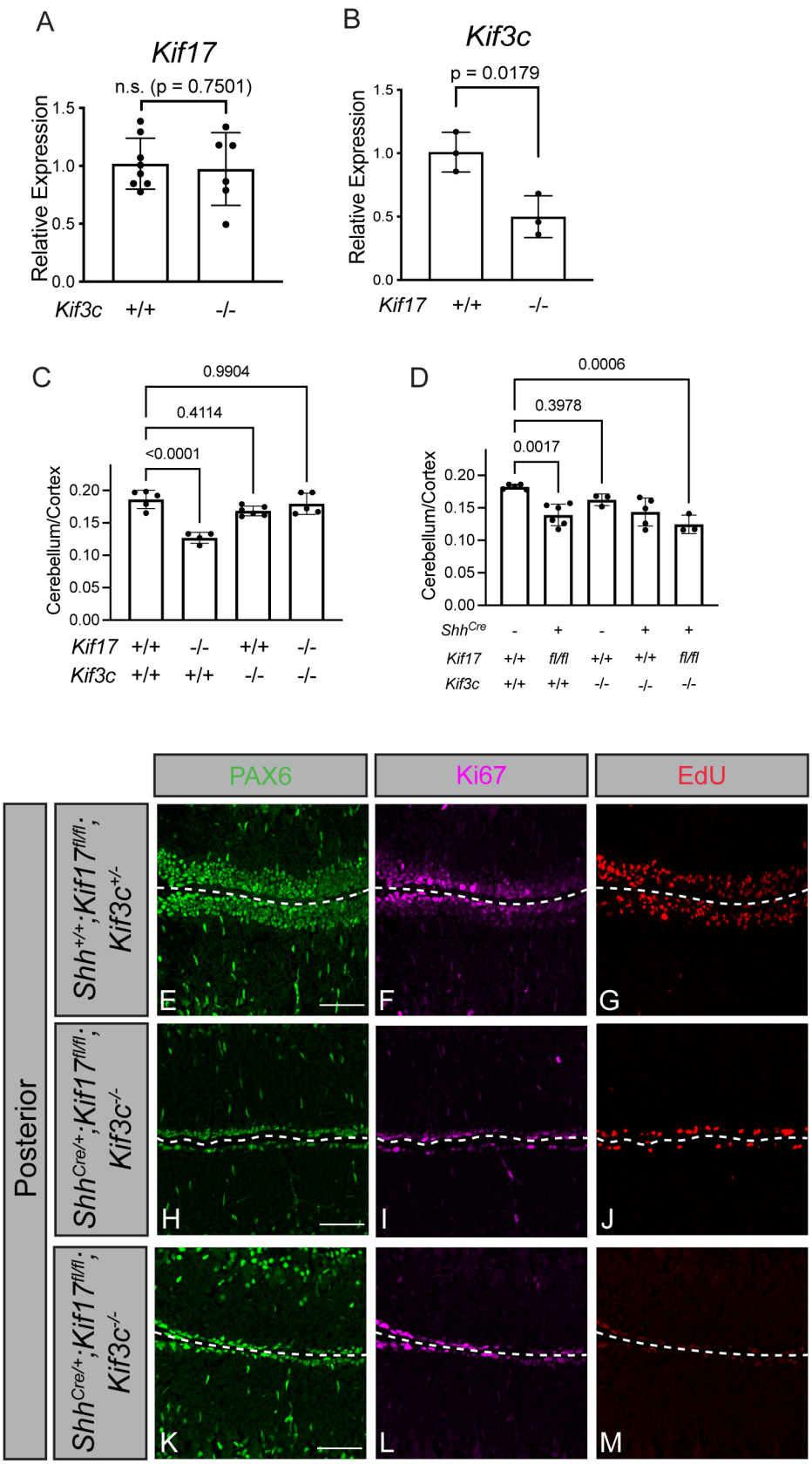
A
Kif17
n.s. (p = 0.7501)
Relative Expression
1.5
1.0
0.5
0.0
Kif3c +/+ -/-
B
Kif3c
p = 0.0179
Relative Expression
1.5
1.0
0.5
0.0
Kif17 +/+ -/-
C
0.9904
0.4114
<0.0001
Cerebellum/Cortex
0.20
0.15
0.10
0.05
0.00
Kif17 +/+ -/- +/+ -/-
Kif3c +/+ +/+ -/- -/-
D
0.0006
0.3978
0.0017
Cerebellum/Cortex
0.20
0.15
0.10
0.05
0.00
ShhCre - + - + +
Kif17 +/+ fl/fl +/+ +/+ fl/fl
Kif3c +/+ +/+ -/- -/- -/-
PAX6
Ki67
EdU
Posterior
Shh+/+;Kif17fl/fl;Kif3c+/-
ShhCre/+;Kif17fl/fl;Kif3c-/-
ShhCre/+;Kif17fl/fl;Kif3c-/-
E
F
G
H
I
J
K
L
M

Figure 3.6 Germline *Kif3c* deletion and Purkinje cell-specific *Kif17* deletion results in cerebellar hypoplasia and reduced CGNP proliferation.

RT-qPCR detection of *Kif17* expression (A) in P10 $Kif3c^{+/+}$ and $Kif3c^{-/-}$ cerebella. RT-qPCR detection of *Kif3c* expression (B) in P10 $Kif17^{+/+}$ and $Kif17^{-/-}$ cerebella. Quantitation of cerebellar weight normalized to cortical weight in *Kif3c;Kif17* germline compound mutants (C) at postnatal day 10. Quantitation of cerebellar weight normalized to cortical weight in *Kif3c* germline;*Kif17* PC conditional deletion compound mutants (D) at postnatal day 10. Each dot represents an individual animal. Data are mean ± s.d. P-values were determined by a two-tailed Student's t-test (A, B) or one way ANOVA analysis (C, D). Immunofluorescent analysis of CGNP proliferation in the posterior lobes of P10 $Kif3c^{+/-};Kif17^{fl/fl}$ (E-G) and $Shh^{Cre/+};Kif17^{fl/fl};Kif3c^{-/-}$ (H-M) cerebella. Antibody detection of PAX6 (green; E, H, K) and Ki67 (magenta; F, I, L). Fluorescent azide detection of EdU (red; G, J, M). Scale bars (E, H, K), 50μm. Dashed line separates individual external granule layers.

3.10 References

Adachi, T., Miyashita, S., Yamashita, M., Shimoda, M., Okonechnikov, K., Chavez, L., Kool, M., Pfister, S.M., Inoue, T., Kawauchi, D., and Hoshino, M. (2021). Notch Signaling between Cerebellar Granule Cell Progenitors. eNeuro *8*. 10.1523/ENEURO.0468-20.2021.

Baas, P.W., Rao, A.N., Matamoros, A.J., and Leo, L. (2016). Stability properties of neuronal microtubules. Cytoskeleton (Hoboken) *73*, 442-460. 10.1002/cm.21286.

Bowie, E., and Goetz, S.C. (2020). TTBK2 and primary cilia are essential for the connectivity and survival of cerebellar Purkinje neurons. Elife *9*. 10.7554/eLife.51166.

Carpenter, B.S., Barry, R.L., Verhey, K.J., and Allen, B.L. (2015). The heterotrimeric kinesin-2 complex interacts with and regulates GLI protein function. J Cell Sci *128*, 1034-1050. 10.1242/jcs.162552.

Corrales, J.D., Blaess, S., Mahoney, E.M., and Joyner, A.L. (2006). The level of sonic hedgehog signaling regulates the complexity of cerebellar foliation. Development *133*, 1811-1821. 10.1242/dev.02351.

Dahmane, N., and Ruiz i Altaba, A. (1999). Sonic hedgehog regulates the growth and patterning of the cerebellum. Development *126*, 3089-3100. 10.1242/dev.126.14.3089.

Engelke, M.F., Waas, B., Kearns, S.E., Suber, A., Boss, A., Allen, B.L., and Verhey, K.J. (2019). Acute Inhibition of Heterotrimeric Kinesin-2 Function Reveals Mechanisms of Intraflagellar Transport in Mammalian Cilia. Curr Biol *29*, 1137-1148 e1134. 10.1016/j.cub.2019.02.043.

Evans, J.E., Snow, J.J., Gunnarson, A.L., Ou, G., Stahlberg, H., McDonald, K.L., and Scholey, J.M. (2006). Functional modulation of IFT kinesins extends the sensory repertoire of ciliated neurons in Caenorhabditis elegans. J Cell Biol *172*, 663-669. 10.1083/jcb.200509115.

Goodrich, L.V., Milenkovic, L., Higgins, K.M., and Scott, M.P. (1997). Altered neural cell fates and medulloblastoma in mouse patched mutants. Science *277*, 1109-1113. 10.1126/science.277.5329.1109.

Gumy, L.F., Chew, D.J., Tortosa, E., Katrukha, E.A., Kapitein, L.C., Tolkovsky, A.M., Hoogenraad, C.C., and Fawcett, J.W. (2013). The kinesin-2 family member KIF3C regulates microtubule dynamics and is required for axon growth and regeneration. J Neurosci *33*, 11329-11345. 10.1523/JNEUROSCI.5221-12.2013.

Guzik-Lendrum, S., Rayment, I., and Gilbert, S.P. (2017). Homodimeric Kinesin-2 KIF3CC Promotes Microtubule Dynamics. Biophys J *113*, 1845-1857. 10.1016/j.bpj.2017.09.015.

Han, Y., Xiong, Y., Shi, X., Wu, J., Zhao, Y., and Jiang, J. (2017). Regulation of Gli ciliary localization and Hedgehog signaling by the PY-NLS/karyopherin-beta2 nuclear import system. PLoS Biol *15*, e2002063. 10.1371/journal.pbio.2002063.

Hiraoka, Y., Komine, O., Nagaoka, M., Bai, N., Hozumi, K., and Tanaka, K. (2013). Delta-like 1 regulates Bergmann glial monolayer formation during cerebellar development. Mol Brain *6*, 25. 10.1186/1756-6606-6-25.

Hirokawa, N., Noda, Y., Tanaka, Y., and Niwa, S. (2009). Kinesin superfamily motor proteins and intracellular transport. Nat Rev Mol Cell Biol *10*, 682-696. 10.1038/nrm2774.

Hor, C.H.H., Lo, J.C.W., Cham, A.L.S., Leong, W.Y., and Goh, E.L.K. (2021). Multifaceted Functions of Rab23 on Primary Cilium-Mediated and Hedgehog Signaling-Mediated Cerebellar Granule Cell Proliferation. J Neurosci *41*, 6850-6863. 10.1523/JNEUROSCI.3005-20.2021.

Huangfu, D., Liu, A., Rakeman, A.S., Murcia, N.S., Niswander, L., and Anderson, K.V. (2003). Hedgehog signalling in the mouse requires intraflagellar transport proteins. Nature *426*, 83-87. 10.1038/nature02061.

Insinna, C., Pathak, N., Perkins, B., Drummond, I., and Besharse, J.C. (2008). The homodimeric kinesin, Kif17, is essential for vertebrate photoreceptor sensory outer segment development. Dev Biol *316*, 160-170. 10.1016/j.ydbio.2008.01.025.

Izzi, L., Levesque, M., Morin, S., Laniel, D., Wilkes, B.C., Mille, F., Krauss, R.S., McMahon, A.P., Allen, B.L., and Charron, F. (2011). Boc and Gas1 each form distinct Shh receptor complexes with Ptch1 and are required for Shh-mediated cell proliferation. Dev Cell *20*, 788-801. 10.1016/j.devcel.2011.04.017.

Jimeno, D., Lillo, C., Roberts, E.A., Goldstein, L.S., and Williams, D.S. (2006). Kinesin-2 and photoreceptor cell death: requirement of motor subunits. Exp Eye Res *82*, 351-353. 10.1016/j.exer.2005.10.026.

Komine, O., Nagaoka, M., Watase, K., Gutmann, D.H., Tanigaki, K., Honjo, T., Radtke, F., Saito, T., Chiba, S., and Tanaka, K. (2007). The monolayer formation of Bergmann glial cells is regulated by Notch/RBP-J signaling. Dev Biol *311*, 238-250. 10.1016/j.ydbio.2007.08.042.

Leto, K., Arancillo, M., Becker, E.B., Buffo, A., Chiang, C., Ding, B., Dobyns, W.B., Dusart, I., Haldipur, P., Hatten, M.E., et al. (2016). Consensus Paper: Cerebellar Development. Cerebellum *15*, 789-828. 10.1007/s12311-015-0724-2.

Lewis, P.M., Gritli-Linde, A., Smeyne, R., Kottmann, A., and McMahon, A.P. (2004). Sonic hedgehog signaling is required for expansion of granule neuron precursors and patterning of the mouse cerebellum. Dev Biol *270*, 393-410. 10.1016/j.ydbio.2004.03.007.

Lewis, T.R., Kundinger, S.R., Link, B.A., Insinna, C., and Besharse, J.C. (2018). Kif17 phosphorylation regulates photoreceptor outer segment turnover. BMC Cell Biol *19*, 25. 10.1186/s12860-018-0177-9.

Lewis, T.R., Kundinger, S.R., Pavlovich, A.L., Bostrom, J.R., Link, B.A., and Besharse, J.C. (2017). Cos2/Kif7 and Osm-3/Kif17 regulate onset of outer segment development in zebrafish

photoreceptors through distinct mechanisms. Dev Biol *425*, 176-190. 10.1016/j.ydbio.2017.03.019.

Louvi, A., and Artavanis-Tsakonas, S. (2006). Notch signalling in vertebrate neural development. Nat Rev Neurosci *7*, 93-102. 10.1038/nrn1847.

Madison, B.B., Braunstein, K., Kuizon, E., Portman, K., Qiao, X.T., and Gumucio, D.L. (2005). Epithelial hedgehog signals pattern the intestinal crypt-villus axis. Development *132*, 279-289. 10.1242/dev.01576.

Nonaka, S., Tanaka, Y., Okada, Y., Takeda, S., Harada, A., Kanai, Y., Kido, M., and Hirokawa, N. (1998). Randomization of left-right asymmetry due to loss of nodal cilia generating leftward flow of extraembryonic fluid in mice lacking KIF3B motor protein. Cell *95*, 829-837. 10.1016/s0092-8674(00)81705-5.

Shimokawa, T., Tostar, U., Lauth, M., Palaniswamy, R., Kasper, M., Toftgard, R., and Zaphiropoulos, P.G. (2008). Novel human glioma-associated oncogene 1 (GLI1) splice variants reveal distinct mechanisms in the terminal transduction of the hedgehog signal. J Biol Chem *283*, 14345-14354. 10.1074/jbc.M800299200.

Snow, J.J., Ou, G., Gunnarson, A.L., Walker, M.R., Zhou, H.M., Brust-Mascher, I., and Scholey, J.M. (2004). Two anterograde intraflagellar transport motors cooperate to build sensory cilia on C. elegans neurons. Nat Cell Biol *6*, 1109-1113. 10.1038/ncb1186.

Solecki, D.J., Liu, X.L., Tomoda, T., Fang, Y., and Hatten, M.E. (2001). Activated Notch2 signaling inhibits differentiation of cerebellar granule neuron precursors by maintaining proliferation. Neuron *31*, 557-568. 10.1016/s0896-6273(01)00395-6.

Spassky, N., Han, Y.G., Aguilar, A., Strehl, L., Besse, L., Laclef, C., Ros, M.R., Garcia-Verdugo, J.M., and Alvarez-Buylla, A. (2008). Primary cilia are required for cerebellar development and Shh-dependent expansion of progenitor pool. Dev Biol *317*, 246-259. 10.1016/j.ydbio.2008.02.026.

Takeda, S., Yonekawa, Y., Tanaka, Y., Okada, Y., Nonaka, S., and Hirokawa, N. (1999). Left-right asymmetry and kinesin superfamily protein KIF3A: new insights in determination of laterality and mesoderm induction by kif3A-/- mice analysis. J Cell Biol *145*, 825-836. 10.1083/jcb.145.4.825.

Wang, S., Tanaka, Y., Xu, Y., Takeda, S., and Hirokawa, N. (2022). KIF3B promotes a PI3K signaling gradient causing changes in a Shh protein gradient and suppressing polydactyly in mice. Dev Cell *57*, 2273-2289 e2211. 10.1016/j.devcel.2022.09.007.

Wechsler-Reya, R.J., and Scott, M.P. (1999). Control of neuronal precursor proliferation in the cerebellum by Sonic Hedgehog. Neuron *22*, 103-114. 10.1016/s0896-6273(00)80682-0.

Weller, M., Krautler, N., Mantei, N., Suter, U., and Taylor, V. (2006). Jagged1 ablation results in cerebellar granule cell migration defects and depletion of Bergmann glia. Dev Neurosci *28*, 70-80. 10.1159/000090754.

Yang, Z., Roberts, E.A., and Goldstein, L.S. (2001). Functional analysis of mouse kinesin motor Kif3C. Mol Cell Biol *21*, 5306-5311. 10.1128/MCB.21.16.5306-5311.2001.

Yin, X., Takei, Y., Kido, M.A., and Hirokawa, N. (2011). Molecular motor KIF17 is fundamental for memory and learning via differential support of synaptic NR2A/2B levels. Neuron *70*, 310-325. 10.1016/j.neuron.2011.02.049.

Zhang, H., Takeda, H., Tsuji, T., Kamiya, N., Rajderkar, S., Louie, K., Collier, C., Scott, G., Ray, M., Mochida, Y., et al. (2015). Generation of Evc2/Limbin global and conditional KO mice and its roles during mineralized tissue formation. Genesis *53*, 612-626. 10.1002/dvg.22879.

Zhao, C., Omori, Y., Brodowska, K., Kovach, P., and Malicki, J. (2012). Kinesin-2 family in vertebrate ciliogenesis. Proc Natl Acad Sci U S A *109*, 2388-2393. 10.1073/pnas.1116035109.

Chapter 4 Discussion and Future Directions

4.1 Summary of Findings

The primary focus for my thesis has been investigating roles for two accessory kinesin-2 motors, KIF17 and KIF3C, in cerebellar development. KIF3A/KIF3B, the main anterograde motor has a well-established role in ciliogenesis and HH signaling. Specifically, both subunits are required for mouse ciliogenesis and cilia maintenance (Engelke *et al*., 2019; Nonaka *et al*., 1998; Takeda *et al*., 1999). Additionally, KIF3A has been demonstrated to bind and regulate GLI transcription factors (Carpenter *et al*., 2015). Unlike KIF3A/KIF3B, loss of either accessory kinesin-2 motor (KIF17 or KIF3C) does not result in any obvious ciliary defects in mouse embryogenesis (Lewis *et al*., 2017; Yang *et al*., 2001; Yin *et al*., 2011). However, these accessory kinesin motors have been implicated in neuronal function (Gumy *et al*., 2013; Yin *et al*., 2011), but they have not been investigated for a role in cerebellar development or HH signaling. In short, my thesis demonstrated two conflicting roles for KIF17 in HH-dependent cerebellar development and a novel role for KIF3C in Notch-dependent patterning in the developing cerebellum.

In chapter 2, I investigated the role(s) of homodimeric KIF17 during cerebellar development. *Kif17* expression was noted in SHH-producing Purkinje cells and HH-responsive CGNPs. Deletion of *Kif17* in Purkinje cells phenocopies germline *Kif17* deletion, resulting in reduced EGL thickness due to decreased CGNP proliferation and reduced HH target gene expression. The loss-of-function phenotype was due to reduced levels of SHH protein observed in Purkinje cells in *Kif17*$^{-/-}$ cerebella. In opposition, CGNP-specific *Kif17* deletion increased HH

target gene expression and EGL thickness due to increased CGNP proliferation. The gain-of-function phenotype was due to reduced levels of $GLI3^R$ in this cell type. This work identifies dual and opposing roles for KIF17 in HH-dependent cerebellar development– first, as a positive regulator of HH signaling through regulation of SHH protein levels within Purkinje cells, and second, as a negative regulator of HH signaling through regulation of GLI transcription factors in CGNPs.

In chapter 3, I explored the contribution of KIF3C to the postnatal cerebellum. Differing from *Kif17*, *Kif3c* expression was detected ubiquitously in the cerebellum. Germline *Kif3c* mutants displayed cerebellar hypoplasia, albeit less severe than *Kif17* germline or Purkinje cell deletion animals. Notably, even with reduced CGNP proliferation, HH signaling remains intact in *Kif3c*$^{-/-}$ cerebella. In addition to decreased expression of Notch target, *Hes1*, we observed abnormal patterning of Bergmann glia in *Kif3c* mutants. Collectively, these data demonstrate KIF3C's requirement in the cerebellum and suggest a novel role in regulating Notch signaling during development.

4.2 Future Directions

4.2.1 Molecular Mechanisms of HH signaling in the Developing Cerebellum

In chapter 2, we demonstrate KIF17 is required for proper levels of SHH ligand. Immunofluorescent detection of SHH revealed reduced levels but no change in localization with *Kif17* deletion (Figure 2.8J-N). Using an antibody which recognizes the C-terminal domain, we observed SHH within the Golgi/ER and cell bodies of Purkinje cells. SHH is initially translated as a 45 kDa precursor including an N-terminal signal sequence, N-terminal signaling molecule and

C-terminal domain (Figure 1.3). Autocleavage of the C-terminal fragment results in cholesterol modification to the C-terminus of the active N-terminal fragment (Lee *et al.*, 1994; Porter *et al.*, 1996a; Porter *et al.*, 1995; Porter *et al.*, 1996b). The C-terminal fragment is not sufficient to drive a HH gain-of-function phenotype (Porter *et al.*, 1995), however full length HH retains a significant level of activity (Tokhunts *et al.*, 2010). In NIH/3T3 and 293T cells, the C-terminal fragment is degraded within the ER (Chen *et al.*, 2011). However, within the developing *Drosophila* retina, the C-terminal domain has been shown to drive localization of the N-terminal ligand to the axons and growth cones of neurons (Chu *et al.*, 2006). Cleaved N-HH is retained in the retina, while the full length HH was transported down axons (Daniele *et al.*, 2017).

The SHH signal we visualized in the cell bodies of Purkinje cells could be the cleaved 25 kDa fragment or unprocessed full length SHH. It remains to be investigated if the C-terminal domain is degraded in the ER or required for trafficking or localization of SHH in cerebellar Purkinje cells. Robust detection of SHH, perhaps through utilization of SHH:GFP mice or tagging SHH with a smaller epitope tag on either the C-terminus or N-terminus (HA:SHH or SHH:HA) will be crucial to understanding SHH processing that occurs in Purkinje cells.

Importantly, CGNPs that lay along the basement membrane display the highest levels of *Gli1* expression, yet they reside furthest from Purkinje cells (Figure 1.5). Additionally, we do not observe a gradient of *Gli1* expression within CGNs that lay closest to Purkinje cells, unlike HH signaling in the neural tube and the developing limb. Is this effect cholesterol-dependent? Or does the C-terminal fragment mediate transport of N-SHH away from the cell body of Purkinje cells?

SCUBE2 function has not been assessed in cerebellar development.

SCUBE2 is believed to drive long-range HH signaling through increasing SHH solubility in the extracellular environment in a cholesterol-dependent manner (Creanga *et al.*, 2012; Hollway *et al.*, 2006; Kawakami *et al.*, 2005; Tukachinsky *et al.*, 2012; Woods and Talbot, 2005). In zebrafish, loss of all SCUBE family members results in a total lack of HH activity (Johnson *et al.*, 2012), while compound mutants of *Scube* in mice have not been published. Individual *Scube2* or *Scube3* deletion in mice does not result in embryonic lethality, but these mice display a defect in endochondral bone formation, a phenotype associated with HH loss-of-function (Lin *et al.*, 2021; Lin *et al.*, 2015). SCUBE contribution to cerebellar development has not been published. We detected *Scube2* expression in wildtype cerebella (Figure 2.8E-F), and we detected *Scube1* and *Scube3* expression in P10 cerebella through RT-qPCR (Figure 4.1A-B). Using data from the Allen Developing Mouse Brain Atlas, *Scube1* expression is detected within Purkinje cells (Figure 4.1C-D). Analysis of individual mutants and compound mutants in mouse embryogenesis and cerebellar morphogenesis will provide insight whether the mechanisms of SHH release are evolutionarily conserved between mice and zebrafish. Analysis of the levels of HH signaling in the Bergmann glia and CGNs versus CGNPs in *Scube* mutants will determine if SCUBE contributes to long-range HH signaling in this tissue. Considering *Kif17* and *Gli1* expression is highest in the posterior lobes of the cerebellum [Figure 2.2A-B, (Corrales *et al.*, 2004)], it will be important to assess if *Scube* family members also display the same pattern of expression.

Cleaved form of BOC is observed in developing cerebellum.

In chapter 2, we investigated if *Kif17* deletion does impacts the abundance of HH co-receptor, BOC (Figure 2.9B-E). Levels of full-length BOC were not altered (Figure 2.9D-E), but we did observe a band at ~110 kDa in postnatal day 10 samples that was not observed in adult

cerebella (Figure 2.9D). Previous work demonstrated BOC has two extracellular cleavage sites, but secreted BOC did not promote HH signal transduction in chick neural tube electroporation experiments (Song et al., 2015). Instead of functioning in the HH responsive cells, BOC could contribute in the SHH-producing cells. HH co-receptor, BOC, can also act further upstream in the pathway than previously thought (Hall *et al*., 2021). It has been demonstrated BOC has a role in cytoneme delivery of SHH (Hall *et al*., 2021). Purkinje cells do express *Boc*, and $Boc^{-/-}$ cerebella display a cell autonomous defect in HH signal transduction in CGNPs [(Izzi *et al*., 2011), Figure 2.11H]. Function of BOC in Purkinje cells has not yet been investigated.

It will be important to validate the BOC western blot using $Boc^{-/-}$ cerebellar tissue from P10. Cell culture media collected from CGNPs and Bergmann glia cultures *in vitro* would be ideal samples to narrow down which cell population(s) are secreting BOC, as there are well-established protocols to grow these two cell types in culture. Purkinje cells isolation and culture methods are currently lacking, but BOC function could be directly assessed through conditional deletion of *Boc* using Shh^{Cre}. Examination of secreted BOC in the developing cerebellum will provide exciting insight into an unknown mechanism of HH signaling.

Reduced levels of GLI3 are sufficient to activate HH signaling in CGNPs during development but not initiation of medulloblastoma.

In chapter 2, we show reduced levels of GLI3 ($Gli3^{+/-}$) were sufficient to cause cerebellar hyperplasia. Further, we demonstrate reduced levels of all three GLIs (GLI1, GLI2 and GLI3) in $Atoh1Cre;Kif17^{fl/fl}$ CGNPs resulted in a HH-gain-of-function phenotype: increased CGNP proliferation and upregulation of HH target genes. These data suggest the reduction of $GLI3^{R}$ is sufficient to activate HH target gene expression in CGNPs. Previous work establishes that GLI1

and GLI2 act as transcriptional activators in the developing cerebellum, but only loss of *Gli2* results in HH loss-of-function phenotype (Corrales *et al*., 2006; Corrales *et al*., 2004). While GLI3 repressor functions in setting up the cerebellum during embryonic development, GLI3 function has not yet been examined in the postnatal cerebellum (Blaess *et al*., 2006; Blaess *et al*., 2008).

Inactivating mutations of *Ptch1* are found in approximately 20% of medulloblastoma cases (Goodrich *et al*., 1997). Additionally, *Sufu* deletion results in a HH gain-of-function phenotype with significant patterning defects (Jiwani *et al*., 2020), as does the loss of RAB23 (Hor *et al*., 2021). Neither medulloblastoma nor patterning defects were detected in $Kif17^{lacZ/lacZ}$, $Atoh1Cre;Kif17^{fl/fl}$ cerebella, suggesting KIF17 regulation of HH signaling is downstream of PTCH1. Furthermore, these data suggest reduced levels of $GLI3^{R}$ are not sufficient to initiate medulloblastoma. It will be important to directly assess if *Gli3* deletion can result in medulloblastoma using conditional deletion ($Atoh1Cre;Gli3^{fl/fl}$) in future work. Evaluating if *Kif17* is differentially expressed in medulloblastoma would be of interest for potential therapeutics, as well as investigating if KIF17 overexpression can restrict medulloblastoma growth.

Active HH signaling is observed in the adult cerebellum.

Expression of HH pathway components has been observed in the adult cerebellum. In particular, *Shh* expression remains in Purkinje cells, while *Gli1*, *Gli2* and *Gli3* are expressed in Bergmann glia and CGNs (Corrales *et al*., 2004). However, it is unknown what the role(s) of HH signaling has in the adult cerebellum. I observed that $Gli1^{lacZ}$ cerebella are sensitive to HH inhibition with LDE225 (Figure 4.2C-D), while $Gli2^{lacZ}$ and $Gli3^{lacZ}$ cerebella do not display changes with LDE225 treatment (Figure 4.2E-H). The reduction of $Gli1^{lacZ}$ activity suggests that HH signaling is indeed active in the adult cerebellum. To determine what the function of HH

signaling is in the adult tissue, use of endogenously tagged *Gli* alleles would make experiments like ChIP-seq or CUT&RUN feasible to determine what genes are downstream of HH activation or repression. Identification of downstream genes would then provide insight to what the function of HH signaling in the adult cerebellum could be. Apoptosis should also be examined with inhibition of HH signaling, as HH is known to promote survival. Could long term inhibition of HH signaling result dysfunction in cerebellar homeostasis or cerebellar ataxia?

Genetic background affects cerebellar development

Mouse genetic backgrounds have been demonstrated to be vital in assessing HH-dependent phenotypes [reviewed in (Hong and Krauss, 2018)]. In severe cases, pups can be born and survive in some genetic backgrounds while that same mutation in other genetic backgrounds result in embryonic lethality (Mecklenburg et al., 2020). In chapter 2, I examined the loss of *Kif17* in two congenic backgrounds – C57BL/6J and 129S4/SvJaeJ (Figure 2.2S, Figure 2.3K). In C57BL/6J, *Kif17* germline deletion results in reduced cerebellar size, while cerebellar size of *Kif17* mutant mice on a 129S4/SvJaeJ background trend upwards. Two possibilities arise from these conflicting data – another kinesin can compensate for the loss of KIF17 in Purkinje cells or loss KIF17 in CGNPs results in a more prominent gain-of-function phenotype on a congenic 129S4/SvJaeJ background.

KIF3C is a candidate for a compensating kinesin. Consistent with this possibility, *Kif3c* expression is reduced in *Kif17* germline mutants on C57BL/6J background (Figure 3.6B). Analysis of *Kif3c* expression in *Kif17*$^{-/-}$ cerebella on a 129S4/SvJaeJ background will be essential to determine if *Kif3c* expression is increased. Further, examination of *Kif3c* expression across the

different cerebellar cell types, in particular Purkinje cells, of *Kif17* mutants on both genetic backgrounds will reveal which cell types could be responsible for compensation.

If this phenotype is not due to compensation, then *Kif17*$^{-/-}$ CGNPs proliferation rate could be driving the difference between the phenotypes on C57BL/6J and 129S4/SvJaeJ backgrounds. Levels of GLI3^{R} will be crucial to analyze in *Kif17* mutants on a 129S4/SvJaeJ background, as reduced levels GLI3 can control cerebellar size (Figure 2.10K). Assessing *in vitro* proliferation rates of *Kif17*$^{-/-}$ CGNPs isolated from on C57BL/6J and 129S4/SvJaeJ backgrounds will reveal any changes in the cell autonomous defect in *Kif17* mutants. Furthermore, sensitivity to HH stimulation could differ in these two genetic backgrounds. Examination of CGNP proliferative response to SAG *in vitro* in both genetic backgrounds will assess any differences in sensitivity to HH stimulation. These data could provide insight to the mechanistic insight to the difference in severity of HH phenotypes across genetic backgrounds.

4.2.2 KIF17 Regulation of HH Signaling

KIF17 interacts with full length SHH and N-SHH

In chapter 2, we demonstrate KIF17 overexpression in COS7 cells increases the abundance of full length SHH:GFP intracellularly and extracellularly, while N-SHH is increased intracellularly (Figure 2.8G-I, Figure 2.9F-H). Furthermore, immunoprecipitation of KIF17:HA followed by western blot reveal KIF17 can interact with full length SHH:GFP; N-SHH can also be detected, albeit at a reduced level (Figure 4.3). Considering intracellular SHH is contained within vesicles, this interaction is likely mediated through an unidentified adaptor protein. MINT1/Lin-10 has a described role as KIF17's adaptor protein in the hippocampus (Guillaud *et al*., 2003; Guillaud *et al*., 2008; Setou *et al*., 2000), and *Lin-10* is expressed in the Purkinje cell

layer (Nakajima et al., 2001). A possible model for KIF17/SHH interaction is that Lin-10 binds to vesicles containing SHH and to the tail domain KIF17 in Purkinje cells. Assessing whether Lin-10 mediates the interaction between KIF17 and SHH will provide important mechanistic data, as Lin-10 release of KIF17 is associated with CaMKII phosphorylation of KIF17's tail domain (Guillaud *et al*., 2008). Examination of the effects of CaMKII phosphorylation sites on KIF17's tail domain on intracellular/extracellular SHH abundance will shed light on the contribution of KIF17 to SHH targeting in Purkinje cells.

Further mapping the interaction between SHH and KIF17 will also provide insights on the mechanism of KIF17 function in Purkinje cells. Further, the observation KIF17 can interact with both full length SHH and N-SHH suggest the interaction is dependent on residues in the N-terminus fragment. This raises the possibility that the interaction is reliant on palmitoylation on the N-terminus. Repeating KIF17/SHH experiments with forms of SHH which cannot be palmitoylated (SHH^{C24S}) will reveal if palmitoylation is required for KIF17 interaction. Furthermore, we observe KIF17 pulls down full length SHH:GFP more efficiently than N-SHH, suggesting there is an additional site on the C-terminal fragment required for interaction or that the interaction can be accentuated with cholesterol modification. Experiments using constructs of SHH that cannot undergo autocleavage or only containing SHH C-terminal fragment will distinguish between these two possibilities.

Lastly, it has been observed removal of KIF17's motor domain does not impact localization in overexpression experiments (Jiang *et al*., 2015; Williams *et al*., 2014). Examination of SHH abundance in the cell lysate and media using a KIF17 construct lacking the motor domain will provide insight to whether motor activity is required for increased SHH abundance extracellularly. If we observe increased abundance of SHH in the cell media with a motorless

KIF17 construct, this provides evidence that KIF17 increases the stability of SHH protein rather controlling its localization. These gain-of-function experiments will provide more insight to KIF17's contribution to SHH ligand during cerebellar development.

Determining if KIF17's regulation of SHH is dependent on SCUBE2 or DISP1.

With *Kif17* deletion, we observed reduced expression of *Scube2* (Figure 2.8E-F). Moreover, expression of *Scube1* and *Scube3* trend downwards *Kif17*$^{-/-}$ cerebella (Figure 4.1A-B), demonstrating *Scube* family members are affected by *Kif17* deletion. Examination of *Scube* family members in *Shh* conditional deletion cerebella (*En2Cre;Shh*$^{fl/fl}$ or *Shh*$^{CreER/lacZ}$) will determine if decreased *Scube* expression is directly due to *Kif17* deletion or whether reduced levels of SHH protein impacts *Scube* expression. Another essential component of SHH release is DISP1; DISP mediates the release of dually lipidated HH ligand from HH-producing cells (Burke *et al.*, 1999; Caspary *et al.*, 2002; Kawakami *et al.*, 2002; Ma *et al.*, 2002; Tian *et al.*, 2005a). Expression and function of *Disp1* have not been examined in the cerebellum, and whether *Kif17* expression impacts *Disp1* expression will be of interest for furthering the mechanism of KIF17 regulation of SHH.

To determine whether KIF17 contributes to SCUBE or DISP1-mediated SHH release, intracellular and extracellular SHH levels could be examined in COS7 cells expressing KIF17 with SCUBE2 or DISP1. Further, utilization of *Scube2*$^{-/-}$ or *Disp1*$^{-/-}$ mouse embryonic fibroblasts as loss-of-function approach in KIF17/SHH overexpression experiments will be crucial. Together, these experiments will discover if KIF17 is upstream or downstream of SCUBE2 or DISP1 for its contribution to SHH in the cerebellum.

KIF17 increases HH signaling in luciferase reporter assay.

In opposition to KIF17's repressive role in CGNPs, I have found that KIF17 overexpression can increase the level of HH signaling in a luciferase reporter assay in NIH/3T3 cells (Figure 4.4). KIF17 has two autoinhibition mechanisms (Hammond *et al.*, 2010). First, a region of the tail domain binds to the motor domain to prevent microtubule binding, while another region in the coiled-coiled 2 domain also binds to the motor to prevent processive movement (Hammond *et al.*, 2010). Importantly, *Kif17* expression is not noted in NIH/3T3 cells, which suggests overexpressed KIF17 is inactive. Consistent with this notion, I do not observe an increase in HH activity when the wildtype form of KIF17 is overexpressed, while there is a significant increase in HH activity in cells transfected with a constitutively active form of KIF17 ($KIF17^{G754E}$). It will be important for future studies to evaluate whether the increase in HH signaling in NIH/3T3 cells with $KIF17^{G754E}$ is associated with a change in ciliary length or altered ciliary or nuclear localization of GLI transcription factors. These data highlight the importance of evaluating cell-specific roles of HH pathway components. Can this activator role of GLIs for KIF17 be observed in other HH-dependent tissues?

KIF17 regulation of GLIs through SUFU.

In chapter 2, I observed reduced ciliary localization of SUFU in *Kif17* deletion CGNPs (Figure 2.14J-R). Similar to KIF17, SUFU has been demonstrated to restrict CGNP proliferation through promoting GLI3 repressor formation (Humke *et al.*, 2010; Jiwani *et al.*, 2020). This is analogous to the effect on GLI protein abundance in CGNPs with *Kif17* deletion (Figure 2.15A-F). These data suggest a mechanism that KIF17 regulates SUFU ciliary localization and therefore SUFU-GLI interaction. Another possibility is that KIF17 independently affects GLI stability. In

support of the latter hypothesis, SUFU ciliary localization is reduced when *Gli2* and *Gli3* are deleted (Tukachinsky *et al.*, 2010). It will be important to evaluate GLI nuclear localization in conditional *Kif17* deletion CGNPs, as disruption of SUFU-GLI1 interaction results in constitute nuclear localization (Dunaeva *et al.*, 2003; Svard *et al.*, 2006). If there is increased GLI nuclear localization in conditional *Kif17* deletion CGNPs, this would shed light on the gain-of-function phenotype in this cell type. Instead of acting through $GLI3^{R}$, loss of KIF17 could increase nuclear GLI activator, resulting upregulation of HH target genes and increased CGNP proliferation. Future studies examining SUFU-GLI interactions in the absence of *Kif17* will be essential to understanding the molecular mechanism of GLI processing in CGNPs.

4.2.3 KIF3C in Embryogenesis

In chapter 3, the loss of *Kif3c* was investigated in the developing cerebellum. Previous literature reported *Kif3c* is not expressed embryonically (Gumy *et al*., 2013; Yang *et al*., 2001). Consistent with these observations, analysis of *Kif3c* mutant embryos at E10.5 do not reveal any significant defects in embryogenesis (Figure 4.5A-D). However, whole mount *in situ* hybridization reveal *Kif3c* is expressed in E16.5 brains (Figure 4.5E-H). Further, embryonic dissections reveal some *Kif3c* mutants display abnormal face development (Figure 4.5I-K). Specifically, some $Kif3c^{-/-}$ embryos display a shortened snout, lower ear and eye placement. This phenotype is not completely penetrant, as surviving $Kif3c^{-/-}$ pups and adults are indistinguishable from their littermates. Examination of more embryos will be essential to evaluate KIF3C contribution to the development of the face.

4.3 Figures

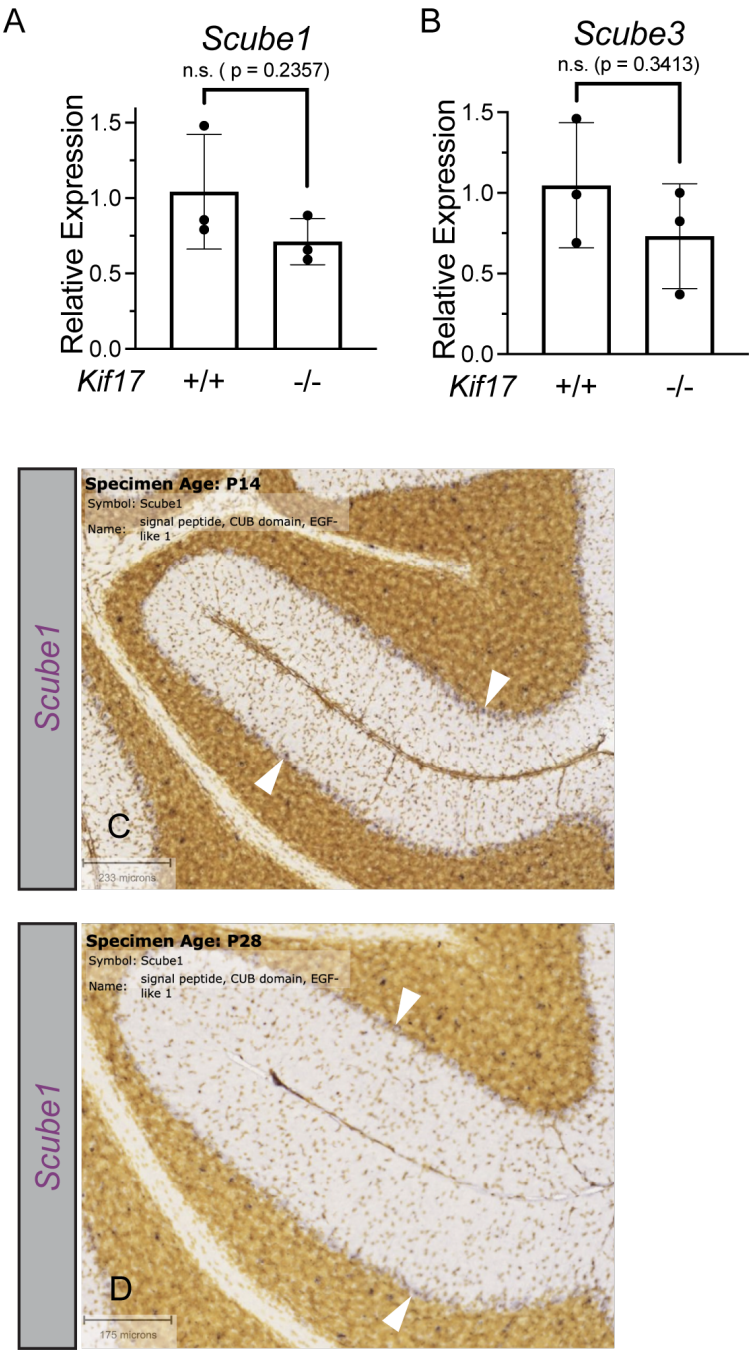

Figure 4.1 *Scube* expression in the cerebellum.

Expression of *Scube1* (A) and *Scube3* (B) measured through RT-qPCR in P10 *Kif17*$^{+/+}$ and *Kif17*$^{-/-}$ cerebella.

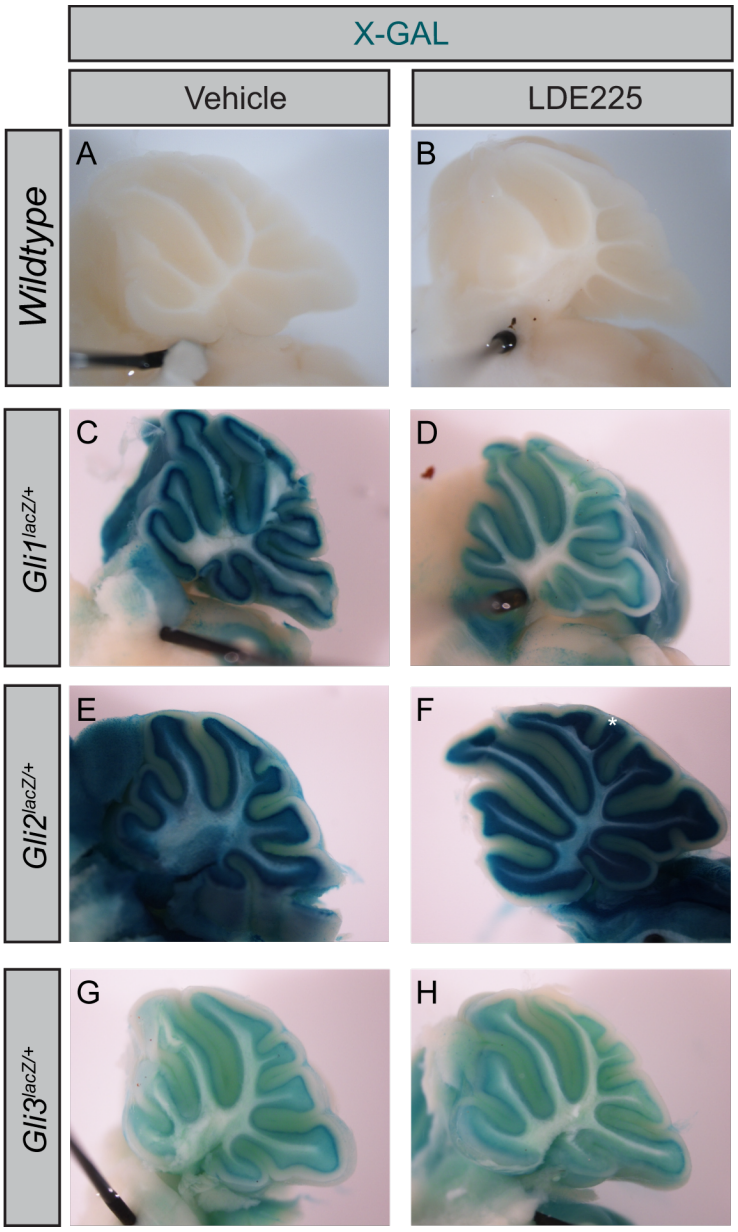

Figure 4.2 Expression of GLI proteins in the adult cerebellum treated HH inhibitor, LDE225.

Whole mount X-GAL stain (blue) of wildtype (A-B), $Gli1^{lacZ/+}$ (C-D), $Gli2^{lacZ/+}$ (E-F), $Gli3^{lacZ/+}$ (G-H) adult cerebella, where animals were treated with vehicle (A, C, E, F) or HH inhibitor, LDE225 (B, D, F, H).

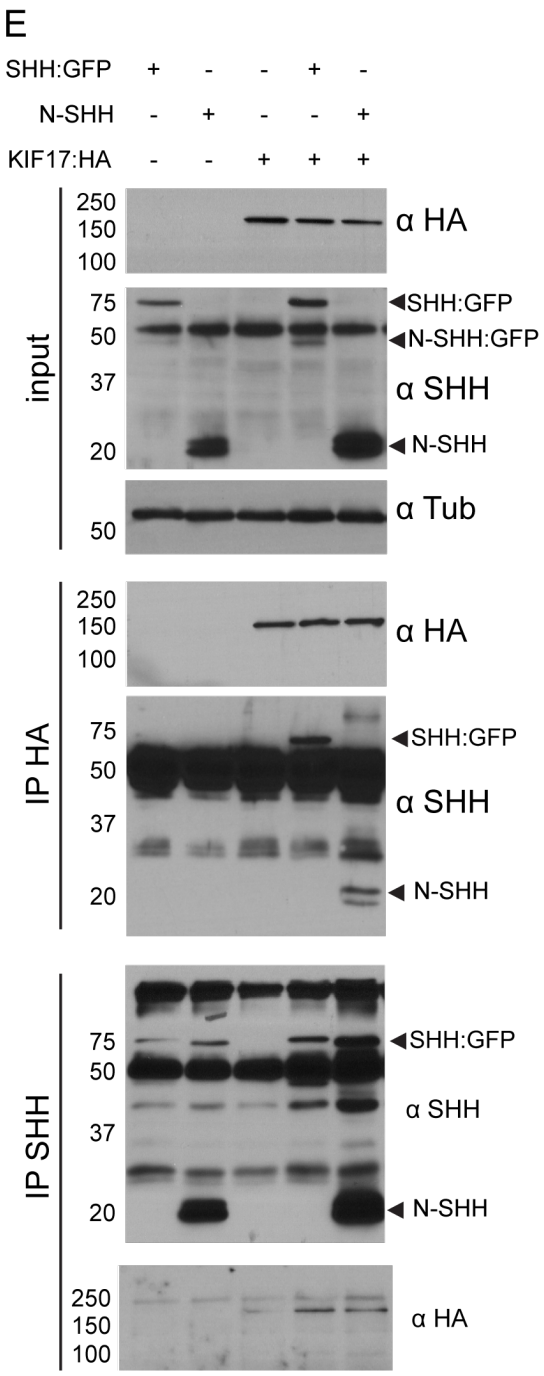

Figure 4.3 KIF17 and SHH physically interact.

Immunoprecipitation of HA-tagged KIF17 (KIF17:HA) from COS-7 cells co-expressing either full length SHH tagged with GFP (SHH:GFP) or N terminal SHH (N-SHH). Immunoprecipitates (IP) and cell lysates (input) were subjected to SDS-PAGE and western blot analysis using antibodies directed against SHH (α-SHH) and HA (α-HA). Antibody detection of β-tubulin (α-Tub) was used to confirm equal loading across lanes. The molecular masses (in kDa) of protein standards are indicated at the left of each blot. Arrowheads denote full length SHH:GFP (68 kDa), N-SHH:GFP (42 kDa) or N-SHH (19 kDa).

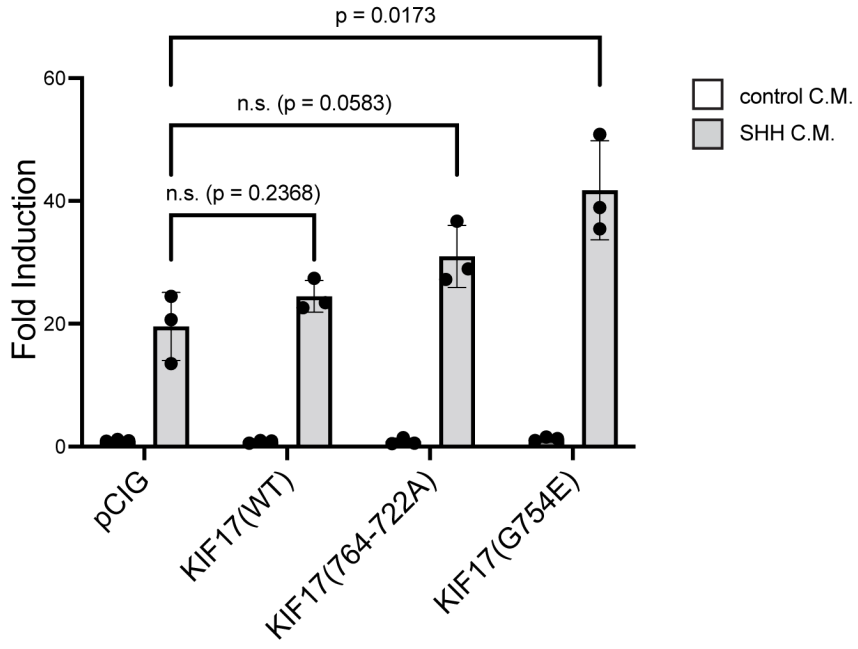

Figure 4.4 Constitutively active KIF17 increase HH activity in luciferase assay in NIH/3T3 cells.

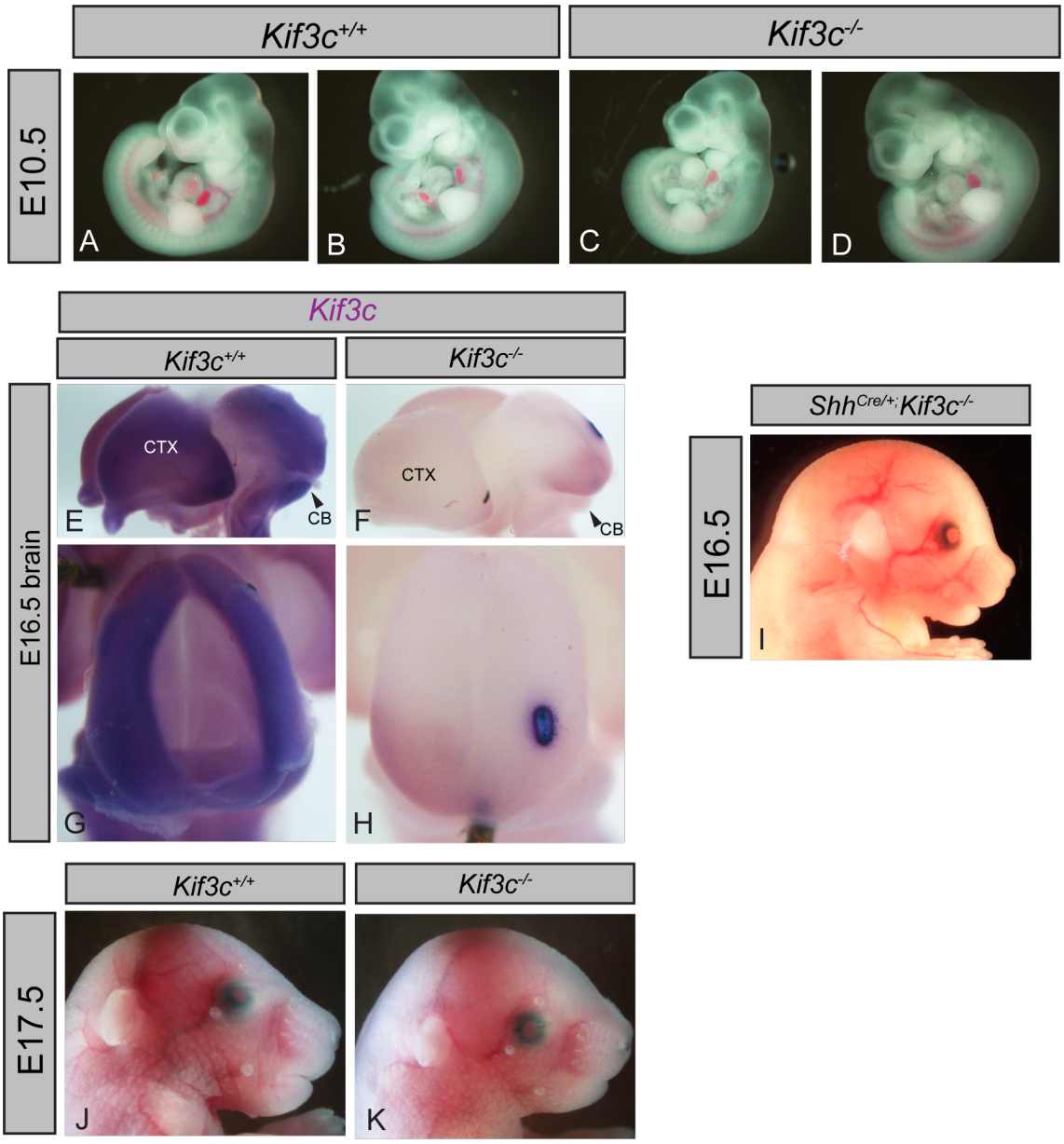

Figure 4.5 Preliminary analysis of KIF3C contribution to embryogenesis.

Dissecting scope images of E10.5 (A-D) of *Kif3c*$^{+/+}$ (A-B) and *Kif3c*$^{-/-}$ embryos. Whole mount in situ hybridization of Kif3c in E16.5 brains of *Kif3c*$^{+/+}$ (E, G) and *Kif3c*$^{-/-}$ (F, H). CTX denotes cortex; CB denotes cerebellum. Dissecting scope images of E16.5 *Shh*$^{Cre/+}$;*Kif3c*$^{-/-}$ embryo, E17.5 *Kif3c*$^{+/+}$ (J) and *Kif3c*$^{-/-}$ (K) embryos.

4.4 References

Aberger, F., and Ruiz i Altaba, A. (2014). Context-dependent signal integration by the GLI code: the oncogenic load, pathways, modifiers and implications for cancer therapy. Semin Cell Dev Biol *33*, 93-104. 10.1016/j.semcdb.2014.05.003.

Adachi, T., Miyashita, S., Yamashita, M., Shimoda, M., Okonechnikov, K., Chavez, L., Kool, M., Pfister, S.M., Inoue, T., Kawauchi, D., and Hoshino, M. (2021). Notch Signaling between Cerebellar Granule Cell Progenitors. eNeuro *8*. 10.1523/ENEURO.0468-20.2021.

Ahn, S., and Joyner, A.L. (2005). In vivo analysis of quiescent adult neural stem cells responding to Sonic hedgehog. Nature *437*, 894-897. 10.1038/nature03994.

Aizawa, H., Sekine, Y., Takemura, R., Zhang, Z., Nangaku, M., and Hirokawa, N. (1992). Kinesin family in murine central nervous system. J Cell Biol *119*, 1287-1296. 10.1083/jcb.119.5.1287.

Alder, J., Lee, K.J., Jessell, T.M., and Hatten, M.E. (1999). Generation of cerebellar granule neurons in vivo by transplantation of BMP-treated neural progenitor cells. Nat Neurosci *2*, 535-540. 10.1038/9189.

Alexandre, C., Jacinto, A., and Ingham, P.W. (1996). Transcriptional activation of hedgehog target genes in Drosophila is mediated directly by the cubitus interruptus protein, a member of the GLI family of zinc finger DNA-binding proteins. Genes Dev *10*, 2003-2013. 10.1101/gad.10.16.2003.

Allen, B.L., Song, J.Y., Izzi, L., Althaus, I.W., Kang, J.S., Charron, F., Krauss, R.S., and McMahon, A.P. (2011). Overlapping roles and collective requirement for the coreceptors GAS1, CDO, and BOC in SHH pathway function. Dev Cell *20*, 775-787. 10.1016/j.devcel.2011.04.018.

Allen, B.L., Tenzen, T., and McMahon, A.P. (2007). The Hedgehog-binding proteins Gas1 and Cdo cooperate to positively regulate Shh signaling during mouse development. Genes Dev *21*, 1244-1257. 10.1101/gad.1543607.

Allen, R.D., Metuzals, J., Tasaki, I., Brady, S.T., and Gilbert, S.P. (1982). Fast axonal transport in squid giant axon. Science *218*, 1127-1129. 10.1126/science.6183744.

Amanai, K., and Jiang, J. (2001). Distinct roles of Central missing and Dispatched in sending the Hedgehog signal. Development *128*, 5119-5127. 10.1242/dev.128.24.5119.

Anne, S.L., Govek, E.E., Ayrault, O., Kim, J.H., Zhu, X., Murphy, D.A., Van Aelst, L., Roussel, M.F., and Hatten, M.E. (2013). WNT3 inhibits cerebellar granule neuron progenitor proliferation and medulloblastoma formation via MAPK activation. PLoS One *8*, e81769. 10.1371/journal.pone.0081769.

Anthony, T.E., and Heintz, N. (2008). Genetic lineage tracing defines distinct neurogenic and gliogenic stages of ventral telencephalic radial glial development. Neural Dev *3*, 30. 10.1186/1749-8104-3-30.

Awan, A., Bernstein, M., Hamasaki, T., and Satir, P. (2004). Cloning and characterization of Kin5, a novel Tetrahymena ciliary kinesin II. Cell Motil Cytoskeleton *58*, 1-9. 10.1002/cm.10170.

Aza-Blanc, P., Ramirez-Weber, F.A., Laget, M.P., Schwartz, C., and Kornberg, T.B. (1997). Proteolysis that is inhibited by hedgehog targets Cubitus interruptus protein to the nucleus and converts it to a repressor. Cell *89*, 1043-1053. 10.1016/s0092-8674(00)80292-5.

Baas, P.W., Rao, A.N., Matamoros, A.J., and Leo, L. (2016). Stability properties of neuronal microtubules. Cytoskeleton (Hoboken) *73*, 442-460. 10.1002/cm.21286.

Bai, C.B., Auerbach, W., Lee, J.S., Stephen, D., and Joyner, A.L. (2002). Gli2, but not Gli1, is required for initial Shh signaling and ectopic activation of the Shh pathway. Development *129*, 4753-4761. 10.1242/dev.129.20.4753.
Bai, C.B., and Joyner, A.L. (2001). Gli1 can rescue the in vivo function of Gli2. Development *128*, 5161-5172. 10.1242/dev.128.24.5161.
Bai, C.B., Stephen, D., and Joyner, A.L. (2004). All mouse ventral spinal cord patterning by hedgehog is Gli dependent and involves an activator function of Gli3. Dev Cell *6*, 103-115. 10.1016/s1534-5807(03)00394-0.
Bangs, F., and Anderson, K.V. (2017). Primary Cilia and Mammalian Hedgehog Signaling. Cold Spring Harb Perspect Biol *9*. 10.1101/cshperspect.a028175.
Bitgood, M.J., and McMahon, A.P. (1995). Hedgehog and Bmp genes are coexpressed at many diverse sites of cell-cell interaction in the mouse embryo. Dev Biol *172*, 126-138. 10.1006/dbio.1995.0010.
Bitgood, M.J., Shen, L., and McMahon, A.P. (1996). Sertoli cell signaling by Desert hedgehog regulates the male germline. Curr Biol *6*, 298-304. 10.1016/s0960-9822(02)00480-3.
Blaess, S., Corrales, J.D., and Joyner, A.L. (2006). Sonic hedgehog regulates Gli activator and repressor functions with spatial and temporal precision in the mid/hindbrain region. Development *133*, 1799-1809. 10.1242/dev.02339.
Blaess, S., Stephen, D., and Joyner, A.L. (2008). Gli3 coordinates three-dimensional patterning and growth of the tectum and cerebellum by integrating Shh and Fgf8 signaling. Development *135*, 2093-2103. 10.1242/dev.015990.
Blasius, T.L., Cai, D., Jih, G.T., Toret, C.P., and Verhey, K.J. (2007). Two binding partners cooperate to activate the molecular motor Kinesin-1. J Cell Biol *176*, 11-17. 10.1083/jcb.200605099.
Bowie, E., and Goetz, S.C. (2020). TTBK2 and primary cilia are essential for the connectivity and survival of cerebellar Purkinje neurons. Elife *9*. 10.7554/eLife.51166.
Brady, S.T., Lasek, R.J., and Allen, R.D. (1982). Fast axonal transport in extruded axoplasm from squid giant axon. Science *218*, 1129-1131. 10.1126/science.6183745.
Breunig, J.J., Sarkisian, M.R., Arellano, J.I., Morozov, Y.M., Ayoub, A.E., Sojitra, S., Wang, B., Flavell, R.A., Rakic, P., and Town, T. (2008). Primary cilia regulate hippocampal neurogenesis by mediating sonic hedgehog signaling. Proc Natl Acad Sci U S A *105*, 13127-13132. 10.1073/pnas.0804558105.
Brown, C.L., Maier, K.C., Stauber, T., Ginkel, L.M., Wordeman, L., Vernos, I., and Schroer, T.A. (2005). Kinesin-2 is a motor for late endosomes and lysosomes. Traffic *6*, 1114-1124. 10.1111/j.1600-0854.2005.00347.x.
Bumcrot, D.A., Takada, R., and McMahon, A.P. (1995). Proteolytic processing yields two secreted forms of sonic hedgehog. Mol Cell Biol *15*, 2294-2303. 10.1128/MCB.15.4.2294.
Burke, R., Nellen, D., Bellotto, M., Hafen, E., Senti, K.A., Dickson, B.J., and Basler, K. (1999). Dispatched, a novel sterol-sensing domain protein dedicated to the release of cholesterol-modified hedgehog from signaling cells. Cell *99*, 803-815. 10.1016/s0092-8674(00)81677-3.
Buttitta, L., Mo, R., Hui, C.C., and Fan, C.M. (2003). Interplays of Gli2 and Gli3 and their requirement in mediating Shh-dependent sclerotome induction. Development *130*, 6233-6243. 10.1242/dev.00851.
Butts, T., Green, M.J., and Wingate, R.J. (2014). Development of the cerebellum: simple steps to make a 'little brain'. Development *141*, 4031-4041. 10.1242/dev.106559.

Carpenter, B.S., Barry, R.L., Verhey, K.J., and Allen, B.L. (2015). The heterotrimeric kinesin-2 complex interacts with and regulates GLI protein function. J Cell Sci *128*, 1034-1050. 10.1242/jcs.162552.
Caspary, T., Garcia-Garcia, M.J., Huangfu, D., Eggenschwiler, J.T., Wyler, M.R., Rakeman, A.S., Alcorn, H.L., and Anderson, K.V. (2002). Mouse Dispatched homolog1 is required for long-range, but not juxtacrine, Hh signaling. Curr Biol *12*, 1628-1632. 10.1016/s0960-9822(02)01147-8.
Chamoun, Z., Mann, R.K., Nellen, D., von Kessler, D.P., Bellotto, M., Beachy, P.A., and Basler, K. (2001). Skinny hedgehog, an acyltransferase required for palmitoylation and activity of the hedgehog signal. Science *293*, 2080-2084. 10.1126/science.1064437.
Chang, C.H., Zanini, M., Shirvani, H., Cheng, J.S., Yu, H., Feng, C.H., Mercier, A.L., Hung, S.Y., Forget, A., Wang, C.H., et al. (2019). Atoh1 Controls Primary Cilia Formation to Allow for SHH-Triggered Granule Neuron Progenitor Proliferation. Dev Cell *48*, 184-199 e185. 10.1016/j.devcel.2018.12.017.
Chen, M.H., Li, Y.J., Kawakami, T., Xu, S.M., and Chuang, P.T. (2004). Palmitoylation is required for the production of a soluble multimeric Hedgehog protein complex and long-range signaling in vertebrates. Genes Dev *18*, 641-659. 10.1101/gad.1185804.
Chen, M.H., Wilson, C.W., Li, Y.J., Law, K.K., Lu, C.S., Gacayan, R., Zhang, X., Hui, C.C., and Chuang, P.T. (2009). Cilium-independent regulation of Gli protein function by Sufu in Hedgehog signaling is evolutionarily conserved. Genes Dev *23*, 1910-1928. 10.1101/gad.1794109.
Chen, X., Tukachinsky, H., Huang, C.H., Jao, C., Chu, Y.R., Tang, H.Y., Mueller, B., Schulman, S., Rapoport, T.A., and Salic, A. (2011). Processing and turnover of the Hedgehog protein in the endoplasmic reticulum. J Cell Biol *192*, 825-838. 10.1083/jcb.201008090.
Chen, Y., Cardinaux, J.R., Goodman, R.H., and Smolik, S.M. (1999). Mutants of cubitus interruptus that are independent of PKA regulation are independent of hedgehog signaling. Development *126*, 3607-3616. 10.1242/dev.126.16.3607.
Chen, Y., and Struhl, G. (1996). Dual roles for patched in sequestering and transducing Hedgehog. Cell *87*, 553-563. 10.1016/s0092-8674(00)81374-4.
Cheng, F.Y., Fleming, J.T., and Chiang, C. (2018). Bergmann glial Sonic hedgehog signaling activity is required for proper cerebellar cortical expansion and architecture. Dev Biol *440*, 152-166. 10.1016/j.ydbio.2018.05.015.
Chennathukuzhi, V., Morales, C.R., El-Alfy, M., and Hecht, N.B. (2003). The kinesin KIF17b and RNA-binding protein TB-RBP transport specific cAMP-responsive element modulator-regulated mRNAs in male germ cells. Proc Natl Acad Sci U S A *100*, 15566-15571. 10.1073/pnas.2536695100.
Chu, T., Chiu, M., Zhang, E., and Kunes, S. (2006). A C-terminal motif targets Hedgehog to axons, coordinating assembly of the Drosophila eye and brain. Dev Cell *10*, 635-646. 10.1016/j.devcel.2006.03.003.
Chung, U.I., Schipani, E., McMahon, A.P., and Kronenberg, H.M. (2001). Indian hedgehog couples chondrogenesis to osteogenesis in endochondral bone development. J Clin Invest *107*, 295-304. 10.1172/JCI11706.
Clark, A.M., Garland, K.K., and Russell, L.D. (2000). Desert hedgehog (Dhh) gene is required in the mouse testis for formation of adult-type Leydig cells and normal development of peritubular cells and seminiferous tubules. Biol Reprod *63*, 1825-1838. 10.1095/biolreprod63.6.1825.

Cobourne, M.T., Miletich, I., and Sharpe, P.T. (2004). Restriction of sonic hedgehog signalling during early tooth development. Development *131*, 2875-2885. 10.1242/dev.01163.
Cole, D.G., Chinn, S.W., Wedaman, K.P., Hall, K., Vuong, T., and Scholey, J.M. (1993). Novel heterotrimeric kinesin-related protein purified from sea urchin eggs. Nature *366*, 268-270. 10.1038/366268a0.
Corbit, K.C., Aanstad, P., Singla, V., Norman, A.R., Stainier, D.Y., and Reiter, J.F. (2005). Vertebrate Smoothened functions at the primary cilium. Nature *437*, 1018-1021. 10.1038/nature04117.
Corrales, J.D., Blaess, S., Mahoney, E.M., and Joyner, A.L. (2006). The level of sonic hedgehog signaling regulates the complexity of cerebellar foliation. Development *133*, 1811-1821. 10.1242/dev.02351.
Corrales, J.D., Rocco, G.L., Blaess, S., Guo, Q., and Joyner, A.L. (2004). Spatial pattern of sonic hedgehog signaling through Gli genes during cerebellum development. Development *131*, 5581-5590. 10.1242/dev.01438.
Creanga, A., Glenn, T.D., Mann, R.K., Saunders, A.M., Talbot, W.S., and Beachy, P.A. (2012). Scube/You activity mediates release of dually lipid-modified Hedgehog signal in soluble form. Genes Dev *26*, 1312-1325. 10.1101/gad.191866.112.
Cruz, C., Ribes, V., Kutejova, E., Cayuso, J., Lawson, V., Norris, D., Stevens, J., Davey, M., Blight, K., Bangs, F., et al. (2010). Foxj1 regulates floor plate cilia architecture and modifies the response of cells to sonic hedgehog signalling. Development *137*, 4271-4282. 10.1242/dev.051714.
Dahmane, N., and Ruiz i Altaba, A. (1999). Sonic hedgehog regulates the growth and patterning of the cerebellum. Development *126*, 3089-3100. 10.1242/dev.126.14.3089.
Dai, P., Akimaru, H., Tanaka, Y., Maekawa, T., Nakafuku, M., and Ishii, S. (1999). Sonic Hedgehog-induced activation of the Gli1 promoter is mediated by GLI3. J Biol Chem *274*, 8143-8152. 10.1074/jbc.274.12.8143.
Daniele, J.R., Chu, T., and Kunes, S. (2017). A novel proteolytic event controls Hedgehog intracellular sorting and distribution to receptive fields. Biol Open *6*, 540-550. 10.1242/bio.024083.
Dimassi, S., Labalme, A., Ville, D., Calender, A., Mignot, C., Boutry-Kryza, N., de Bellescize, J., Rivier-Ringenbach, C., Bourel-Ponchel, E., Cheillan, D., et al. (2016). Whole-exome sequencing improves the diagnosis yield in sporadic infantile spasm syndrome. Clin Genet *89*, 198-204. 10.1111/cge.12636.
Ding, Q., Fukami, S., Meng, X., Nishizaki, Y., Zhang, X., Sasaki, H., Dlugosz, A., Nakafuku, M., and Hui, C. (1999). Mouse suppressor of fused is a negative regulator of sonic hedgehog signaling and alters the subcellular distribution of Gli1. Curr Biol *9*, 1119-1122. 10.1016/s0960-9822(99)80482-5.
Ding, Q., Motoyama, J., Gasca, S., Mo, R., Sasaki, H., Rossant, J., and Hui, C.C. (1998). Diminished Sonic hedgehog signaling and lack of floor plate differentiation in Gli2 mutant mice. Development *125*, 2533-2543. 10.1242/dev.125.14.2533.
Dishinger, J.F., Kee, H.L., Jenkins, P.M., Fan, S., Hurd, T.W., Hammond, J.W., Truong, Y.N., Margolis, B., Martens, J.R., and Verhey, K.J. (2010). Ciliary entry of the kinesin-2 motor KIF17 is regulated by importin-beta2 and RanGTP. Nat Cell Biol *12*, 703-710. 10.1038/ncb2073.
Dominguez, M., Brunner, M., Hafen, E., and Basler, K. (1996). Sending and receiving the hedgehog signal: control by the Drosophila Gli protein Cubitus interruptus. Science *272*, 1621-1625. 10.1126/science.272.5268.1621.

Dunaeva, M., Michelson, P., Kogerman, P., and Toftgard, R. (2003). Characterization of the physical interaction of Gli proteins with SUFU proteins. J Biol Chem *278*, 5116-5122. 10.1074/jbc.M209492200.
Echelard, Y., Epstein, D.J., St-Jacques, B., Shen, L., Mohler, J., McMahon, J.A., and McMahon, A.P. (1993). Sonic hedgehog, a member of a family of putative signaling molecules, is implicated in the regulation of CNS polarity. Cell *75*, 1417-1430. 10.1016/0092-8674(93)90627-3.
Eggenschwiler, J.T., Bulgakov, O.V., Qin, J., Li, T., and Anderson, K.V. (2006). Mouse Rab23 regulates hedgehog signaling from smoothened to Gli proteins. Dev Biol *290*, 1-12. 10.1016/j.ydbio.2005.09.022.
Eggenschwiler, J.T., Espinoza, E., and Anderson, K.V. (2001). Rab23 is an essential negative regulator of the mouse Sonic hedgehog signalling pathway. Nature *412*, 194-198. 10.1038/35084089.
Elliott, K.H., Chen, X., Salomone, J., Chaturvedi, P., Schultz, P.A., Balchand, S.K., Servetas, J.D., Zuniga, A., Zeller, R., Gebelein, B., et al. (2020). Gli3 utilizes Hand2 to synergistically regulate tissue-specific transcriptional networks. Elife *9*. 10.7554/eLife.56450.
Endoh-Yamagami, S., Evangelista, M., Wilson, D., Wen, X., Theunissen, J.W., Phamluong, K., Davis, M., Scales, S.J., Solloway, M.J., de Sauvage, F.J., and Peterson, A.S. (2009). The mammalian Cos2 homolog Kif7 plays an essential role in modulating Hh signal transduction during development. Curr Biol *19*, 1320-1326. 10.1016/j.cub.2009.06.046.
Engelke, M.F., Waas, B., Kearns, S.E., Suber, A., Boss, A., Allen, B.L., and Verhey, K.J. (2019). Acute Inhibition of Heterotrimeric Kinesin-2 Function Reveals Mechanisms of Intraflagellar Transport in Mammalian Cilia. Curr Biol *29*, 1137-1148 e1134. 10.1016/j.cub.2019.02.043.
Epstein, D.J., Marti, E., Scott, M.P., and McMahon, A.P. (1996). Antagonizing cAMP-dependent protein kinase A in the dorsal CNS activates a conserved Sonic hedgehog signaling pathway. Development *122*, 2885-2894. 10.1242/dev.122.9.2885.
Evans, J.E., Snow, J.J., Gunnarson, A.L., Ou, G., Stahlberg, H., McDonald, K.L., and Scholey, J.M. (2006). Functional modulation of IFT kinesins extends the sensory repertoire of ciliated neurons in Caenorhabditis elegans. J Cell Biol *172*, 663-669. 10.1083/jcb.200509115.
Falkenstein, K.N., and Vokes, S.A. (2014). Transcriptional regulation of graded Hedgehog signaling. Semin Cell Dev Biol *33*, 73-80. 10.1016/j.semcdb.2014.05.010.
Feng, J., White, B., Tyurina, O.V., Guner, B., Larson, T., Lee, H.Y., Karlstrom, R.O., and Kohtz, J.D. (2004). Synergistic and antagonistic roles of the Sonic hedgehog N- and C-terminal lipids. Development *131*, 4357-4370. 10.1242/dev.01301.
Gao, Y., Zheng, H., Li, L., Zhou, C., Chen, X., Zhou, X., and Cao, Y. (2020). KIF3C Promotes Proliferation, Migration, and Invasion of Glioma Cells by Activating the PI3K/AKT Pathway and Inducing EMT. Biomed Res Int *2020*, 6349312. 10.1155/2020/6349312.
Goetz, S.C., and Anderson, K.V. (2010). The primary cilium: a signalling centre during vertebrate development. Nat Rev Genet *11*, 331-344. 10.1038/nrg2774.
Goffinet, A.M. (1983). The embryonic development of the cerebellum in normal and reeler mutant mice. Anat Embryol (Berl) *168*, 73-86. 10.1007/BF00305400.
Goldstein, O., Gana-Weisz, M., Shiner, T., Attar, R., Mordechai, Y., Waldman, Y.Y., Bar-Shira, A., Thaler, A., Gurevich, T., Mirelman, A., et al. (2021). R869C mutation in molecular motor KIF17 gene is involved in dementia with Lewy bodies. Alzheimers Dement (Amst) *13*, e12143. 10.1002/dad2.12143.

Goodrich, L.V., Milenkovic, L., Higgins, K.M., and Scott, M.P. (1997). Altered neural cell fates and medulloblastoma in mouse patched mutants. Science *277*, 1109-1113. 10.1126/science.277.5329.1109.
Gorivodsky, M., Mukhopadhyay, M., Wilsch-Braeuninger, M., Phillips, M., Teufel, A., Kim, C., Malik, N., Huttner, W., and Westphal, H. (2009). Intraflagellar transport protein 172 is essential for primary cilia formation and plays a vital role in patterning the mammalian brain. Dev Biol *325*, 24-32. 10.1016/j.ydbio.2008.09.019.
Grimmond, S., Larder, R., Van Hateren, N., Siggers, P., Hulsebos, T.J., Arkell, R., and Greenfield, A. (2000). Cloning, mapping, and expression analysis of a gene encoding a novel mammalian EGF-related protein (SCUBE1). Genomics *70*, 74-81. 10.1006/geno.2000.6370.
Grimmond, S., Larder, R., Van Hateren, N., Siggers, P., Morse, S., Hacker, T., Arkell, R., and Greenfield, A. (2001). Expression of a novel mammalian epidermal growth factor-related gene during mouse neural development. Mech Dev *102*, 209-211. 10.1016/s0925-4773(00)00586-4.
Guillaud, L., Setou, M., and Hirokawa, N. (2003). KIF17 dynamics and regulation of NR2B trafficking in hippocampal neurons. J Neurosci *23*, 131-140. 10.1523/JNEUROSCI.23-01-00131.2003.
Guillaud, L., Wong, R., and Hirokawa, N. (2008). Disruption of KIF17-Mint1 interaction by CaMKII-dependent phosphorylation: a molecular model of kinesin-cargo release. Nat Cell Biol *10*, 19-29. 10.1038/ncb1665.
Gumy, L.F., Chew, D.J., Tortosa, E., Katrukha, E.A., Kapitein, L.C., Tolkovsky, A.M., Hoogenraad, C.C., and Fawcett, J.W. (2013). The kinesin-2 family member KIF3C regulates microtubule dynamics and is required for axon growth and regeneration. J Neurosci *33*, 11329-11345. 10.1523/JNEUROSCI.5221-12.2013.
Guo, A., Wang, T., Ng, E.L., Aulia, S., Chong, K.H., Teng, F.Y., Wang, Y., and Tang, B.L. (2006). Open brain gene product Rab23: expression pattern in the adult mouse brain and functional characterization. J Neurosci Res *83*, 1118-1127. 10.1002/jnr.20788.
Guzik-Lendrum, S., Rayment, I., and Gilbert, S.P. (2017). Homodimeric Kinesin-2 KIF3CC Promotes Microtubule Dynamics. Biophys J *113*, 1845-1857. 10.1016/j.bpj.2017.09.015.
Hall, E.T., Dillard, M.E., Stewart, D.P., Zhang, Y., Wagner, B., Levine, R.M., Pruett-Miller, S.M., Sykes, A., Temirov, J., Cheney, R.E., et al. (2021). Cytoneme delivery of Sonic Hedgehog from ligand-producing cells requires Myosin 10 and a Dispatched-BOC/CDON co-receptor complex. Elife *10*. 10.7554/eLife.61432.
Hammerschmidt, M., Bitgood, M.J., and McMahon, A.P. (1996). Protein kinase A is a common negative regulator of Hedgehog signaling in the vertebrate embryo. Genes Dev *10*, 647-658. 10.1101/gad.10.6.647.
Hammond, J.W., Blasius, T.L., Soppina, V., Cai, D., and Verhey, K.J. (2010). Autoinhibition of the kinesin-2 motor KIF17 via dual intramolecular mechanisms. J Cell Biol *189*, 1013-1025. 10.1083/jcb.201001057.
Han, Y., Xiong, Y., Shi, X., Wu, J., Zhao, Y., and Jiang, J. (2017). Regulation of Gli ciliary localization and Hedgehog signaling by the PY-NLS/karyopherin-beta2 nuclear import system. PLoS Biol *15*, e2002063. 10.1371/journal.pbio.2002063.
Han, Y.G., Spassky, N., Romaguera-Ros, M., Garcia-Verdugo, J.M., Aguilar, A., Schneider-Maunoury, S., and Alvarez-Buylla, A. (2008). Hedgehog signaling and primary cilia are required for the formation of adult neural stem cells. Nat Neurosci *11*, 277-284. 10.1038/nn2059.

Haque, F., Freniere, C., Ye, Q., Mani, N., Wilson-Kubalek, E.M., Ku, P.I., Milligan, R.A., and Subramanian, R. (2022). Cytoskeletal regulation of a transcription factor by DNA mimicry via coiled-coil interactions. Nat Cell Biol *24*, 1088-1098. 10.1038/s41556-022-00935-7.
Harfe, B.D., Scherz, P.J., Nissim, S., Tian, H., McMahon, A.P., and Tabin, C.J. (2004). Evidence for an expansion-based temporal Shh gradient in specifying vertebrate digit identities. Cell *118*, 517-528. 10.1016/j.cell.2004.07.024.
Haycraft, C.J., Banizs, B., Aydin-Son, Y., Zhang, Q., Michaud, E.J., and Yoder, B.K. (2005). Gli2 and Gli3 localize to cilia and require the intraflagellar transport protein polaris for processing and function. PLoS Genet *1*, e53. 10.1371/journal.pgen.0010053.
He, M., Agbu, S., and Anderson, K.V. (2017). Microtubule Motors Drive Hedgehog Signaling in Primary Cilia. Trends Cell Biol *27*, 110-125. 10.1016/j.tcb.2016.09.010.
He, M., Subramanian, R., Bangs, F., Omelchenko, T., Liem, K.F., Jr., Kapoor, T.M., and Anderson, K.V. (2014). The kinesin-4 protein Kif7 regulates mammalian Hedgehog signalling by organizing the cilium tip compartment. Nat Cell Biol *16*, 663-672. 10.1038/ncb2988.
Hiraoka, Y., Komine, O., Nagaoka, M., Bai, N., Hozumi, K., and Tanaka, K. (2013). Delta-like 1 regulates Bergmann glial monolayer formation during cerebellar development. Mol Brain *6*, 25. 10.1186/1756-6606-6-25.
Hirokawa, N., Noda, Y., Tanaka, Y., and Niwa, S. (2009). Kinesin superfamily motor proteins and intracellular transport. Nat Rev Mol Cell Biol *10*, 682-696. 10.1038/nrm2774.
Holloway, E.M., Czerwinski, M., Tsai, Y.H., Wu, J.H., Wu, A., Childs, C.J., Walton, K.D., Sweet, C.W., Yu, Q., Glass, I., et al. (2021). Mapping Development of the Human Intestinal Niche at Single-Cell Resolution. Cell Stem Cell *28*, 568-580 e564. 10.1016/j.stem.2020.11.008.
Hollway, G.E., Maule, J., Gautier, P., Evans, T.M., Keenan, D.G., Lohs, C., Fischer, D., Wicking, C., and Currie, P.D. (2006). Scube2 mediates Hedgehog signalling in the zebrafish embryo. Dev Biol *294*, 104-118. 10.1016/j.ydbio.2006.02.032.
Hong, M., and Krauss, R.S. (2018). Modeling the complex etiology of holoprosencephaly in mice. Am J Med Genet C Semin Med Genet *178*, 140-150. 10.1002/ajmg.c.31611.
Hooper, J.E., and Scott, M.P. (1989). The Drosophila patched gene encodes a putative membrane protein required for segmental patterning. Cell *59*, 751-765. 10.1016/0092-8674(89)90021-4.
Hor, C.H.H., Lo, J.C.W., Cham, A.L.S., Leong, W.Y., and Goh, E.L.K. (2021). Multifaceted Functions of Rab23 on Primary Cilium-Mediated and Hedgehog Signaling-Mediated Cerebellar Granule Cell Proliferation. J Neurosci *41*, 6850-6863. 10.1523/JNEUROSCI.3005-20.2021.
Huangfu, D., and Anderson, K.V. (2005). Cilia and Hedgehog responsiveness in the mouse. Proc Natl Acad Sci U S A *102*, 11325-11330. 10.1073/pnas.0505328102.
Huangfu, D., and Anderson, K.V. (2006). Signaling from Smo to Ci/Gli: conservation and divergence of Hedgehog pathways from Drosophila to vertebrates. Development *133*, 3-14. 10.1242/dev.02169.
Huangfu, D., Liu, A., Rakeman, A.S., Murcia, N.S., Niswander, L., and Anderson, K.V. (2003). Hedgehog signalling in the mouse requires intraflagellar transport proteins. Nature *426*, 83-87. 10.1038/nature02061.
Hui, C.C., and Angers, S. (2011). Gli proteins in development and disease. Annu Rev Cell Dev Biol *27*, 513-537. 10.1146/annurev-cellbio-092910-154048.
Humke, E.W., Dorn, K.V., Milenkovic, L., Scott, M.P., and Rohatgi, R. (2010). The output of Hedgehog signaling is controlled by the dynamic association between Suppressor of Fused and the Gli proteins. Genes Dev *24*, 670-682. 10.1101/gad.1902910.

Ingham, P.W., Nakano, Y., and Seger, C. (2011). Mechanisms and functions of Hedgehog signalling across the metazoa. Nat Rev Genet *12*, 393-406. 10.1038/nrg2984.
Insinna, C., Pathak, N., Perkins, B., Drummond, I., and Besharse, J.C. (2008). The homodimeric kinesin, Kif17, is essential for vertebrate photoreceptor sensory outer segment development. Dev Biol *316*, 160-170. 10.1016/j.ydbio.2008.01.025.
Irla, M., Saade, M., Fernandez, C., Chasson, L., Victorero, G., Dahmane, N., Chazal, G., and Nguyen, C. (2007). Neuronal distribution of spatial in the developing cerebellum and hippocampus and its somatodendritic association with the kinesin motor KIF17. Exp Cell Res *313*, 4107-4119. 10.1016/j.yexcr.2007.09.006.
Izzi, L., Levesque, M., Morin, S., Laniel, D., Wilkes, B.C., Mille, F., Krauss, R.S., McMahon, A.P., Allen, B.L., and Charron, F. (2011). Boc and Gas1 each form distinct Shh receptor complexes with Ptch1 and are required for Shh-mediated cell proliferation. Dev Cell *20*, 788-801. 10.1016/j.devcel.2011.04.017.
Jia, J., Amanai, K., Wang, G., Tang, J., Wang, B., and Jiang, J. (2002). Shaggy/GSK3 antagonizes Hedgehog signalling by regulating Cubitus interruptus. Nature *416*, 548-552. 10.1038/nature733.
Jia, J., Zhang, L., Zhang, Q., Tong, C., Wang, B., Hou, F., Amanai, K., and Jiang, J. (2005). Phosphorylation by double-time/CKIepsilon and CKIalpha targets cubitus interruptus for Slimb/beta-TRCP-mediated proteolytic processing. Dev Cell *9*, 819-830. 10.1016/j.devcel.2005.10.006.
Jiang, J., and Struhl, G. (1998). Regulation of the Hedgehog and Wingless signalling pathways by the F-box/WD40-repeat protein Slimb. Nature *391*, 493-496. 10.1038/35154.
Jiang, L., Tam, B.M., Ying, G., Wu, S., Hauswirth, W.W., Frederick, J.M., Moritz, O.L., and Baehr, W. (2015). Kinesin family 17 (osmotic avoidance abnormal-3) is dispensable for photoreceptor morphology and function. FASEB J *29*, 4866-4880. 10.1096/fj.15-275677.
Jimeno, D., Lillo, C., Roberts, E.A., Goldstein, L.S., and Williams, D.S. (2006). Kinesin-2 and photoreceptor cell death: requirement of motor subunits. Exp Eye Res *82*, 351-353. 10.1016/j.exer.2005.10.026.
Jiwani, T., Kim, J.J., and Rosenblum, N.D. (2020). Suppressor of fused controls cerebellum granule cell proliferation by suppressing Fgf8 and spatially regulating Gli proteins. Development *147*. 10.1242/dev.170274.
Johnson, J.L., Hall, T.E., Dyson, J.M., Sonntag, C., Ayers, K., Berger, S., Gautier, P., Mitchell, C., Hollway, G.E., and Currie, P.D. (2012). Scube activity is necessary for Hedgehog signal transduction in vivo. Dev Biol *368*, 193-202. 10.1016/j.ydbio.2012.05.007.
Kaesler, S., Luscher, B., and Ruther, U. (2000). Transcriptional activity of GLI1 is negatively regulated by protein kinase A. Biol Chem *381*, 545-551. 10.1515/BC.2000.070.
Kawakami, A., Nojima, Y., Toyoda, A., Takahoko, M., Satoh, M., Tanaka, H., Wada, H., Masai, I., Terasaki, H., Sakaki, Y., et al. (2005). The zebrafish-secreted matrix protein you/scube2 is implicated in long-range regulation of hedgehog signaling. Curr Biol *15*, 480-488. 10.1016/j.cub.2005.02.018.
Kawakami, T., Kawcak, T., Li, Y.J., Zhang, W., Hu, Y., and Chuang, P.T. (2002). Mouse dispatched mutants fail to distribute hedgehog proteins and are defective in hedgehog signaling. Development *129*, 5753-5765. 10.1242/dev.00178.
Keady, B.T., Samtani, R., Tobita, K., Tsuchya, M., San Agustin, J.T., Follit, J.A., Jonassen, J.A., Subramanian, R., Lo, C.W., and Pazour, G.J. (2012). IFT25 links the signal-dependent

movement of Hedgehog components to intraflagellar transport. Dev Cell *22*, 940-951. 10.1016/j.devcel.2012.04.009.
Kerjan, G., Dolan, J., Haumaitre, C., Schneider-Maunoury, S., Fujisawa, H., Mitchell, K.J., and Chedotal, A. (2005). The transmembrane semaphorin Sema6A controls cerebellar granule cell migration. Nat Neurosci *8*, 1516-1524. 10.1038/nn1555.
Kim, J., Kato, M., and Beachy, P.A. (2009). Gli2 trafficking links Hedgehog-dependent activation of Smoothened in the primary cilium to transcriptional activation in the nucleus. Proc Natl Acad Sci U S A *106*, 21666-21671. 10.1073/pnas.0912180106.
Kimmins, S., Kotaja, N., Fienga, G., Kolthur, U.S., Brancorsini, S., Hogeveen, K., Monaco, L., and Sassone-Corsi, P. (2004). A specific programme of gene transcription in male germ cells. Reprod Biomed Online *8*, 496-500. 10.1016/s1472-6483(10)61094-2.
Kohtz, J.D., Lee, H.Y., Gaiano, N., Segal, J., Ng, E., Larson, T., Baker, D.P., Garber, E.A., Williams, K.P., and Fishell, G. (2001). N-terminal fatty-acylation of sonic hedgehog enhances the induction of rodent ventral forebrain neurons. Development *128*, 2351-2363. 10.1242/dev.128.12.2351.
Komine, O., Nagaoka, M., Watase, K., Gutmann, D.H., Tanigaki, K., Honjo, T., Radtke, F., Saito, T., Chiba, S., and Tanaka, K. (2007). The monolayer formation of Bergmann glial cells is regulated by Notch/RBP-J signaling. Dev Biol *311*, 238-250. 10.1016/j.ydbio.2007.08.042.
Kondo, S., Sato-Yoshitake, R., Noda, Y., Aizawa, H., Nakata, T., Matsuura, Y., and Hirokawa, N. (1994). KIF3A is a new microtubule-based anterograde motor in the nerve axon. J Cell Biol *125*, 1095-1107. 10.1083/jcb.125.5.1095.
Kotaja, N., Lin, H., Parvinen, M., and Sassone-Corsi, P. (2006). Interplay of PIWI/Argonaute protein MIWI and kinesin KIF17b in chromatoid bodies of male germ cells. J Cell Sci *119*, 2819-2825. 10.1242/jcs.03022.
Krauss, S., Concordet, J.P., and Ingham, P.W. (1993). A functionally conserved homolog of the Drosophila segment polarity gene hh is expressed in tissues with polarizing activity in zebrafish embryos. Cell *75*, 1431-1444. 10.1016/0092-8674(93)90628-4.
Lee, C.S., Buttitta, L., and Fan, C.M. (2001a). Evidence that the WNT-inducible growth arrest-specific gene 1 encodes an antagonist of sonic hedgehog signaling in the somite. Proc Natl Acad Sci U S A *98*, 11347-11352. 10.1073/pnas.201418298.
Lee, H.Y., Greene, L.A., Mason, C.A., and Manzini, M.C. (2009). Isolation and culture of post-natal mouse cerebellar granule neuron progenitor cells and neurons. J Vis Exp. 10.3791/990.
Lee, J.D., Kraus, P., Gaiano, N., Nery, S., Kohtz, J., Fishell, G., Loomis, C.A., and Treisman, J.E. (2001b). An acylatable residue of Hedgehog is differentially required in Drosophila and mouse limb development. Dev Biol *233*, 122-136. 10.1006/dbio.2001.0218.
Lee, J.J., Ekker, S.C., von Kessler, D.P., Porter, J.A., Sun, B.I., and Beachy, P.A. (1994). Autoproteolysis in hedgehog protein biogenesis. Science *266*, 1528-1537. 10.1126/science.7985023.
Lee, J.J., von Kessler, D.P., Parks, S., and Beachy, P.A. (1992). Secretion and localized transcription suggest a role in positional signaling for products of the segmentation gene hedgehog. Cell *71*, 33-50. 10.1016/0092-8674(92)90264-d.
Leto, K., Arancillo, M., Becker, E.B., Buffo, A., Chiang, C., Ding, B., Dobyns, W.B., Dusart, I., Haldipur, P., Hatten, M.E., et al. (2016). Consensus Paper: Cerebellar Development. Cerebellum *15*, 789-828. 10.1007/s12311-015-0724-2.
Lewis, P.M., Dunn, M.P., McMahon, J.A., Logan, M., Martin, J.F., St-Jacques, B., and McMahon, A.P. (2001). Cholesterol modification of sonic hedgehog is required for long-range

signaling activity and effective modulation of signaling by Ptc1. Cell *105*, 599-612. 10.1016/s0092-8674(01)00369-5.
Lewis, P.M., Gritli-Linde, A., Smeyne, R., Kottmann, A., and McMahon, A.P. (2004). Sonic hedgehog signaling is required for expansion of granule neuron precursors and patterning of the mouse cerebellum. Dev Biol *270*, 393-410. 10.1016/j.ydbio.2004.03.007.
Lewis, T.R., Kundinger, S.R., Link, B.A., Insinna, C., and Besharse, J.C. (2018). Kif17 phosphorylation regulates photoreceptor outer segment turnover. BMC Cell Biol *19*, 25. 10.1186/s12860-018-0177-9.
Lewis, T.R., Kundinger, S.R., Pavlovich, A.L., Bostrom, J.R., Link, B.A., and Besharse, J.C. (2017). Cos2/Kif7 and Osm-3/Kif17 regulate onset of outer segment development in zebrafish photoreceptors through distinct mechanisms. Dev Biol *425*, 176-190. 10.1016/j.ydbio.2017.03.019.
Li, Y., Zhang, H., Litingtung, Y., and Chiang, C. (2006). Cholesterol modification restricts the spread of Shh gradient in the limb bud. Proc Natl Acad Sci U S A *103*, 6548-6553. 10.1073/pnas.0600124103.
Liao, W.J., Tsao, K.C., and Yang, R.B. (2016). Electrostatics and N-glycan-mediated membrane tethering of SCUBE1 is critical for promoting bone morphogenetic protein signalling. Biochem J *473*, 661-672. 10.1042/BJ20151041.
Lim, Y.S., and Tang, B.L. (2015). A role for Rab23 in the trafficking of Kif17 to the primary cilium. J Cell Sci *128*, 2996-3008. 10.1242/jcs.163964.
Lin, Y.C., Niceta, M., Muto, V., Vona, B., Pagnamenta, A.T., Maroofian, R., Beetz, C., van Duyvenvoorde, H., Dentici, M.L., Lauffer, P., et al. (2021). SCUBE3 loss-of-function causes a recognizable recessive developmental disorder due to defective bone morphogenetic protein signaling. Am J Hum Genet *108*, 115-133. 10.1016/j.ajhg.2020.11.015.
Lin, Y.C., Roffler, S.R., Yan, Y.T., and Yang, R.B. (2015). Disruption of Scube2 Impairs Endochondral Bone Formation. J Bone Miner Res *30*, 1255-1267. 10.1002/jbmr.2451.
Liu, A., Wang, B., and Niswander, L.A. (2005). Mouse intraflagellar transport proteins regulate both the activator and repressor functions of Gli transcription factors. Development *132*, 3103-3111. 10.1242/dev.01894.
Liu, H., Liu, R., Hao, M., Zhao, X., and Li, C. (2021). Kinesin family member 3C (KIF3C) is a novel non-small cell lung cancer (NSCLC) oncogene whose expression is modulated by microRNA-150-5p (miR-150-5p) and microRNA-186-3p (miR-186-3p). Bioengineered *12*, 3077-3088. 10.1080/21655979.2021.1942768.
Liu, J., Zeng, H., and Liu, A. (2015a). The loss of Hh responsiveness by a non-ciliary Gli2 variant. Development *142*, 1651-1660. 10.1242/dev.119669.
Liu, M., Liu, Y., Hou, B., Bu, D., Shi, L., Gu, X., and Ma, Z. (2015b). Kinesin superfamily protein 17 contributes to the development of bone cancer pain by participating in NR2B transport in the spinal cord of mice. Oncol Rep *33*, 1365-1371. 10.3892/or.2015.3706.
Liu, Y., Liang, Y., Hou, B., Liu, M., Yang, X., Liu, C., Zhang, J., Zhang, W., Ma, Z., and Gu, X. (2014). The inhibitor of calcium/calmodulin-dependent protein kinase II KN93 attenuates bone cancer pain via inhibition of KIF17/NR2B trafficking in mice. Pharmacol Biochem Behav *124*, 19-26. 10.1016/j.pbb.2014.05.003.
Liu, Y., Tian, X., Ke, P., Gu, J., Ma, Y., Guo, Y., Xu, X., Chen, Y., Yang, M., Wang, X., and Xiao, F. (2022). KIF17 Modulates Epileptic Seizures and Membrane Expression of the NMDA Receptor Subunit NR2B. Neurosci Bull *38*, 841-856. 10.1007/s12264-022-00888-9.

Louvi, A., and Artavanis-Tsakonas, S. (2006). Notch signalling in vertebrate neural development. Nat Rev Neurosci *7*, 93-102. 10.1038/nrn1847.
Lum, L., Yao, S., Mozer, B., Rovescalli, A., Von Kessler, D., Nirenberg, M., and Beachy, P.A. (2003). Identification of Hedgehog pathway components by RNAi in Drosophila cultured cells. Science *299*, 2039-2045. 10.1126/science.1081403.
Ma, H., Zhang, F., Zhong, Q., and Hou, J. (2021). METTL3-mediated m6A modification of KIF3C-mRNA promotes prostate cancer progression and is negatively regulated by miR-320d. Aging (Albany NY) *13*, 22332-22344. 10.18632/aging.203541.
Ma, Y., Erkner, A., Gong, R., Yao, S., Taipale, J., Basler, K., and Beachy, P.A. (2002). Hedgehog-mediated patterning of the mammalian embryo requires transporter-like function of dispatched. Cell *111*, 63-75. 10.1016/s0092-8674(02)00977-7.
Macho, B., Brancorsini, S., Fimia, G.M., Setou, M., Hirokawa, N., and Sassone-Corsi, P. (2002). CREM-dependent transcription in male germ cells controlled by a kinesin. Science *298*, 2388-2390. 10.1126/science.1077265.
Machold, R., and Fishell, G. (2005). Math1 is expressed in temporally discrete pools of cerebellar rhombic-lip neural progenitors. Neuron *48*, 17-24. 10.1016/j.neuron.2005.08.028.
Machold, R., Hayashi, S., Rutlin, M., Muzumdar, M.D., Nery, S., Corbin, J.G., Gritli-Linde, A., Dellovade, T., Porter, J.A., Rubin, L.L., et al. (2003). Sonic hedgehog is required for progenitor cell maintenance in telencephalic stem cell niches. Neuron *39*, 937-950. 10.1016/s0896-6273(03)00561-0.
Marigo, V., Davey, R.A., Zuo, Y., Cunningham, J.M., and Tabin, C.J. (1996). Biochemical evidence that patched is the Hedgehog receptor. Nature *384*, 176-179. 10.1038/384176a0.
Marigo, V., and Tabin, C.J. (1996). Regulation of patched by sonic hedgehog in the developing neural tube. Proc Natl Acad Sci U S A *93*, 9346-9351. 10.1073/pnas.93.18.9346.
Markantoni, M., Sarafidou, T., Kyrgiafini, M.A., Chatziparasidou, A., Christoforidis, N., Dafopoulos, K., and Mamuris, Z. (2021). Replicating a GWAS: two novel candidate markers for oligospermia in Greek population. Mol Biol Rep *48*, 4967-4972. 10.1007/s11033-021-06470-2.
Martinelli, D.C., and Fan, C.M. (2007). Gas1 extends the range of Hedgehog action by facilitating its signaling. Genes Dev *21*, 1231-1243. 10.1101/gad.1546307.
Matei, V., Pauley, S., Kaing, S., Rowitch, D., Beisel, K.W., Morris, K., Feng, F., Jones, K., Lee, J., and Fritzsch, B. (2005). Smaller inner ear sensory epithelia in Neurog 1 null mice are related to earlier hair cell cycle exit. Dev Dyn *234*, 633-650. 10.1002/dvdy.20551.
McDermott, A., Gustafsson, M., Elsam, T., Hui, C.C., Emerson, C.P., Jr., and Borycki, A.G. (2005). Gli2 and Gli3 have redundant and context-dependent function in skeletal muscle formation. Development *132*, 345-357. 10.1242/dev.01537.
Mecklenburg, N., Kowalczyk, I., Witte, F., Görne, J., Laier, A., Gonschior, H., Lehmann, M., Richter, M., Sporbert, A., Purfürst, B., et al. (2020). Identification of novel disease relevant genetic modifiers affecting the SHH pathway in the developing brain. bioRxiv, 2020.2011.2003.366302. 10.1101/2020.11.03.366302.
Methot, N., and Basler, K. (1999). Hedgehog controls limb development by regulating the activities of distinct transcriptional activator and repressor forms of Cubitus interruptus. Cell *96*, 819-831. 10.1016/s0092-8674(00)80592-9.
Miale, I.L., and Sidman, R.L. (1961). An autoradiographic analysis of histogenesis in the mouse cerebellum. Exp Neurol *4*, 277-296. 10.1016/0014-4886(61)90055-3.

Micchelli, C.A., The, I., Selva, E., Mogila, V., and Perrimon, N. (2002). Rasp, a putative transmembrane acyltransferase, is required for Hedgehog signaling. Development *129*, 843-851. 10.1242/dev.129.4.843.
Mo, R., Freer, A.M., Zinyk, D.L., Crackower, M.A., Michaud, J., Heng, H.H., Chik, K.W., Shi, X.M., Tsui, L.C., Cheng, S.H., et al. (1997). Specific and redundant functions of Gli2 and Gli3 zinc finger genes in skeletal patterning and development. Development *124*, 113-123. 10.1242/dev.124.1.113.
Mohler, J., and Vani, K. (1992). Molecular organization and embryonic expression of the hedgehog gene involved in cell-cell communication in segmental patterning of Drosophila. Development *115*, 957-971. 10.1242/dev.115.4.957.
Mori, T., Tanaka, K., Buffo, A., Wurst, W., Kuhn, R., and Gotz, M. (2006). Inducible gene deletion in astroglia and radial glia--a valuable tool for functional and lineage analysis. Glia *54*, 21-34. 10.1002/glia.20350.
Morris, R.L., Hoffman, M.P., Obar, R.A., McCafferty, S.S., Gibbons, I.R., Leone, A.D., Cool, J., Allgood, E.L., Musante, A.M., Judkins, K.M., et al. (2006). Analysis of cytoskeletal and motility proteins in the sea urchin genome assembly. Dev Biol *300*, 219-237. 10.1016/j.ydbio.2006.08.052.
Motoyama, J., Liu, J., Mo, R., Ding, Q., Post, M., and Hui, C.C. (1998). Essential function of Gli2 and Gli3 in the formation of lung, trachea and oesophagus. Nat Genet *20*, 54-57. 10.1038/1711.
Muresan, V., Abramson, T., Lyass, A., Winter, D., Porro, E., Hong, F., Chamberlin, N.L., and Schnapp, B.J. (1998). KIF3C and KIF3A form a novel neuronal heteromeric kinesin that associates with membrane vesicles. Mol Biol Cell *9*, 637-652. 10.1091/mbc.9.3.637.
Nagase, T., Kikuno, R., Ishikawa, K.I., Hirosawa, M., and Ohara, O. (2000). Prediction of the coding sequences of unidentified human genes. XVI. The complete sequences of 150 new cDNA clones from brain which code for large proteins in vitro. DNA Res *7*, 65-73. 10.1093/dnares/7.1.65.
Nakagawa, T., Tanaka, Y., Matsuoka, E., Kondo, S., Okada, Y., Noda, Y., Kanai, Y., and Hirokawa, N. (1997). Identification and classification of 16 new kinesin superfamily (KIF) proteins in mouse genome. Proc Natl Acad Sci U S A *94*, 9654-9659. 10.1073/pnas.94.18.9654.
Nakajima, Y., Okamoto, M., Nishimura, H., Obata, K., Kitano, H., Sugita, M., and Matsuyama, T. (2001). Neuronal expression of mint1 and mint2, novel multimodular proteins, in adult murine brain. Brain Res Mol Brain Res *92*, 27-42. 10.1016/s0169-328x(01)00126-7.
Nakano, Y., Guerrero, I., Hidalgo, A., Taylor, A., Whittle, J.R., and Ingham, P.W. (1989). A protein with several possible membrane-spanning domains encoded by the Drosophila segment polarity gene patched. Nature *341*, 508-513. 10.1038/341508a0.
Nakano, Y., Kim, H.R., Kawakami, A., Roy, S., Schier, A.F., and Ingham, P.W. (2004). Inactivation of dispatched 1 by the chameleon mutation disrupts Hedgehog signalling in the zebrafish embryo. Dev Biol *269*, 381-392. 10.1016/j.ydbio.2004.01.022.
Niewiadomski, P., Kong, J.H., Ahrends, R., Ma, Y., Humke, E.W., Khan, S., Teruel, M.N., Novitch, B.G., and Rohatgi, R. (2014). Gli protein activity is controlled by multisite phosphorylation in vertebrate Hedgehog signaling. Cell Rep *6*, 168-181. 10.1016/j.celrep.2013.12.003.
Niewiadomski, P., Zhujiang, A., Youssef, M., and Waschek, J.A. (2013). Interaction of PACAP with Sonic hedgehog reveals complex regulation of the hedgehog pathway by PKA. Cell Signal *25*, 2222-2230. 10.1016/j.cellsig.2013.07.012.

Nonaka, S., Tanaka, Y., Okada, Y., Takeda, S., Harada, A., Kanai, Y., Kido, M., and Hirokawa, N. (1998). Randomization of left-right asymmetry due to loss of nodal cilia generating leftward flow of extraembryonic fluid in mice lacking KIF3B motor protein. Cell *95*, 829-837. 10.1016/s0092-8674(00)81705-5.
Nusslein-Volhard, C., and Wieschaus, E. (1980). Mutations affecting segment number and polarity in Drosophila. Nature *287*, 795-801. 10.1038/287795a0.
Ocbina, P.J., Eggenschwiler, J.T., Moskowitz, I., and Anderson, K.V. (2011). Complex interactions between genes controlling trafficking in primary cilia. Nat Genet *43*, 547-553. 10.1038/ng.832.
Pan, Y., Bai, C.B., Joyner, A.L., and Wang, B. (2006). Sonic hedgehog signaling regulates Gli2 transcriptional activity by suppressing its processing and degradation. Mol Cell Biol *26*, 3365-3377. 10.1128/MCB.26.9.3365-3377.2006.
Pan, Y., and Wang, B. (2007). A novel protein-processing domain in Gli2 and Gli3 differentially blocks complete protein degradation by the proteasome. J Biol Chem *282*, 10846-10852. 10.1074/jbc.M608599200.
Pan, Y., Wang, C., and Wang, B. (2009). Phosphorylation of Gli2 by protein kinase A is required for Gli2 processing and degradation and the Sonic Hedgehog-regulated mouse development. Dev Biol *326*, 177-189. 10.1016/j.ydbio.2008.11.009.
Park, H.L., Bai, C., Platt, K.A., Matise, M.P., Beeghly, A., Hui, C.C., Nakashima, M., and Joyner, A.L. (2000). Mouse Gli1 mutants are viable but have defects in SHH signaling in combination with a Gli2 mutation. Development *127*, 1593-1605. 10.1242/dev.127.8.1593.
Parmantier, E., Lynn, B., Lawson, D., Turmaine, M., Namini, S.S., Chakrabarti, L., McMahon, A.P., Jessen, K.R., and Mirsky, R. (1999). Schwann cell-derived Desert hedgehog controls the development of peripheral nerve sheaths. Neuron *23*, 713-724. 10.1016/s0896-6273(01)80030-1.
Pepinsky, R.B., Zeng, C., Wen, D., Rayhorn, P., Baker, D.P., Williams, K.P., Bixler, S.A., Ambrose, C.M., Garber, E.A., Miatkowski, K., et al. (1998). Identification of a palmitic acid-modified form of human Sonic hedgehog. J Biol Chem *273*, 14037-14045. 10.1074/jbc.273.22.14037.
Peterson, K.A., Nishi, Y., Ma, W., Vedenko, A., Shokri, L., Zhang, X., McFarlane, M., Baizabal, J.M., Junker, J.P., van Oudenaarden, A., et al. (2012). Neural-specific Sox2 input and differential Gli-binding affinity provide context and positional information in Shh-directed neural patterning. Genes Dev *26*, 2802-2816. 10.1101/gad.207142.112.
Petrov, K., Wierbowski, B.M., and Salic, A. (2017). Sending and Receiving Hedgehog Signals. Annu Rev Cell Dev Biol *33*, 145-168. 10.1146/annurev-cellbio-100616-060847.
Porter, J.A., Ekker, S.C., Park, W.J., von Kessler, D.P., Young, K.E., Chen, C.H., Ma, Y., Woods, A.S., Cotter, R.J., Koonin, E.V., and Beachy, P.A. (1996a). Hedgehog patterning activity: role of a lipophilic modification mediated by the carboxy-terminal autoprocessing domain. Cell *86*, 21-34. 10.1016/s0092-8674(00)80074-4.
Porter, J.A., von Kessler, D.P., Ekker, S.C., Young, K.E., Lee, J.J., Moses, K., and Beachy, P.A. (1995). The product of hedgehog autoproteolytic cleavage active in local and long-range signalling. Nature *374*, 363-366. 10.1038/374363a0.
Porter, J.A., Young, K.E., and Beachy, P.A. (1996b). Cholesterol modification of hedgehog signaling proteins in animal development. Science *274*, 255-259. 10.1126/science.274.5285.255.
Preat, T. (1992). Characterization of Suppressor of fused, a complete suppressor of the fused segment polarity gene of Drosophila melanogaster. Genetics *132*, 725-736. 10.1093/genetics/132.3.725.

Preat, T., Therond, P., Limbourg-Bouchon, B., Pham, A., Tricoire, H., Busson, D., and Lamour-Isnard, C. (1993). Segmental polarity in Drosophila melanogaster: genetic dissection of fused in a Suppressor of fused background reveals interaction with costal-2. Genetics *135*, 1047-1062. 10.1093/genetics/135.4.1047.
Price, M.A., and Kalderon, D. (2002). Proteolysis of the Hedgehog signaling effector Cubitus interruptus requires phosphorylation by Glycogen Synthase Kinase 3 and Casein Kinase 1. Cell *108*, 823-835. 10.1016/s0092-8674(02)00664-5.
Qin, J., Lin, Y., Norman, R.X., Ko, H.W., and Eggenschwiler, J.T. (2011). Intraflagellar transport protein 122 antagonizes Sonic Hedgehog signaling and controls ciliary localization of pathway components. Proc Natl Acad Sci U S A *108*, 1456-1461. 10.1073/pnas.1011410108.
Raffel, C., Jenkins, R.B., Frederick, L., Hebrink, D., Alderete, B., Fults, D.W., and James, C.D. (1997). Sporadic medulloblastomas contain PTCH mutations. Cancer Res *57*, 842-845.
Renaud, J., Kerjan, G., Sumita, I., Zagar, Y., Georget, V., Kim, D., Fouquet, C., Suda, K., Sanbo, M., Suto, F., et al. (2008). Plexin-A2 and its ligand, Sema6A, control nucleus-centrosome coupling in migrating granule cells. Nat Neurosci *11*, 440-449. 10.1038/nn2064.
Riddle, R.D., Johnson, R.L., Laufer, E., and Tabin, C. (1993). Sonic hedgehog mediates the polarizing activity of the ZPA. Cell *75*, 1401-1416. 10.1016/0092-8674(93)90626-2.
Rios, I., Alvarez-Rodriguez, R., Marti, E., and Pons, S. (2004). Bmp2 antagonizes sonic hedgehog-mediated proliferation of cerebellar granule neurones through Smad5 signalling. Development *131*, 3159-3168. 10.1242/dev.01188.
Riva, A., Gambadauro, A., Dipasquale, V., Casto, C., Ceravolo, M.D., Accogli, A., Scala, M., Ceravolo, G., Iacomino, M., Zara, F., et al. (2021). Biallelic Variants in KIF17 Associated with Microphthalmia and Coloboma Spectrum. Int J Mol Sci *22*. 10.3390/ijms22094471.
Roelink, H., Augsburger, A., Heemskerk, J., Korzh, V., Norlin, S., Ruiz i Altaba, A., Tanabe, Y., Placzek, M., Edlund, T., Jessell, T.M., and et al. (1994). Floor plate and motor neuron induction by vhh-1, a vertebrate homolog of hedgehog expressed by the notochord. Cell *76*, 761-775. 10.1016/0092-8674(94)90514-2.
Roelink, H., Porter, J.A., Chiang, C., Tanabe, Y., Chang, D.T., Beachy, P.A., and Jessell, T.M. (1995). Floor plate and motor neuron induction by different concentrations of the amino-terminal cleavage product of sonic hedgehog autoproteolysis. Cell *81*, 445-455. 10.1016/0092-8674(95)90397-6.
Rohatgi, R., Milenkovic, L., and Scott, M.P. (2007). Patched1 regulates hedgehog signaling at the primary cilium. Science *317*, 372-376. 10.1126/science.1139740.
Saade, M., Irla, M., Govin, J., Victorero, G., Samson, M., and Nguyen, C. (2007). Dynamic distribution of Spatial during mouse spermatogenesis and its interaction with the kinesin KIF17b. Exp Cell Res *313*, 614-626. 10.1016/j.yexcr.2006.11.011.
Santos, N., and Reiter, J.F. (2014). A central region of Gli2 regulates its localization to the primary cilium and transcriptional activity. J Cell Sci *127*, 1500-1510. 10.1242/jcs.139253.
Sasaki, H., Hui, C., Nakafuku, M., and Kondoh, H. (1997). A binding site for Gli proteins is essential for HNF-3beta floor plate enhancer activity in transgenics and can respond to Shh in vitro. Development *124*, 1313-1322. 10.1242/dev.124.7.1313.
Sasaki, H., Nishizaki, Y., Hui, C., Nakafuku, M., and Kondoh, H. (1999). Regulation of Gli2 and Gli3 activities by an amino-terminal repression domain: implication of Gli2 and Gli3 as primary mediators of Shh signaling. Development *126*, 3915-3924. 10.1242/dev.126.17.3915.

Scholey, J.M. (2013). Kinesin-2: a family of heterotrimeric and homodimeric motors with diverse intracellular transport functions. Annu Rev Cell Dev Biol *29*, 443-469. 10.1146/annurev-cellbio-101512-122335.
Setou, M., Nakagawa, T., Seog, D.H., and Hirokawa, N. (2000). Kinesin superfamily motor protein KIF17 and mLin-10 in NMDA receptor-containing vesicle transport. Science *288*, 1796-1802. 10.1126/science.288.5472.1796.
Signor, D., Wedaman, K.P., Rose, L.S., and Scholey, J.M. (1999). Two heteromeric kinesin complexes in chemosensory neurons and sensory cilia of Caenorhabditis elegans. Mol Biol Cell *10*, 345-360. 10.1091/mbc.10.2.345.
Smelkinson, M.G., and Kalderon, D. (2006). Processing of the Drosophila hedgehog signaling effector Ci-155 to the repressor Ci-75 is mediated by direct binding to the SCF component Slimb. Curr Biol *16*, 110-116. 10.1016/j.cub.2005.12.012.
Snow, J.J., Ou, G., Gunnarson, A.L., Walker, M.R., Zhou, H.M., Brust-Mascher, I., and Scholey, J.M. (2004). Two anterograde intraflagellar transport motors cooperate to build sensory cilia on C. elegans neurons. Nat Cell Biol *6*, 1109-1113. 10.1038/ncb1186.
Solecki, D.J., Liu, X.L., Tomoda, T., Fang, Y., and Hatten, M.E. (2001). Activated Notch2 signaling inhibits differentiation of cerebellar granule neuron precursors by maintaining proliferation. Neuron *31*, 557-568. 10.1016/s0896-6273(01)00395-6.
Song, J.Y., Holtz, A.M., Pinskey, J.M., and Allen, B.L. (2015). Distinct structural requirements for CDON and BOC in the promotion of Hedgehog signaling. Dev Biol *402*, 239-252. 10.1016/j.ydbio.2015.03.015.
Spassky, N., Han, Y.G., Aguilar, A., Strehl, L., Besse, L., Laclef, C., Ros, M.R., Garcia-Verdugo, J.M., and Alvarez-Buylla, A. (2008). Primary cilia are required for cerebellar development and Shh-dependent expansion of progenitor pool. Dev Biol *317*, 246-259. 10.1016/j.ydbio.2008.02.026.
Stauber, T., Simpson, J.C., Pepperkok, R., and Vernos, I. (2006). A role for kinesin-2 in COPI-dependent recycling between the ER and the Golgi complex. Curr Biol *16*, 2245-2251. 10.1016/j.cub.2006.09.060.
Stewart, D.P., Marada, S., Bodeen, W.J., Truong, A., Sakurada, S.M., Pandit, T., Pruett-Miller, S.M., and Ogden, S.K. (2018). Cleavage activates dispatched for Sonic Hedgehog ligand release. Elife *7*. 10.7554/eLife.31678.
Stone, D.M., Hynes, M., Armanini, M., Swanson, T.A., Gu, Q., Johnson, R.L., Scott, M.P., Pennica, D., Goddard, A., Phillips, H., et al. (1996). The tumour-suppressor gene patched encodes a candidate receptor for Sonic hedgehog. Nature *384*, 129-134. 10.1038/384129a0.
Svard, J., Heby-Henricson, K., Persson-Lek, M., Rozell, B., Lauth, M., Bergstrom, A., Ericson, J., Toftgard, R., and Teglund, S. (2006). Genetic elimination of Suppressor of fused reveals an essential repressor function in the mammalian Hedgehog signaling pathway. Dev Cell *10*, 187-197. 10.1016/j.devcel.2005.12.013.
Tabata, T., Eaton, S., and Kornberg, T.B. (1992). The Drosophila hedgehog gene is expressed specifically in posterior compartment cells and is a target of engrailed regulation. Genes Dev *6*, 2635-2645. 10.1101/gad.6.12b.2635.
Taipale, J., Cooper, M.K., Maiti, T., and Beachy, P.A. (2002). Patched acts catalytically to suppress the activity of Smoothened. Nature *418*, 892-897. 10.1038/nature00989.
Takeda, S., Yamazaki, H., Seog, D.H., Kanai, Y., Terada, S., and Hirokawa, N. (2000). Kinesin superfamily protein 3 (KIF3) motor transports fodrin-associating vesicles important for neurite building. J Cell Biol *148*, 1255-1265. 10.1083/jcb.148.6.1255.

Takeda, S., Yonekawa, Y., Tanaka, Y., Okada, Y., Nonaka, S., and Hirokawa, N. (1999). Left-right asymmetry and kinesin superfamily protein KIF3A: new insights in determination of laterality and mesoderm induction by kif3A-/- mice analysis. J Cell Biol *145*, 825-836. 10.1083/jcb.145.4.825.
Tarabeux, J., Champagne, N., Brustein, E., Hamdan, F.F., Gauthier, J., Lapointe, M., Maios, C., Piton, A., Spiegelman, D., Henrion, E., et al. (2010). De novo truncating mutation in Kinesin 17 associated with schizophrenia. Biol Psychiatry *68*, 649-656. 10.1016/j.biopsych.2010.04.018.
Taylor, A.M., Nakano, Y., Mohler, J., and Ingham, P.W. (1993). Contrasting distributions of patched and hedgehog proteins in the Drosophila embryo. Mech Dev *42*, 89-96. 10.1016/0925-4773(93)90101-3.
Tempe, D., Casas, M., Karaz, S., Blanchet-Tournier, M.F., and Concordet, J.P. (2006). Multisite protein kinase A and glycogen synthase kinase 3beta phosphorylation leads to Gli3 ubiquitination by SCFbetaTrCP. Mol Cell Biol *26*, 4316-4326. 10.1128/MCB.02183-05.
Tenzen, T., Allen, B.L., Cole, F., Kang, J.S., Krauss, R.S., and McMahon, A.P. (2006). The cell surface membrane proteins Cdo and Boc are components and targets of the Hedgehog signaling pathway and feedback network in mice. Dev Cell *10*, 647-656. 10.1016/j.devcel.2006.04.004.
Therond, P., Busson, D., Guillemet, E., Limbourg-Bouchon, B., Preat, T., Terracol, R., Tricoire, H., and Lamour-Isnard, C. (1993). Molecular organisation and expression pattern of the segment polarity gene fused of Drosophila melanogaster. Mech Dev *44*, 65-80. 10.1016/0925-4773(93)90017-r.
Tian, H., Jeong, J., Harfe, B.D., Tabin, C.J., and McMahon, A.P. (2005a). Mouse Disp1 is required in sonic hedgehog-expressing cells for paracrine activity of the cholesterol-modified ligand. Development *132*, 133-142. 10.1242/dev.01563.
Tian, L., Holmgren, R.A., and Matouschek, A. (2005b). A conserved processing mechanism regulates the activity of transcription factors Cubitus interruptus and NF-kappaB. Nat Struct Mol Biol *12*, 1045-1053. 10.1038/nsmb1018.
Tokhunts, R., Singh, S., Chu, T., D'Angelo, G., Baubet, V., Goetz, J.A., Huang, Z., Yuan, Z., Ascano, M., Zavros, Y., et al. (2010). The full-length unprocessed hedgehog protein is an active signaling molecule. J Biol Chem *285*, 2562-2568. 10.1074/jbc.M109.078626.
Traiffort, E., Charytoniuk, D.A., Faure, H., and Ruat, M. (1998). Regional distribution of Sonic Hedgehog, patched, and smoothened mRNA in the adult rat brain. J Neurochem *70*, 1327-1330. 10.1046/j.1471-4159.1998.70031327.x.
Trifonov, S., Yamashita, Y., Kase, M., Maruyama, M., and Sugimoto, T. (2016). Overview and assessment of the histochemical methods and reagents for the detection of beta-galactosidase activity in transgenic animals. Anat Sci Int *91*, 56-67. 10.1007/s12565-015-0300-3.
Tsai, M.T., Cheng, C.J., Lin, Y.C., Chen, C.C., Wu, A.R., Wu, M.T., Hsu, C.C., and Yang, R.B. (2009). Isolation and characterization of a secreted, cell-surface glycoprotein SCUBE2 from humans. Biochem J *422*, 119-128. 10.1042/BJ20090341.
Tukachinsky, H., Kuzmickas, R.P., Jao, C.Y., Liu, J., and Salic, A. (2012). Dispatched and scube mediate the efficient secretion of the cholesterol-modified hedgehog ligand. Cell Rep *2*, 308-320. 10.1016/j.celrep.2012.07.010.
Tukachinsky, H., Lopez, L.V., and Salic, A. (2010). A mechanism for vertebrate Hedgehog signaling: recruitment to cilia and dissociation of SuFu-Gli protein complexes. J Cell Biol *191*, 415-428. 10.1083/jcb.201004108.

Tuson, M., He, M., and Anderson, K.V. (2011). Protein kinase A acts at the basal body of the primary cilium to prevent Gli2 activation and ventralization of the mouse neural tube. Development *138*, 4921-4930. 10.1242/dev.070805.
Vale, R.D., Reese, T.S., and Sheetz, M.P. (1985). Identification of a novel force-generating protein, kinesin, involved in microtubule-based motility. Cell *42*, 39-50. 10.1016/s0092-8674(85)80099-4.
van Eeden, F.J., Granato, M., Schach, U., Brand, M., Furutani-Seiki, M., Haffter, P., Hammerschmidt, M., Heisenberg, C.P., Jiang, Y.J., Kane, D.A., et al. (1996). Mutations affecting somite formation and patterning in the zebrafish, Danio rerio. Development *123*, 153-164. 10.1242/dev.123.1.153.
Verhey, K.J., and Hammond, J.W. (2009). Traffic control: regulation of kinesin motors. Nat Rev Mol Cell Biol *10*, 765-777. 10.1038/nrm2782.
Vortkamp, A., Lee, K., Lanske, B., Segre, G.V., Kronenberg, H.M., and Tabin, C.J. (1996). Regulation of rate of cartilage differentiation by Indian hedgehog and PTH-related protein. Science *273*, 613-622. 10.1126/science.273.5275.613.
Wallace, V.A. (1999). Purkinje-cell-derived Sonic hedgehog regulates granule neuron precursor cell proliferation in the developing mouse cerebellum. Curr Biol *9*, 445-448. 10.1016/s0960-9822(99)80195-x.
Wang, B., Fallon, J.F., and Beachy, P.A. (2000). Hedgehog-regulated processing of Gli3 produces an anterior/posterior repressor gradient in the developing vertebrate limb. Cell *100*, 423-434. 10.1016/s0092-8674(00)80678-9.
Wang, B., and Li, Y. (2006). Evidence for the direct involvement of betaTrCP in Gli3 protein processing. Proc Natl Acad Sci U S A *103*, 33-38. 10.1073/pnas.0509927103.
Wang, C., Pan, Y., and Wang, B. (2010). Suppressor of fused and Spop regulate the stability, processing and function of Gli2 and Gli3 full-length activators but not their repressors. Development *137*, 2001-2009. 10.1242/dev.052126.
Wang, C., Wang, C., Wei, Z., Li, Y., Wang, W., Li, X., Zhao, J., Zhou, X., Qu, X., and Xiang, F. (2015). Suppression of motor protein KIF3C expression inhibits tumor growth and metastasis in breast cancer by inhibiting TGF-beta signaling. Cancer Lett *368*, 105-114. 10.1016/j.canlet.2015.07.037.
Wang, G., Wang, B., and Jiang, J. (1999). Protein kinase A antagonizes Hedgehog signaling by regulating both the activator and repressor forms of Cubitus interruptus. Genes Dev *13*, 2828-2837. 10.1101/gad.13.21.2828.
Wang, S., Tanaka, Y., Xu, Y., Takeda, S., and Hirokawa, N. (2022). KIF3B promotes a PI3K signaling gradient causing changes in a Shh protein gradient and suppressing polydactyly in mice. Dev Cell *57*, 2273-2289 e2211. 10.1016/j.devcel.2022.09.007.
Wang, V.Y., Rose, M.F., and Zoghbi, H.Y. (2005). Math1 expression redefines the rhombic lip derivatives and reveals novel lineages within the brainstem and cerebellum. Neuron *48*, 31-43. 10.1016/j.neuron.2005.08.024.
Wechsler-Reya, R.J., and Scott, M.P. (1999). Control of neuronal precursor proliferation in the cerebellum by Sonic Hedgehog. Neuron *22*, 103-114. 10.1016/s0896-6273(00)80682-0.
Weller, M., Krautler, N., Mantei, N., Suter, U., and Taylor, V. (2006). Jagged1 ablation results in cerebellar granule cell migration defects and depletion of Bergmann glia. Dev Neurosci *28*, 70-80. 10.1159/000090754.

Wen, X., Lai, C.K., Evangelista, M., Hongo, J.A., de Sauvage, F.J., and Scales, S.J. (2010). Kinetics of hedgehog-dependent full-length Gli3 accumulation in primary cilia and subsequent degradation. Mol Cell Biol *30*, 1910-1922. 10.1128/MCB.01089-09.
Williams, C.L., McIntyre, J.C., Norris, S.R., Jenkins, P.M., Zhang, L., Pei, Q., Verhey, K., and Martens, J.R. (2014). Direct evidence for BBSome-associated intraflagellar transport reveals distinct properties of native mammalian cilia. Nat Commun *5*, 5813. 10.1038/ncomms6813.
Wong, R.W., Setou, M., Teng, J., Takei, Y., and Hirokawa, N. (2002). Overexpression of motor protein KIF17 enhances spatial and working memory in transgenic mice. Proc Natl Acad Sci U S A *99*, 14500-14505. 10.1073/pnas.222371099.
Wong, S.Y., Seol, A.D., So, P.L., Ermilov, A.N., Bichakjian, C.K., Epstein, E.H., Jr., Dlugosz, A.A., and Reiter, J.F. (2009). Primary cilia can both mediate and suppress Hedgehog pathway-dependent tumorigenesis. Nat Med *15*, 1055-1061. 10.1038/nm.2011.
Woods, I.G., and Talbot, W.S. (2005). The you gene encodes an EGF-CUB protein essential for Hedgehog signaling in zebrafish. PLoS Biol *3*, e66. 10.1371/journal.pbio.0030066.
Wu, Y., Wang, C., Sun, H., LeRoith, D., and Yakar, S. (2009). High-efficient FLPo deleter mice in C57BL/6J background. PLoS One *4*, e8054. 10.1371/journal.pone.0008054.
Yamazaki, H., Nakata, T., Okada, Y., and Hirokawa, N. (1995). KIF3A/B: a heterodimeric kinesin superfamily protein that works as a microtubule plus end-directed motor for membrane organelle transport. J Cell Biol *130*, 1387-1399. 10.1083/jcb.130.6.1387.
Yang, N., Li, L., Eguether, T., Sundberg, J.P., Pazour, G.J., and Chen, J. (2015). Intraflagellar transport 27 is essential for hedgehog signaling but dispensable for ciliogenesis during hair follicle morphogenesis. Development *142*, 2860. 10.1242/dev.128751.
Yang, Z., and Goldstein, L.S. (1998). Characterization of the KIF3C neural kinesin-like motor from mouse. Mol Biol Cell *9*, 249-261. 10.1091/mbc.9.2.249.
Yang, Z., Hanlon, D.W., Marszalek, J.R., and Goldstein, L.S. (1997). Identification, partial characterization, and genetic mapping of kinesin-like protein genes in mouse. Genomics *45*, 123-131. 10.1006/geno.1997.4901.
Yang, Z., Roberts, E.A., and Goldstein, L.S. (2001). Functional analysis of mouse kinesin motor Kif3C. Mol Cell Biol *21*, 5306-5311. 10.1128/MCB.21.16.5306-5311.2001.
Yao, S., Lum, L., and Beachy, P. (2006). The ihog cell-surface proteins bind Hedgehog and mediate pathway activation. Cell *125*, 343-357. 10.1016/j.cell.2006.02.040.
Yao, W., Jia, X., Xu, L., Li, S., and Wei, L. (2021). MicroRNA-2053 involves in the progression of esophageal cancer by targeting KIF3C. Cell Cycle *20*, 1163-1172. 10.1080/15384101.2021.1929675.
Yin, X., Feng, X., Takei, Y., and Hirokawa, N. (2012). Regulation of NMDA receptor transport: a KIF17-cargo binding/releasing underlies synaptic plasticity and memory in vivo. J Neurosci *32*, 5486-5499. 10.1523/JNEUROSCI.0718-12.2012.
Yin, X., Takei, Y., Kido, M.A., and Hirokawa, N. (2011). Molecular motor KIF17 is fundamental for memory and learning via differential support of synaptic NR2A/2B levels. Neuron *70*, 310-325. 10.1016/j.neuron.2011.02.049.
Yuasa, S. (1996). Bergmann glial development in the mouse cerebellum as revealed by tenascin expression. Anat Embryol (Berl) *194*, 223-234. 10.1007/BF00187133.
Yuasa, S., Kawamura, K., Ono, K., Yamakuni, T., and Takahashi, Y. (1991). Development and migration of Purkinje cells in the mouse cerebellar primordium. Anat Embryol (Berl) *184*, 195-212. 10.1007/BF01673256.

Zeng, H., Jia, J., and Liu, A. (2010). Coordinated translocation of mammalian Gli proteins and suppressor of fused to the primary cilium. PLoS One *5*, e15900. 10.1371/journal.pone.0015900.
Zhang, H., Takeda, H., Tsuji, T., Kamiya, N., Rajderkar, S., Louie, K., Collier, C., Scott, G., Ray, M., Mochida, Y., et al. (2015). Generation of Evc2/Limbin global and conditional KO mice and its roles during mineralized tissue formation. Genesis *53*, 612-626. 10.1002/dvg.22879.
Zhao, C., Omori, Y., Brodowska, K., Kovach, P., and Malicki, J. (2012). Kinesin-2 family in vertebrate ciliogenesis. Proc Natl Acad Sci U S A *109*, 2388-2393. 10.1073/pnas.1116035109.
Zhao, H., Ayrault, O., Zindy, F., Kim, J.H., and Roussel, M.F. (2008). Post-transcriptional down-regulation of Atoh1/Math1 by bone morphogenic proteins suppresses medulloblastoma development. Genes Dev *22*, 722-727. 10.1101/gad.1636408.